CASE FILE
COPY

NASA TECHNICAL REPORT

NASA TR R-199

NASA TR R-199

DYNAMIC RESPONSE OF AIRPLANES TO ATMOSPHERIC TURBULENCE INCLUDING FLIGHT DATA ON INPUT AND RESPONSE

by John C. Houbolt, Roy Steiner, and Kermit G. Pratt

Langley Research Center
Langley Station, Hampton, Va.

NATIONAL AERONAUTICS AND SPACE ADMINISTRATION • WASHINGTON, D. C. • JUNE 1964

DYNAMIC RESPONSE OF AIRPLANES TO ATMOSPHERIC TURBULENCE

INCLUDING FLIGHT DATA ON INPUT AND RESPONSE

By John C. Houbolt, Roy Steiner,
and Kermit G. Pratt

Langley Research Center
Langley Station, Hampton, Va.

NATIONAL AERONAUTICS AND SPACE ADMINISTRATION

For sale by the Office of Technical Services, Department of Commerce,
Washington, D.C. 20230 -- Price $2.50

CONTENTS

DYNAMIC RESPONSE OF AIRPLANES TO ATMOSPHERIC TURBULENCE INCLUDING FLIGHT DATA ON INPUT AND RESPONSE*

By John C. Houbolt, Roy Steiner,
and Kermit G. Pratt
Langley Research Center

SUMMARY

A coordinated account of flight measurements of random atmospheric turbulence input, of calculated and experimentally determined airplane transfer functions, and of analytical procedures for determining output or airplane response is given based on the concepts of power spectral techniques. Atmospheric turbulence results for several meteorological conditions and altitudes (including new information from thunderstorms) are described and consideration is given to the numerical values of the root-mean-square gust velocities and the turbulence scale parameter. Transfer functions obtained both by calculation and as deduced from flight tests are compared for rigid and flexible airplanes at subsonic speeds and for a rigid airplane at supersonic speeds. Some of the implications of power spectral techniques for load prediction and for design are discussed. An outline of the origin and derivation of the correlation and spectral relations used in the paper, the effect of extraneous signals on determination of the scale of turbulence, and a review of the basic procedures and mathematics that are involved in the practical applications of power spectral techniques are given in the appendixes.

INTRODUCTION

This report deals with the science and art of treating the gust loads problem of airplanes as a random-process phenomenon; subjects included are (1) the establishment of a realistic and usable description of continuous atmospheric turbulence by power spectral techniques and (2) the allied treatment of the dynamic response of airplanes to such turbulence. In this coverage, analytical techniques and data - past, present, and new - and statistical inference are considered.

---

*An earlier version of this paper bearing the title "Flight Data and Considerations of the Dynamic Response of Airplanes to Atmospheric Turbulence" was presented to the AGARD panels on Structures and Materials and on Flight Mechanics in Paris, July 1962.

Much information on gust problems has been generated over the past decade, as is attested by the first three sections of the bibliography. It is now appropriate to ask, "Where do we stand today in our ability to predict gust loads, particularly with power spectral techniques?" and "Where does one begin?" Therefore, in addition to presenting new data and information, the purpose of this report is twofold - first, to examine the present state of the art and to indicate what data are available, and second, to determine a starting point for the selection of appropriate procedures and techniques applicable to the gust loads problem.

The development of the present report is essentially as follows: Data on and analytical representation of the turbulence in the atmosphere are first given, including results of recent flights through cumulus clouds and thunderstorms for both subsonic and supersonic flight. Next the means for determining the airplane transfer function are considered, both analytically and by flight experimentation methods. A comparison of recent results is given for a subsonic and a supersonic case. Then several suggestions are outlined for the possibility of establishing the gust design of airplanes by power spectral techniques. The body of the paper is concluded with a listing of the main elements which deserve further consideration. A list of principal symbols is presented in appendix A. In appendixes B to E details of the mathematical derivations are given and the mathematical representation and analytical procedures involved in the application of power spectral techniques are reviewed. Analog equipment for analyzing random functions is described in appendix F.

EVOLUTION OF GUST DESIGN

This résumé of the evolution of gust design is restricted to developments within the United States, but it should be kept in mind that significant contributions have also been made in the past 30 years by investigators in several countries.

The early design for gusts was based on a discrete-gust approach involving the concept of a rigid airplane and a ramp-type gust with a gradient distance of 10 chords and specified maximum vertical velocity. A somewhat arbitrary alleviation curve was used to attempt to adjust for differences in such factors as wing chord and pitching effects; although improper in a rigorous sense, it was expressed in terms of the convenient design parameter W/S, the wing loading. This alleviation curve, when used in the gust-load formula, gave results which were, in effect, the same as if the airplane had encountered a step-type gust of less magnitude than the maximum design velocity used in the ramp gust; hence, the concept of "sharp-edge gust encounter" frequently mentioned.

Later the design procedure was changed so that the alleviation curve was expressed in terms of the more fundamental and less restrictive parameter μ, the mass ratio. (For small business or pleasure types of airplanes, however, the wing-loading parameter is still used.) Also considered was the shape of the discrete gust - whether it should be a triangular type, sine type, or 1 - cosine type - and many arguments ensued over what shape was the "proper"

one to use. The shape adopted was a compromise, the 1 - cosine type with a gradient distance of 12.5 chords.

It should be recognized that the use of the discrete-gust concept is, in principle, a convenient and simple way of relating the accelerations experienced by one airplane to those which are likely to be experienced by another, and further implies that the relative loads for single isolated gusts are a measure of the relative loads in a sequence of gusts. This concept seems justifiable if different aircraft have essentially the same response characteristics and are used in roughly the same manner. Indeed, the concept has been a useful and simple one through the past years.

As airplanes began to change markedly in their configuration and response characteristics - as sweep was introduced, as the airplanes became more flexible and the distributions of their masses differed, as speeds and altitudes of operation changed - a more general approach was needed. Hence the power spectral techniques of generalized harmonic analysis were introduced. The pioneers of the applications of these techniques are, in particular, Harry Press, G. C. Clementson, Norbert Wiener, S. O. Rice, and J. W. Tukey. References 1 and 2 summarize some of the earlier applications to airplane dynamics.

As these spectral techniques were being developed for airplane application, however, much work was also done in attempting to extend the application of the discrete-gust concept from rigid bodies to flexible bodies. In this flexible-body approach, the attempt is to include dynamic-response effects by mathematically flying the flexible airplane through discrete gusts of varying wavelengths. (See, for example, ref. 3.) Rough indications of amplification or overshoot effects are obtained in this way, but serious deficiencies exist, such as the inherent inability to take into account the continuous nature of atmospheric turbulence, particularly in the case of lightly damped systems. Design for gusts, nevertheless, had to rely on this approach for several years until the power spectral approach was developed to a usable point. At present, design philosophy makes use of both the discrete gust and the spectral approach. Essentially, the design is first established on the basis of a discrete-gust analysis. It is then examined or checked in greater detail by means of a power spectral approach, and comparisons may be made with results for an older or proven airplane. As the spectral approach becomes further developed, it may replace the discrete-gust concepts altogether.

The main assets offered by the power spectral approach are as follows:

1. It allows for a more realistic representation of the continuous nature of atmospheric turbulence.

2. It allows airplane configurations and response characteristics to be taken into account in a rational manner.

3. It allows more rational consideration of design and operational variations such as configuration changes, mission changes, and airplane degrees of freedom.

Since application and tests of these techniques are relatively recent, not all the ramifications and aspects are known. It is significant and encouraging, however, to note that agreement between calculation and experiment on the whole has been good.

DESCRIPTION OF ATMOSPHERIC TURBULENCE

The nature of atmospheric turbulence in terms of power spectral representation is discussed in this section. First, the relations required to obtain time histories of the components of "true gust velocities" from flight measurements are presented with some considerations of the flight instrumentation requirements. The term "true gust velocity" is used herein to denote the actual velocity of the air particles as distinguished from an equivalent velocity that has been used in discrete-gust studies. The description of the atmospheric turbulence consists of a review of available spectra for low-altitude (less than 5,000 feet) clear-air turbulence and, in addition, the presentation of new spectra for more severe turbulence recently measured in cumulus clouds and thunderstorms to altitudes of 40,000 feet. Analytical representation of these spectra is considered in some detail.

Method of Evaluation

The basic measurement for the description of the atmospheric turbulence by power-spectral-density techniques is the angle of attack or angle of sideslip measured by flow vanes or differential-pressure probes on booms ahead of the airplane. The flow angles are corrected for effects of airplane motions to provide a continuous time history of the components of true gust velocity. The vertical component of true gust velocity is given by

$$w_g = V\alpha_V - V\theta + \int a_Z \, dt + l_X\dot{\theta} \tag{1}$$

the lateral component by

$$v_g = -V\beta_V - V\psi + l_X\dot{\psi} + \int \left(a_Y + g\varphi\right)dt + l_Z\dot{\varphi} \tag{2}$$

and the longitudinal component by

$$u_g = (V - \overline{V}) - \int (a_X - g\theta)dt \tag{3}$$

(Primary symbols are defined in appendix A; $\overline{V}$ is the mean value of the airspeed.) Equations (1) to (3) are based on the following assumptions:

1. All disturbances are small enough to allow use of the angle in radians in place of the sine of the angle.

2. Boom flexure is negligible.

3. Effects of variation in upwash on vane indications are negligible or are allowed for by calibration.

The measurements are normally taken as increments from the mean values for the entire record. The actual evaluation procedures to obtain the time history of the vertical component of gust velocities are, for example, given by

$$w_g = V(\alpha_v - \bar{\alpha}_v) - V(\theta - \bar{\theta}) + \int_0^t (a_z - \bar{a}_z)dt + l_x(\dot{\theta} - \bar{\dot{\theta}}) \qquad (4)$$

where the bar denotes the average value for the record length being evaluated (see ref. 4). This evaluation yields a time history of a component of the true gust velocity in continuous turbulence at equally spaced time intervals, say 0.05 second. The reading interval ϵ depends on airplane speed and the highest frequency to be evaluated and is given by the relation $\epsilon = \pi/V\Omega_0$, where $\Omega_0 = 0.1$ is representative of the highest spatial frequency of concern in turbulence investigations (see appendix D).

The time history is then analyzed to determine the power spectrum of turbulence. This analysis, as shown in appendix E, consists generally of prewhitening, estimating values of the autocovariance function, obtaining raw estimates of power, smoothing the estimates of the power, and postdarkening these to obtain the final estimates of the power spectrum.

Instrumentation

An airplane is usually used as the platform for transporting the instrumentation for measuring the three components of gust velocity. If all three components are to be evaluated, the instrumentation must furnish measurements to satisfy all the terms in equations (1) to (3). If the term cannot be measured directly, then a quantity is measured from which the desired quantity may be calculated. For example, the vertical acceleration can be integrated to obtain the vertical velocity of the airplane.

The instrumentation used in several flight investigations has provided measurements of dynamic pressure, static pressure, temperature, three components of linear acceleration, three attitudes (pitch, roll, and yaw), three angular rates (pitch velocity, etc.), and the angle of attack and angle of sideslip from flow vanes or differential pressure probes. Care is required to obtain the greatest possible accuracy in the measured quantities and to reduce the time lag between the measured quantities. These factors become increasingly important if low-intensity turbulence is being surveyed or long wavelengths are to be measured. In some cases it may become necessary to use a stable platform to obtain the measurements of the attitudes and attitude rates of the airplane.

In the investigation of high-intensity turbulence the accuracy may not be as critical, since the errors become a smaller proportion of the measured quantities.

The boom should be long enough to place the angle-of-attack and sideslip sensor ahead of the disturbed airflow around the airplane. A practical length of approximately 1.5 fuselage diameters is normally used, which reduces the effect of steady-state upwash to approximately 5 percent. The boom should have a natural frequency above the highest frequency of gust velocity to be evaluated; specifically, the angular frequency should be greater than $V\Omega_0$, where $\Omega_0 \approx 0.1$ as stated earlier. Also, the natural frequency should not be in the same range as the natural frequency of the sensor.

Evaluated Turbulence Spectra

Considerable effort has been expended in the past several years on the development of the techniques of measuring atmospheric turbulence and the application of power spectral techniques to the description of turbulence and to the response studies of aircraft. The early investigations were generally made in the more prevalent turbulence of clear air at low altitudes (below 5,000 feet) and sufficient spectra were obtained to indicate the practical compliance of turbulence in clear air with the properties of a stationary random Gaussian process (ref. 5). These data and additional new spectra for turbulence in cumulus clouds and severe storms are reviewed.

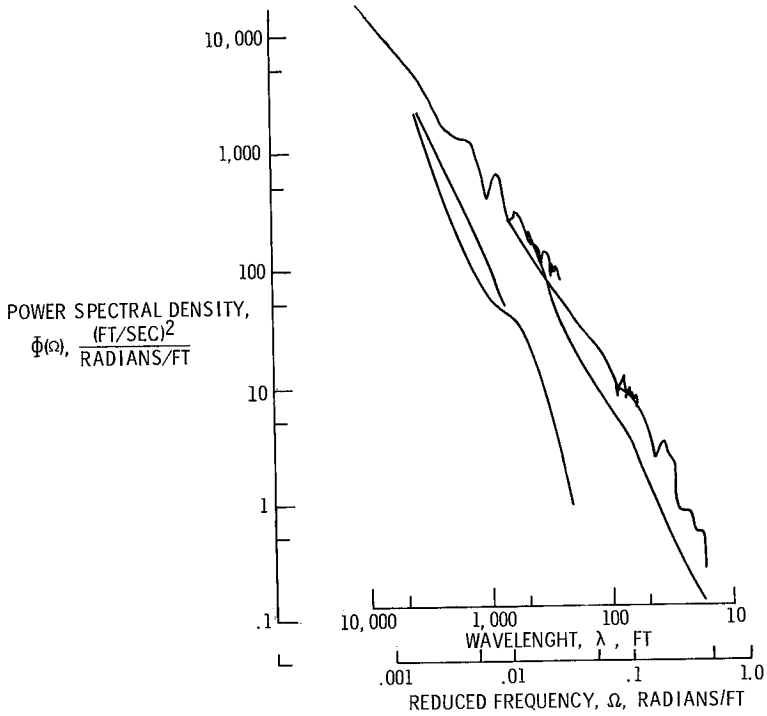

Figure 1.- Power spectra of the vertical components of turbulence in clear air at an altitude of approximately 5,000 feet.

Turbulence in clear air.- Several representative power-spectral-density curves for the vertical components of true gust velocities measured in clear air at an altitude of approximately 5,000 feet are given in figure 1. In this and other figures the power spectral density in $(ft/sec)^2$ per radians/ft is plotted against the reduced frequency in radians/ft with an auxiliary scale of wavelengths in feet. The data cover a range of wavelengths of approximately 10 to 5,000 feet. For this range the spectra show a characteristic rapid decrease in power with increasing frequency, and the rates of power decrease are similar for the various spectra The heights of the spectra are a measure of the intensity of the turbulence; thus, the intensity of the turbulent samples varies over

an appreciable range. More definitely, the root-mean-square gust velocity defined as the square root of the area under the portion of the spectrum evaluated, and herein designated σ_1, is often given as a measure of the intensity of the turbulence. For an average spectrum in figure 1 this truncated rms gust velocity is about 3 ft/sec. The actual rms value σ_w, which is associated with the area under the complete spectra, may be 2 to 2.5 times as large, as will be discussed subsequently.

Other spectra (at least 100) from flights in clear-air turbulence at lower altitudes (200 to 1,000 feet) are given in reference 6. However, the method of evaluation for these spectra differs significantly in certain details from that for the spectra presented herein, and therefore direct comparison is not made.

Turbulence in cumulus clouds.- In 1959 an instrumented F-86 jet airplane was used to measure turbulence in cumulus clouds at altitudes of about 15,000 feet near Langley Field, Virginia. Typical power-spectral-density curves for the vertical, longitudinal, and lateral components of gust velocities measured during two traverses are shown in figure 2.

The w_g, or vertical velocity, spectra are similar to the spectra of clear-air turbulence (fig. 1) with respect to the decrease in power with frequency and the variation in intensity for different traverses. As expected, the intensity of turbulence is greater than for clear air, as indicated by the range of truncated rms values of 3.4 to 9.2 feet per second for nine traverses through cumulus clouds (spectra for seven additional traverses are not shown).

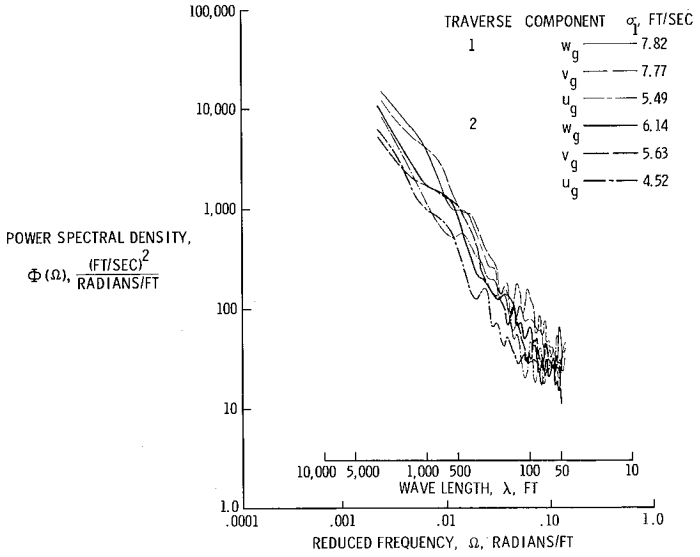

Figure 2.- Spectra of three components of gust velocity in cumulus clouds.

From the theory of isotropic turbulence and use of airplane flight measurements to define the turbulence, the lateral v_g and vertical w_g components should have similar spectra while the longitudinal u_g spectra should be different but similar in shape (appendix B and ref. 5). The longitudinal spectra should be above the lateral or vertical spectra by a factor of 2 in the range near zero frequency and below by a factor of 3/4 at the higher frequencies. Figure 2 roughly substantiates the situation at the higher frequencies.

Turbulence in thunderstorms.- More recently, jet airplanes have been used to obtain measurements in the severe turbulence in thunderstorms to altitudes of 40,000 feet

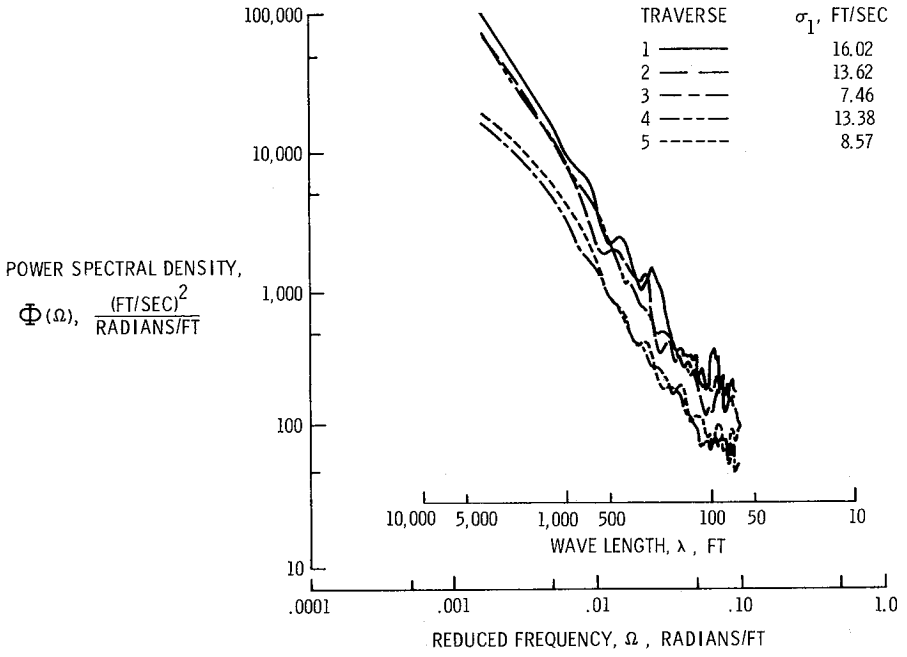

(a) Vertical components.

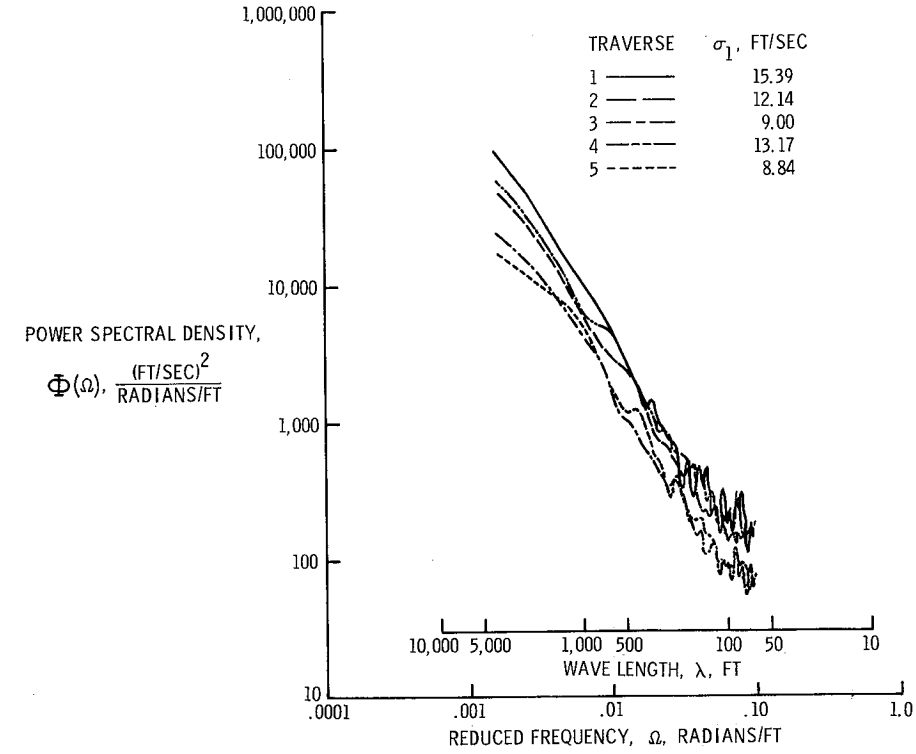

(b) Lateral components.

Figure 3.- Comparison of power spectra of turbulence measured in successive traverses of a thunderstorm at an altitude of approximately 40,000 feet.

over the southwest United States. A T-33 airplane was used in the spring of 1960 and an F-106 airplane flown at low supersonic speeds was used in the spring of 1961. The spectra of the vertical and lateral components of gust velocity are shown in figure 3 for five traverses of the T-33 airplane through one storm at 40,000 feet. (The longitudinal spectra were not obtained because water from the cloud collected in the pitot head in sufficient quantity to dampen the high-frequency airspeed fluctuations.)

A comparison of figures 3(a) and 3(b) indicates that the vertical and lateral components are similar in shape and intensity; this comparison is shown more clearly in figure 3(c). The intensity of the turbulence indicated by the truncated rms gust velocities for some 15 traverses ranged from 6.1 to 16.0 ft/sec.

Comparison of spectra for different weather conditions.- Typical spectra for clear air, cumulus clouds, and thunderstorms are compared in figure 4. These spectra show two general features: The similarity of the slopes of the spectra, and the variation in the intensity of turbulence with weather conditions as indicated by the relative heights of the

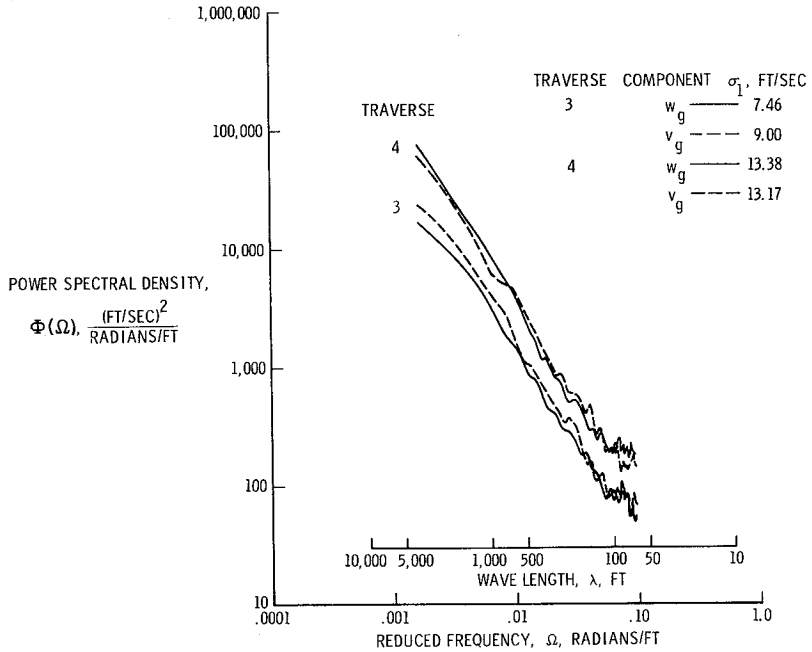

(c) Thunderstorm traverses 3 and 4.

Figure 3.- Concluded.

curves. Many samples for each weather condition would yield overlapping bands of spectra. (See figs. 1 to 3.) Thus, it appears that a composite picture made up from measured spectra for all types of turbulence would cover a continuous band of intensities having associated truncated rms values of turbulence velocities ranging from near zero to as much as 16 ft/sec.

Turbulence Characteristics

The practical compliance of severe atmospheric turbulence with the properties of a stationary random Gaussian process is examined in this section. The property of isotropy has been suggested in figure 2 and will be discussed further in a subsequent section.

Stationarity and homogeneity of severe turbulence.- The properties of stationarity and homogeneity of a random process specify an invariance in the statistical characteristics of turbulence with respect to the position along the time history where the sampling interval is taken, the positioning in the turbulence, and the direction through the turbulence. Inasmuch as the intensity of the turbulence is dependent upon the weather conditions, which are known to change with time, these properties can apply only in a very limited sense. For large-scale patterns of air motion the stationarity and homogeneity conditions might be expected to apply within regions of perhaps 100 miles and time durations of perhaps an hour. In the case of severe turbulence, such as that encountered in thunderstorms, these distances and times would not be expected

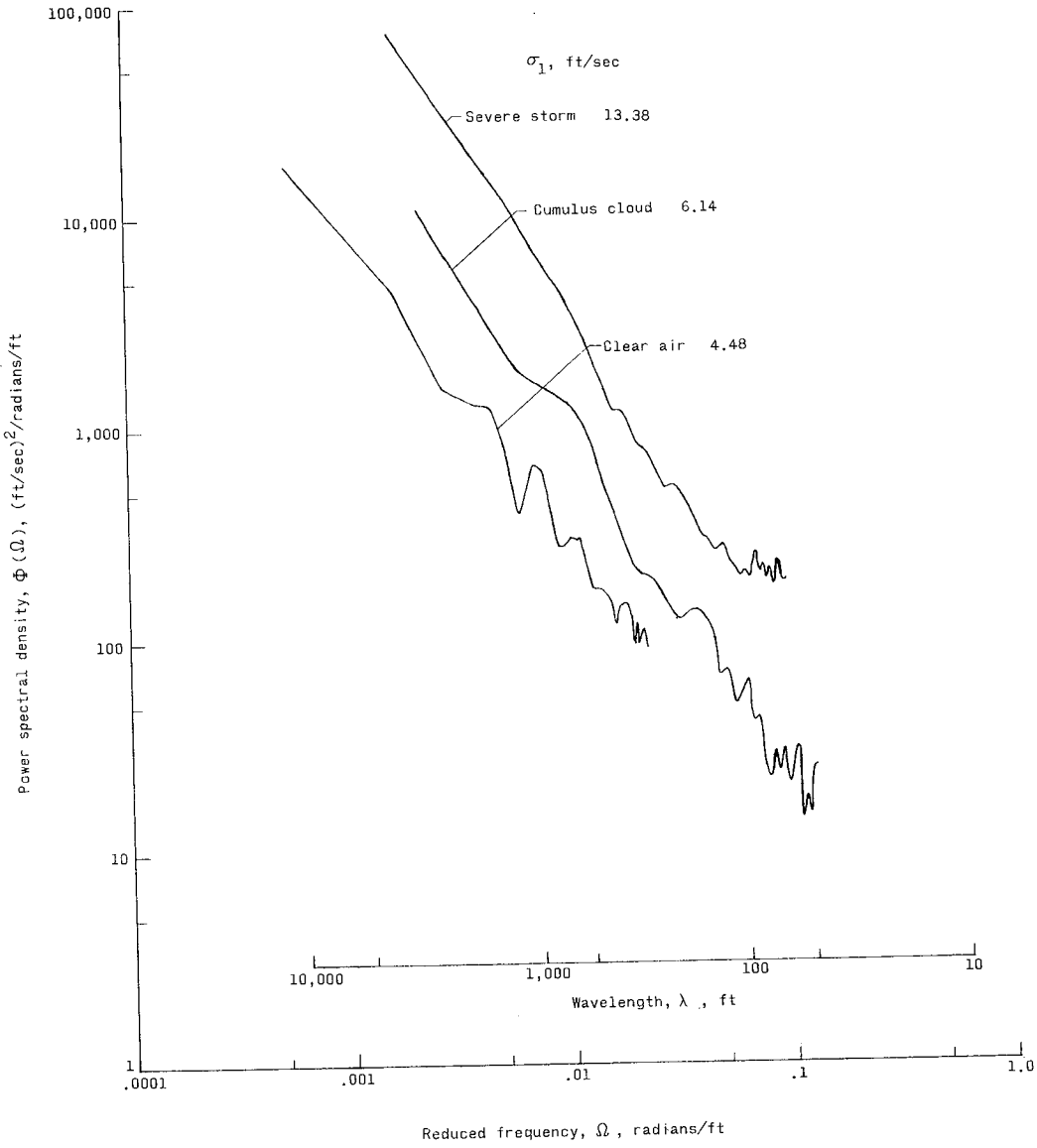

Figure 4.- Typical power spectra of vertical component of turbulence measured in clear air, cumulus cloud, and thunderstorm.

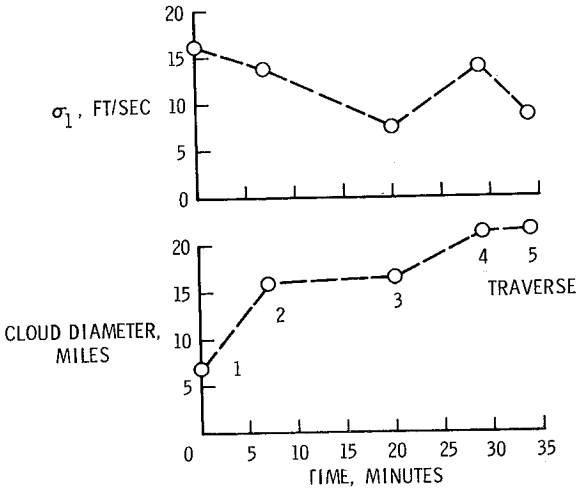

Figure 5.- Variation of turbulence intensity and cloud diameter with time at an altitude of 40,000 feet.

to apply; some available data that have a bearing on these factors are presented.

In figure 5 are given the root-mean-square values of the vertical component of gust velocity and the cloud diameter as determined from five surveys through a storm during an elapsed time of approximately 35 minutes, where all traverses were made at the same altitude. The cloud grew rapidly in size during two periods and it may be noted that the intensity of turbulence varied, having relatively high rms values (14 to 15 ft/sec) during the periods of growth and smaller rms values (9 to 10 ft/sec) during periods of little growth. From these data it appears that the time duration for homogeneous and stationary conditions may be about 5 minutes. Of course, the spatial region for these conditions would be limited to the approximate size of the storm - in this case, about 21 miles.

In figure 6, a comparison is given of the power spectra of vertical gust velocity obtained from the two successive half-sections of traverse 4 through the storm; the spectra for the complete traverse are given in figure 3(a). The individual spectra covered approximately 12 miles, or 100 seconds of time. The two spectra agree in general form, considering that differences in both time and space are involved. Thus, there appears to be some degree of stationarity and homogeneity present even in severe storm turbulence.

Gaussian test of severe turbulence.- For the turbulence to be Gaussian, the fluctuations of the turbulence must have a normal probability distribution. In the past, it has been customary to consider that if a component of the turbulence - the vertical component, for

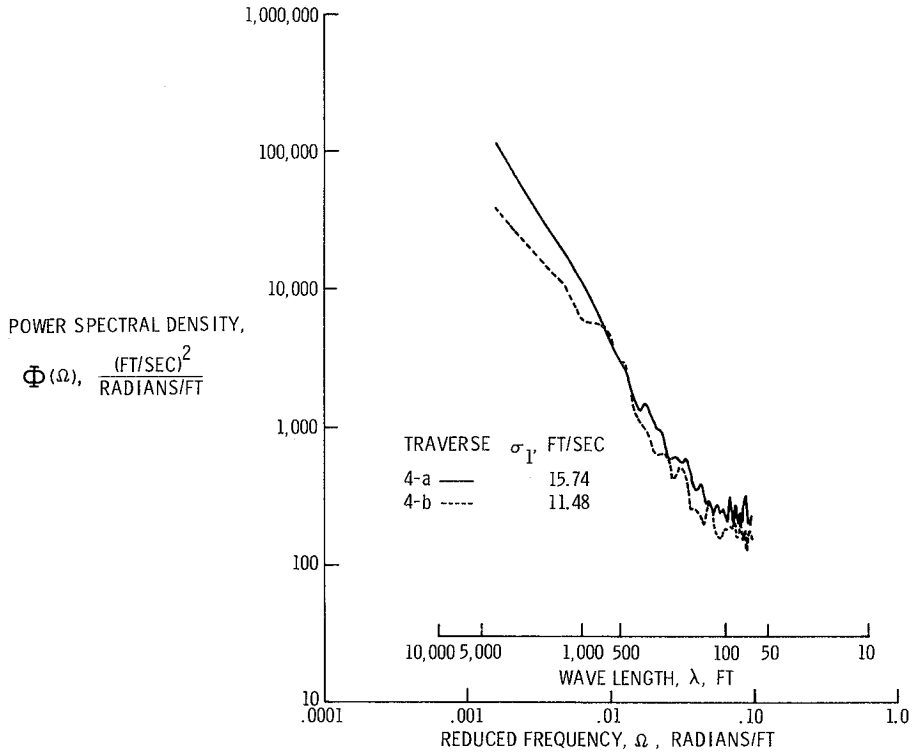

Figure 6.- Comparison of power spectra of vertical component of turbulence for two parts of thunderstorm (traverse 4).

instance - has a normal distribution, then for practical purposes normality of the turbulence is indicated (ignoring higher order Gaussian tests).

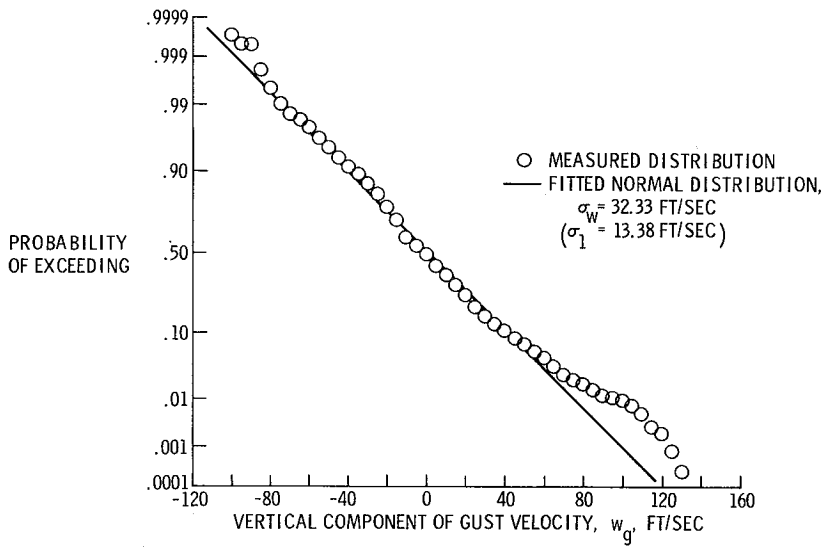

Figure 7.- Probability of equaling or exceeding given values of vertical gust velocity for thunderstorm (traverse 4).

The test for traverse 4 through a thunderstorm is shown in figure 7. The figure presents the cumulative frequency distribution of the vertical component of gust velocity w_g plotted on probability paper. The paper is scaled so as to yield a straight line for a normal distribution. The data shown were obtained from a 200-second traverse read each 1/10 second (a total of 2,000 points). A fitted normal distribution is also shown for comparison with the measured distribution. It can be seen that the fitted curve approximates the measured distribution quite well except at the large positive values. Therefore, for many practical purposes, a Gaussian assumption appears reasonable. (Even the measured distributions for clear-air turbulence depart slightly from a straight line at large values of w_g.)

Spectral Shape and Analytical Representation

Several analytical representations of turbulence spectra have been used in the past in connection with wind-tunnel turbulence studies. (See refs. 7 and 8.) Two of these representations are considered here for application to atmospheric turbulence. One is a representation due to Von Kármán which seems to have been overlooked in recent years; the other is an often-quoted case which was selected for convenience several years ago as being representative of atmospheric turbulence.

Analytical representation.- The autocorrelation and associated spectrum functions that were considered with respect to their appropriateness as analytical representations of atmospheric turbulence are as follows (see appendix B for their development):

Case I (isotropic turbulence),

$$R(r) = \sigma_w^2 \frac{2^{2/3}}{\Gamma\left(\frac{1}{3}\right)}\left(\frac{r}{1.339L}\right)^{1/3}\left[K_{1/3}\left(\frac{r}{1.339L}\right) - \frac{1}{2}\left(\frac{r}{1.339L}\right)K_{2/3}\left(\frac{r}{1.339L}\right)\right] \qquad (5)$$

where the numerical factor $\frac{2^{2/3}}{\Gamma\left(\frac{1}{3}\right)}$ is equal to 0.59253.

$$\Phi_w(\Omega) = \frac{\sigma_w^2 L}{\pi} \frac{1 + \frac{8}{3}(1.339L\Omega)^2}{\left[1 + (1.339L\Omega)^2\right]^{11/6}} \tag{6}$$

Case II (has been used for fitting wind-tunnel turbulence data),

$$R(r) = \sigma_w^2 \left(1 - \frac{r}{2L}\right) e^{-r/L} \tag{7}$$

$$\Phi_w(\Omega) = \frac{\sigma_w^2 L}{\pi} \frac{1 + 3L^2\Omega^2}{\left(1 + \Omega^2 L^2\right)^2} \tag{8}$$

where

σ_w^2 mean-square value of vertical (or lateral) turbulence velocity

L "scale" of the turbulence $L = L_u = 2L_w$ (as shown in appendix B)

r correlation distance $V\tau$, where τ is the time shift on a time-history basis

Ω spatial frequency defined by $2\pi/\lambda$, where λ is the wavelength of a sinusoidal component

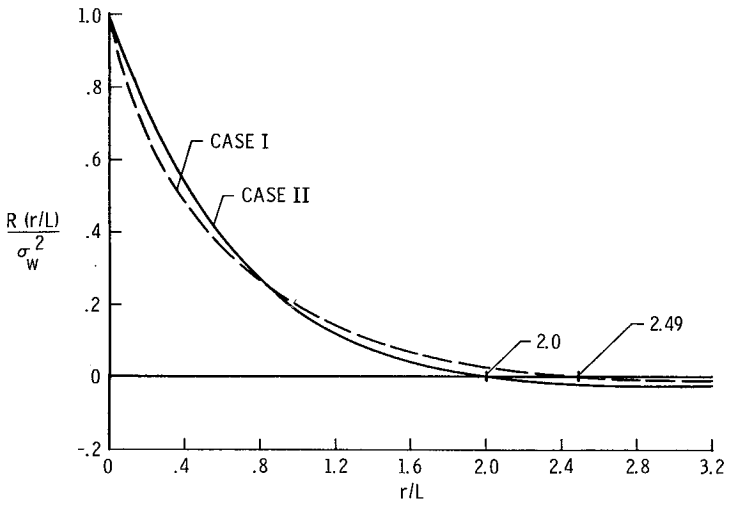

Figure 8.- Analytical autocorrelation functions.

These equations are plotted in figures 8 and 9. It may be noted that for Case I the spectra vary in proportion to $\Omega^{-5/3}$ at the high frequencies, whereas for Case II they vary in proportion to Ω^{-2}. A question of concern is which of these two representations best fits the data. In order to attempt to answer this question, the evaluation of the two parameters σ_w and L must be considered.

Evaluation of rms values.- Two different values of rms are useful, as will be seen. The one

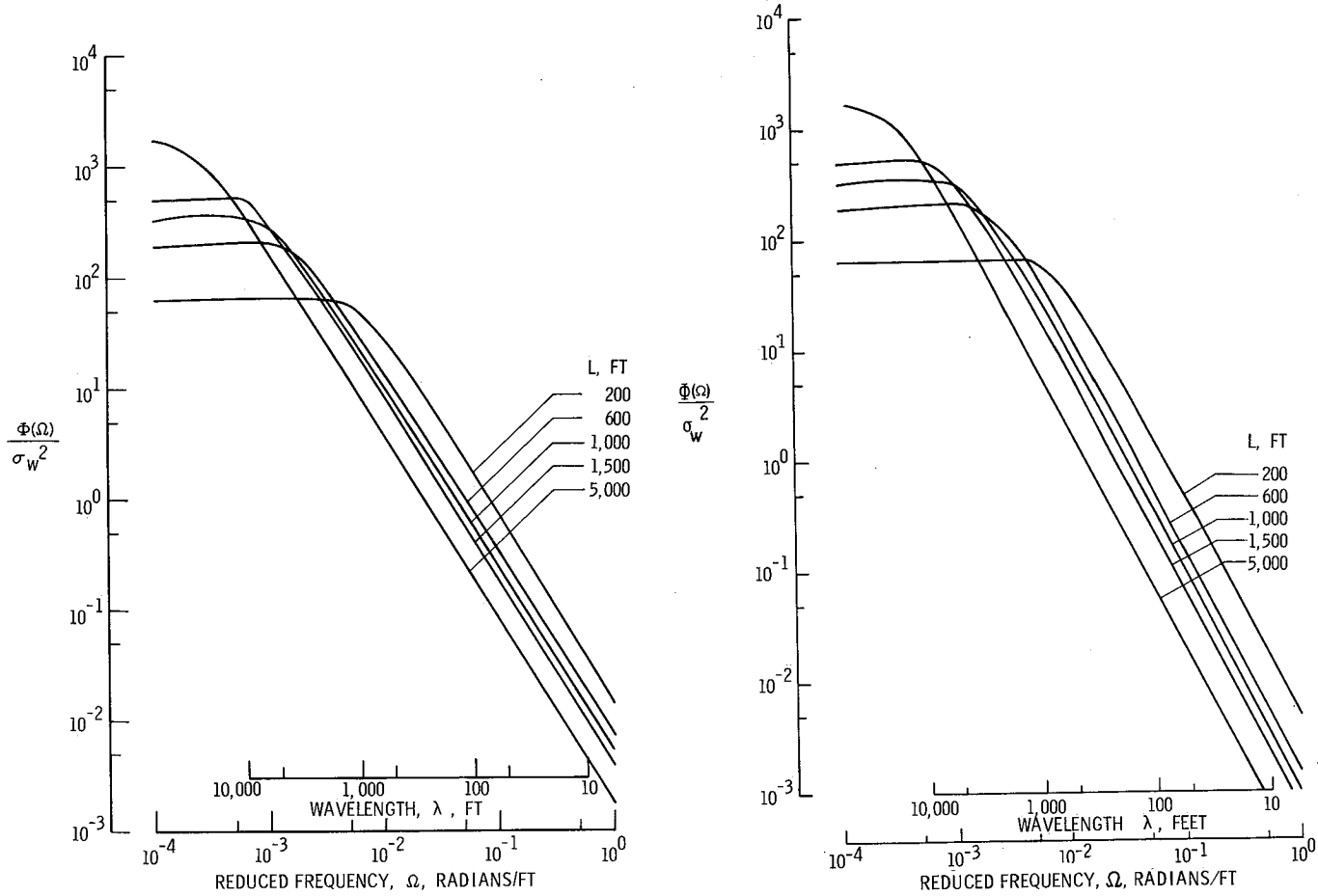

(a) Isotropic turbulence; Case I;

$$\Phi(\Omega) = \frac{\sigma_w^2 L}{\pi} \frac{1 + \frac{8}{3}(1.339L\Omega)^2}{\left[1 + (1.339L\Omega)^2\right]^{11/6}}.$$

(b) Isotropic turbulence; Case II;

$$\Phi(\Omega) = \frac{\sigma_w^2 L}{\pi} \frac{1 + 3L^2\Omega^2}{(1 + \Omega^2 L^2)^2}.$$

Figure 9.- Analytical representation of atmospheric turbulence spectra.

most commonly quoted for atmospheric turbulence, as has been done in the previous section dealing with the description of the turbulence, is σ_1, the square root of the area under the measured spectra; that is, the truncated values obtained as the square root of the area contained between the low- and high-frequency values of the spectral estimates (as obtained by numerical integration).

The other and more significant value is σ_w, the square root of the total area under the complete spectrum (value required in analytical representation); this is given also as the square root of the initial value of the autocovariance function of vertical gust velocity (correlation function associated with vertical velocity record having zero mean). That is,

$$R(0) = \sigma_w^2$$

Evaluation of L.- Several methods associated with the autocorrelation function or with the power spectrum are available for determining the numerical value of L.

From autocorrelation function:

The first method to be considered makes use of the autocorrelation function. It is known that (see, e.g., table I)

$$\Phi(0) = \frac{2}{\pi} \int_0^\infty R(r)dr$$

and for either equation (6) or (8), Case I or Case II, it is also true that

$$\Phi(0) = \frac{\sigma_w^2 L}{\pi}$$

These equations lead automatically to the relation

$$L = 2 \int_0^\infty \frac{R(r)}{R(0)} dr = 2V \int_0^\infty \frac{\tilde{R}(\tau)}{\tilde{R}(0)} d\tau \tag{9}$$

since $\sigma_w^2 = R(0)$ and $r = V\tau$.

It is interesting to note that other analytically exact methods for determining L from the autocorrelation functions are possible and useful; two such methods are mentioned. One involves the location at which the correlation function crosses zero; the other is an alteration of equation (9) involving the area under the normalized correlation function out to a specific value of r instead of to infinity. Specific relations are:

For Case I,

$$L = 0.402r_c \tag{10}$$

$$L = 0.746r_1 = 2 \int_0^{r_1} \frac{R(r)}{R(0)} dr \tag{11}$$

For Case II,

$$L = 0.5r_c \tag{12}$$

$$L = 2 \int_0^L \frac{R(r)}{R(0)} dr \tag{13}$$

where r_c designates the value of r at which the correlation function crosses zero. From a graphical viewpoint r_1 in equation (11) is such that twice the area under the normalized function up to r_1 equals $0.746r_1$, a product which can be shown to equal L, whereas in equation (13), L is such that twice the area under the function up to L equals L. In general, to use equations (10) and (12) the correlation functions, equation (5) or (7), must be fitted to the data, either by a rough visual technique or more accurately by a least-square process, from which r_c then follows. Equations (11) and (13) are to be preferred since they can be applied directly to the correlation data.

From spectrum values:

Evaluation of L may also be made by consideration of the truncated and total rms values and the analytical representations of spectrum shape as follows. Consider the straight-line portion of the spectra shown in figures 9(a) and 9(b); from equations (6) and (8) good approximations to the spectrum in the high-frequency range are for Case I,

$$\Phi_w(\Omega) = 0.521 \frac{\sigma_w^2}{L^{2/3}\Omega^{5/3}} \tag{14}$$

and for Case II,

$$\Phi_w(\Omega) = \frac{3\sigma_w^2}{\pi} \frac{1}{L\Omega^2} \tag{15}$$

Integration of these equations from Ω_1 to Ω_0, the lowest frequency and highest frequency of the measured spectrum, gives the truncated value of mean-square gust velocity for Case I,

$$\sigma_1^2 = 0.782 \frac{\sigma_w^2}{L^{2/3}}\left(\frac{1}{\Omega_1^{2/3}} - \frac{1}{\Omega_0^{2/3}}\right)$$

and for Case II,

$$\sigma_1^2 = \frac{3}{\pi} \frac{\sigma_w^2}{L}\left(\frac{1}{\Omega_1} - \frac{1}{\Omega_0}\right)$$

Solution of these equations for L leads to the following relations which allow a direct calculation of the scale in terms of the two rms values of vertical gust velocity:

Case I,

$$L = 0.692\left(\frac{\sigma_w}{\sigma_1}\right)^3\left(\frac{1}{\Omega_1^{2/3}} - \frac{1}{\Omega_0^{2/3}}\right)^{3/2} \tag{16a}$$

which reduces simply to

$$L = 0.692\left(\frac{\sigma_w}{\sigma_1}\right)^3 \frac{1}{\Omega_1} \tag{16b}$$

when very little power exists beneath the spectrum beyond Ω_0. For Case II,

$$L = \frac{3}{\pi}\left(\frac{\sigma_w}{\sigma_1}\right)^2\left(\frac{1}{\Omega_1} - \frac{1}{\Omega_0}\right) \tag{17a}$$

which reduces simply to

$$L = \frac{3}{\pi}\left(\frac{\sigma_w}{\sigma_1}\right)^2 \frac{1}{\Omega_1} \tag{17b}$$

Equations (16b) and (17b) yield results with errors arbitrarily selected as 5 percent or less as long as $\Omega_1/\Omega_0 < 0.001$ for equation (16b) and $\Omega_1/\Omega_0 < 0.02$ for equation (17b).

The value of L for the vertical gust velocity for traverse 4 through a thunderstorm (see fig. 3(c)) was obtained from these relations. For these data $\sigma_w = 32.33$ ft/sec, and $\sigma_1 = 13.38$ ft/sec for the frequency range of $\Omega_1 = 0.0016$ radian/ft to $\Omega_0 = 0.096$ radian/ft. The values of L are as follows:

	L, feet	
	Case I	Case II
Spectrum:		
With $\Omega_0 = 0.096$ (eqs. (16a) and (17a))	5,550	3,430
With $\Omega_0 = \infty$ (eqs. (16b) and (17b))	6,120	3,490
Autocorrelation: (eqs. (11) and 13))	5,720	4,750

Fitting of spectrum curve.- Values of $\sigma_w = 32.33$ ft/sec and L = 5,600 feet for Case I and L = 3,400 and 4,800 feet for Case II were used to fit the respective spectra to the measured spectra for traverse 4 through a thunderstorm. Spectrum results are shown in figure 10; autocorrelation functions based on the value of L = 5,600 feet for Case I and 3,400 and 4,800 feet for Case II are shown in figure 11. Case I provides an excellent fit of the data for both the autocorrelation function and the spectrum. By comparison Case II does not fit very well and there is a conflict as to what value of L should be used; a value of L = 3,400 feet seems to fit the spectrum data best (and if Case I had not been considered, the fit would probably be judged reasonably good) but does not lead to a good correlation function fit, whereas for L = 4,800 feet the situation is just the reverse.

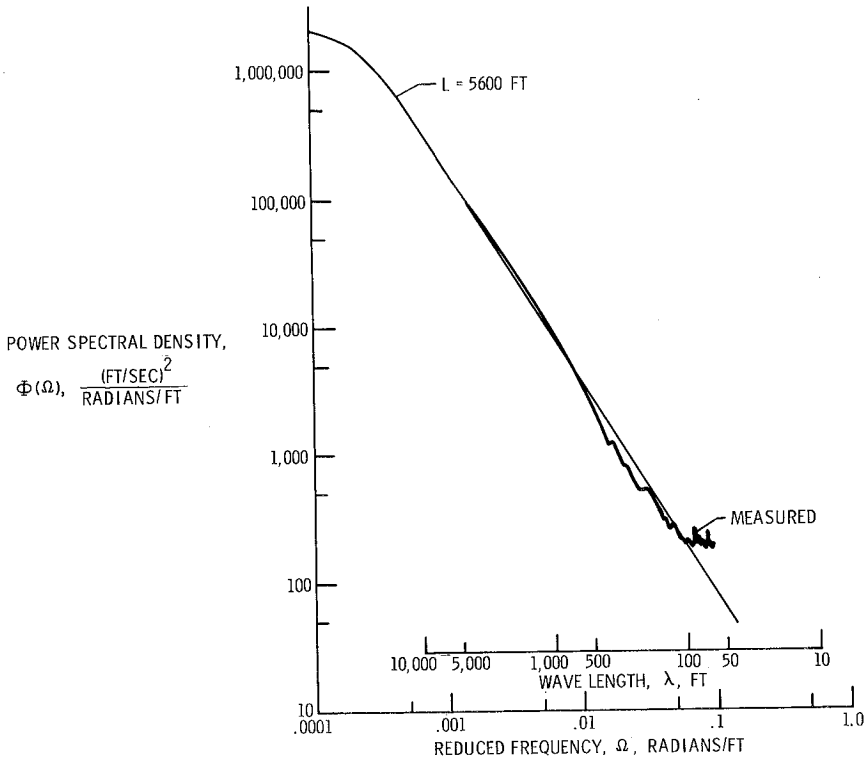

(a) Case I.

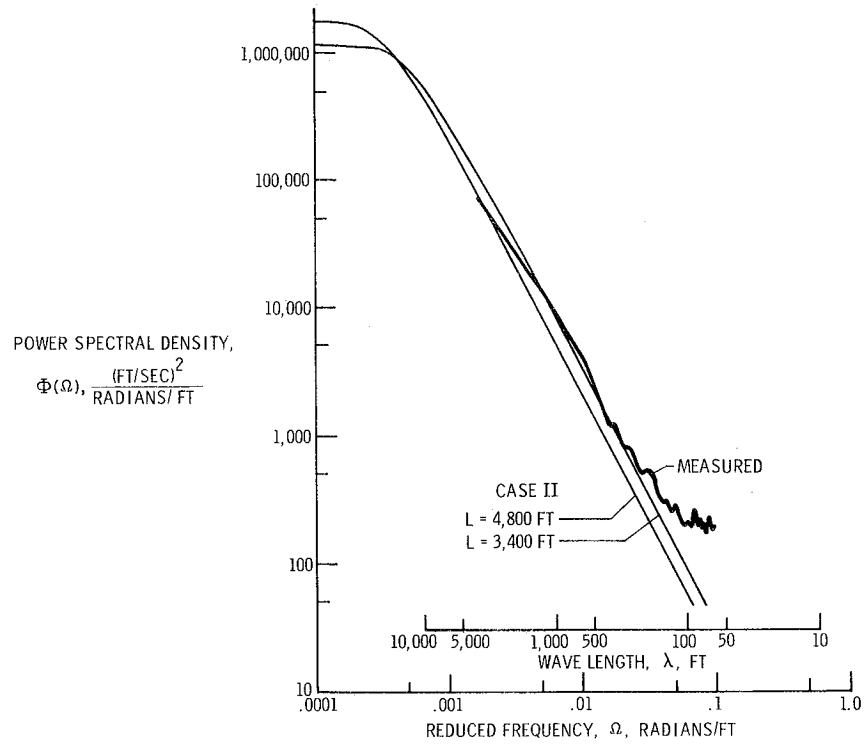

(b) Case II.

Figure 10.- Measured and fitted spectra for thunderstorm.

It is concluded, therefore, that the analytical representation based on the theory of isotropic turbulence (Case I) best fits these data. In addition, it is indicated that L is fairly large, apparently of the order of 5,000 feet.

As additional evidence that the scale is of the order indicated, recourse is made to the spectral data that were obtained from the F-106 tests. For several cases these data extend to frequencies lower than those just presented (down to $\Omega = 0.00045$, or λ up to 14,000 feet), and even so, no flattening of the spectrum was apparent. From figure 9(a) it may be seen that the scale must be large to fulfill this condition of no flattening. Similarly, the spectrum of clear-air turbulence given in reference 9 did not indicate a flattening of the spectrum at a frequency of $\Omega = 0.0005$. Again, the scale must be large to fulfill this condition of no flattening.

A reexamination was made of some clear-air turbulence data (ref. 4) by the procedures outlined herein (eqs. (9) to (13) and (16a) to (17b)), where the appropriate numerical values were available. These data yielded values of L

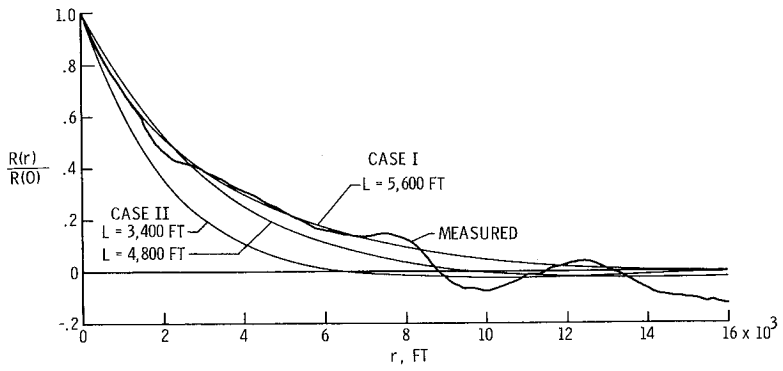

Figure 11.- Measured and fitted autocorrelation functions.

of approximately 3,000 to 6,000 feet for the different runs and methods of evaluation.

A simple means of fitting the analytical representation to the measured spectrum for the higher frequencies is derivable; L from equations (16b) and (17b) is substituted into equations (14) and (15), respectively, to yield for Case I,

$$\Phi(\Omega_1) = \frac{2}{3}\frac{\sigma_1^2}{\Omega_1} \qquad (18)$$

and for Case II,

$$\Phi(\Omega_1) = \frac{\sigma_1^2}{\Omega_1} \qquad (19)$$

Thus, a spectrum curve is easily fitted by evaluating $\Phi(\Omega_1)$ from equation (18) and then passing a $\Omega^{-5/3}$ line through the point $\left(\Omega=\Omega_1,\ \Phi=\Phi(\Omega_1)\right)$. For equation (19) a Ω^{-2} line is used.

Statistical description of atmospheric turbulence.- Although the foregoing material implies that the spectral shape of the atmospheric turbulence is similar for wide ranges of weather conditions, for application of this information additional statistical parameters must be known, such as the probability of occurrence of turbulence of various intensities. Recourse has been made to the large mass of airplane response data collected over many years during routine airline operations to provide information of this type on the description of the atmosphere. References 10 to 12 are examples of such studies. Since such results are of interest from a loads prediction standpoint, they are discussed subsequently in the section entitled "Prediction of Gusts Based on Spectral Techniques."

RESPONSE OF AIRPLANES TO RANDOM ATMOSPHERIC TURBULENCE

In this section the dynamic response of the aircraft structure to atmospheric turbulence is considered. Basic in this consideration is the input-output relation which relates the input and output power spectra through the frequency-response function for the response quantity under consideration, such as acceleration or wing bending strain (see appendix D and table II). The frequency-response function, which is defined as the response due to a unit sinusoidal gust of varying frequencies, is thus the mechanism by which the various degrees of freedom of the airplane become reflected in the output response. In general, the desire is to use the power spectrum of input and the

frequency-response function to establish the power spectrum of the output; from this power spectrum statistical properties of the output time history are then deduced without actually evaluating the time history.

On the other hand, it is sometimes desired to measure the input and output spectra and to deduce the frequency-response function so as to assess the degree of complexity to which the airplane structure must be represented to make response calculations.

The basic spectral relations, the frequency responses, the associated equations of motion, and results of frequency-response calculations are presented in this section together with comparisons with flight-test results.

Basic Relations

The basic relations between the spectra of atmospheric turbulence and the spectra of airplane responses such as motions, deformations, and loads are as follows (see ref. 13):

General relation.-

$$\Phi_y = \Phi_{11}H_1\overline{H}_1 + \Phi_{22}H_2\overline{H}_2 + \Phi_{33}H_3\overline{H}_3 + \cdots + 2\mathrm{Re}\left(\Phi_{12}\overline{H}_1H_2 + \Phi_{13}\overline{H}_1H_3 + \cdots + \Phi_{23}\overline{H}_2H_3 + \cdots\right) \tag{20}$$

where

$\Phi_y = \Phi_y(\omega)$ power spectrum of airplane response quantity y

$\Phi_{ij} = \Phi_{ij}(\omega)$ cross spectrum of turbulence velocities at center of the ith and jth segmented areas of the airplane

$H_i = H_i(\omega)$ frequency-response function of y due to a unit sinusoidal gust velocity over the segment of the surface associated with the ith point

$\overline{H}_i = \overline{H}_i(\omega)$ complex conjugate of H_i or $\overline{H}_i(\omega) = H_i(-\omega)$

Re denotes the real part

The preceding equation is general within linear theory; for airplane response applications it reduces to a simpler form, depending on whether the assumed turbulence model is two-dimensional (nonuniform gust variation across the span) or one-dimensional (uniform gust velocities spanwise).

Relations for two-dimensional isotropic turbulence.- Earlier results, as well as the results presented in the preceding section, indicate that atmospheric turbulence may be considered to be locally isotropic. For this situation the following spectral relations apply:

$$\Phi_{11} = \Phi_{22} = \Phi_{33} = \cdots = \Phi_{nn}$$

$$\Phi_{12} = \Phi_{23} = \Phi_{34} = \cdots = \Phi_{n,n+1}$$

$$\Phi_{13} = \Phi_{24} = \Phi_{35} = \cdots = \Phi_{n,n+2}$$

and so on. Correlation of turbulence velocities for this case is independent of orientation and depends only on the distance between points.

With these relations, equation (20) becomes

$$\Phi_y = \Phi_{11}\left\{H_1\overline{H}_1 + H_2\overline{H}_2 + \cdots + 2\mathrm{Re}\left[\frac{\Phi_{12}}{\Phi_{11}}\left(\overline{H}_1H_2 + \overline{H}_2H_3 + \cdots\right)\right.\right.$$

$$\left.\left. + \frac{\Phi_{13}}{\Phi_{11}}\left(\overline{H}_1H_3 + \overline{H}_2H_4 + \cdots\right) + \cdots + \frac{\Phi_{1n}}{\Phi_{11}}\left(\overline{H}_1H_n + \overline{H}_2H_{n+1} + \cdots\right)\right]\right\} \qquad (21)$$

Relations for one-dimensional isotropic turbulence.- When the scale of the turbulence is large, as results indicate it to be for atmospheric turbulence, some of the more significant airplane loads problems can be treated in an even simpler manner by considering that the turbulence velocities vary randomly in the direction of flight but are uniform along the span; for this model,

$$\Phi_w = \Phi_{11} = \Phi_{12} = \Phi_{13} = \cdots \Phi_{1n}$$

where Φ_w denotes the power spectrum of the vertical gust velocities. Substitution of these relations into equation (21) leads to the significant input-output relation

$$\Phi_y(\omega) = \Phi_w(\omega)\left|H(\omega)\right|^2 \qquad (22)$$

where

$$H = H_1 + H_2 + \cdots + H_n \qquad (23)$$

Alternate equations based on the same model (ref. 13), involving cross spectra, are

$$\Phi_{wy}(\omega) = H(\omega)\Phi_w(\omega) \qquad (24)$$

or

$$\Phi_y(\omega) = H(\omega)\Phi_{yw}(\omega) \qquad (25)$$

where Φ_{wy} is the cross spectrum between the one-dimensional turbulence w and the response y, and $\Phi_{yw}(\omega) = \Phi_{wy}(-\omega)$. Additional information concerning these relations is given in appendix D.

Equation (22) provides a direct relation between the turbulence and the response spectra in terms of the square of the amplitude of the frequency-response function; phase information is not involved. Equations (24) and (25), on the other hand, retain phase information. This fact is particularly useful for determination of complete frequency-response functions from experimental data.

Frequency-Response Functions

In a general sense, the frequency-response functions which appear in the preceding equations would include the effects of all components of the airplane motion - all rigid-body motions and structural deformation. For practical response calculations, however, it is customary to treat the longitudinal and lateral motions separately (at least for conventional airplane configurations). Sinusoidal gust velocities are applied to the aerodynamic surfaces appropriate to the mode of motion being considered; that is, the wing and horizontal-tail surfaces for longitudinal motion and the wing and vertical-tail surfaces for lateral motion.

Usually, the most significant loads due to turbulence arise from the response in the longitudinal modes of motion. Therefore, more attention is given to this motion in the following discussion. The equations of motion employed are those which follow from a linearized treatment involving small perturbations about an otherwise steady flight. The treatment assumes a one-dimensional vertical-velocity turbulence field; that is, the velocities are uniform in the spanwise direction. (See refs. 13 and 14 for two-dimensional turbulence application that would be required if the scale of turbulence is small.) Degrees of freedom of the airplane include pitch, vertical motions, and those representing flexible-body deformations.

Generally, the equations of motion are conveniently formulated either by a modal approach involving the use of Lagrange's dynamical equation or by a lumped-parameter method which is based on structural influence functions. For an airplane which can be considered rigid, classical dynamic-stability equations with gust forces added are also suitable. In the modal approach the elastic deformations are described by a series of modal functions, usually but not necessarily possessing orthogonal properties. The lumped-parameter method generally involves a relatively large number of degrees of freedom compared with the modal approach.

The modal approach is reviewed briefly here. Let the motion of the airplane be expressed by the equation

$$z(x,y,t) = a_1(t)z_1(x,y) + a_2(t)z_2(x,y) + a_3(t)z_3(x,y) + \ldots \qquad (26)$$

or $$z(x,y,t) = \sum_{i=1}^{n} a_i(t) z_i(x,y)$$

where $i = 1, 2, 3, \ldots n$ and where the a_i's are generalized coordinates and the z_i's are modal shapes including rigid-body modes; for example, $z_1 = 1$ and $z_2 = x$ represent the rigid modes, while z_3, z_4, . . . z_n are the mode shapes of the flexible modes. When the flexible modes are chosen to be the natural modes of vibration of the free-free airplane, the Lagrangian formulation yields the following equations of motion:

$$M_i \ddot{a}_i + \omega_i^2 M_i a_i = Q_i \quad (i = 1, 2, 3, \ldots n) \quad (27)$$

where

$M_i = \int z_i^2 dm$ generalized mass where dm is differential mass

ω_i natural frequency of the ith mode

$Q_i = \iint p(x,y) z_i(x,y) dx\, dy$ generalized force in which p is the aerodynamic pressure acting on the airframe due to motion and impressed gust velocities

For sinusoidal motions, let

$$z = z_0 e^{i\omega t}$$

$$a_i = a_{i,0} e^{i\omega t}$$

$$Q_i = Q_{i,0} e^{i\omega t}$$

$$p = p_0 e^{i\omega t}$$

Equations (26) and (27) then yield

$$z_0 = a_{1,0} z_1 + a_{2,0} z_2 + a_{3,0} z_3 + \ldots \quad (28)$$

$$M_i \left(\omega_i^2 - \omega^2\right) a_{i,0} = Q_{i,0}$$

$$= \iint p_0(x,y) z_i(x,y) dx\, dy \qquad (i = 1, 2, 3, \ldots n) \quad (29)$$

Aerodynamic forces.- The generalized aerodynamic forces $Q_{i,0}$ may be calculated from the nonsteady surface pressures p_0 as obtained by several methods such as a strip theory, quasi-steady or nonsteady lifting-line or surface theory. These methods differ in complexity and the choice will depend on the particular application. In the nonsteady lifting-surface theory, one of the most advanced methods, the pressure p_0 is related to the downwash on the aerodynamic surfaces by the following linear equation:

$$w_0(x,y,k) = \frac{V}{8\pi q} \iint p_0(x,y,k)K(x-\xi,y-\eta;k,M)d\xi\ d\eta \tag{30}$$

where sinusoidal motion is implied and

w_0 local downwash

V airspeed

q dynamic pressure

K kernel of integral equation which denotes downwash at a field point (x,y) due to a unit pressure dipole at a point (ξ,η)

$k = \frac{\omega c_r}{2V}$, in which c_r is the root chord

M free-stream Mach number

The kernel K and numerical methods of solving equation (30) for p_0 for given values of w_0 have been developed at the NASA Langley Research Center for both subsonic and supersonic Mach numbers (subsonic leading edges). (See refs. 15 to 17.) The numerical methods may be applied to wings of arbitrary planform and are, therefore, particularly suitable for swept or delta wings. These methods have been programed on high-speed digital computers for known values of w_0 at as many as 16 positions on a wing semispan. Rapid solutions are obtained for downwashes due to both sinusoidal motion and sinusoidal gust velocities on a consistent basis.

The applied downwash w_0 may be written (with sinusoidal term suppressed) as

$$w_0 = \left(V\frac{\partial}{\partial x} + i\omega\right)z_0 + w_{g,0}e^{-i\omega\frac{x_c}{V}} \tag{31}$$

$$w_0 = \left(V\frac{\partial}{\partial x} + i2\frac{Vk}{c_r}\right)z_0 + w_{g,0}e^{-i2\frac{x_c k}{c_r}} \tag{32}$$

where $w_{g,0}$ is the magnitude of the sinusoidal gust velocity and x_c is the location of the downwash point relative to a convenient reference point, say the leading edge of the root chord of the lifting surface.

To determine p_0, equation (32) is substituted into equation (30) with z_0 replaced by its definition, equation (28). The resulting equation is then solved by numerical procedure and leads to an expression for p_0 given by

$$p_0 = a_{1,0}p_1 + a_{2,0}p_2 + \cdots + a_{n,0}p_n + w_{g,0}p_g \tag{33}$$

where the p_i's are the pressure or loading distributions associated with the shapes of z_i, and p_g is the pressure distribution due to the gust velocity $w_{g,0}$. In general, these pressure distributions are complex; that is, they have a component that is in phase with the sinusoidal motion and a component 90^o out of phase.

Solution for frequency-response functions.- The substitution of equation (33) into equations (29) gives simultaneous equations which are solved for the complex generalized coordinates $a_{1,0}$, $a_{2,0}$, ... Solutions are made at various frequencies and hence the results are the frequency-response functions for these coordinates, which represent, of course, the modal displacement coefficients. From the solution for the $a_{i,0}$'s the frequency-response functions for other response quantities, such as bending moment or shear, can be determined (the H in eqs. (22) to (25)). With the bending moment at a particular station as an example,

$$H(\omega) = \bar{M}_0(\omega) = a_{1,0}(\omega)\bar{M}_1 + a_{2,0}\bar{M}_2 + \cdots + a_{n,0}\bar{M}_n + w_{g,0}\bar{M}_g \tag{34}$$

where $\bar{M}_0(\omega)$ is the bending-moment frequency-response function. This equation may be established by two basic means, as will be outlined briefly. One is the so-called loads-summation approach, and the other, a mode-displacement procedure.

In the loads-summation approach the total loading on the structure, consisting of the inertia and aerodynamic loading, is used. Thus,

$$p_{t,0} = m\omega^2 z_0 + p_0 \tag{35}$$

Integration of this loading to obtain bending moments leads directly to equation (34).

In the mode-displacement procedure the moment is considered to be the superposition of the moments due to the flexible modes only. In this case, equation (34) becomes

$$\bar{M}_0 = a_{3,0}\bar{M}_3 + a_{4,0}\bar{M}_4 + \cdots + a_{n,0}\bar{M}_n \tag{36}$$

where the $\bar{M}_i$'s are here the moments associated with the deflection shape z_i. For example, for a wing treated as a beam $\bar{M}_i = EI \frac{\partial^2 z_i}{\partial x^2}$.

The choice of procedure for the determination of $\bar{M}_i$ depends upon the purpose. The loads-summation method provides better accuracy for a given number of flexible modes than does the mode-displacement method. The effort, however, is considerably greater.

Lateral motion.- Significant motions and localized loads (vertical-tail loads, for example) are generated by the response of the lateral modes of motion to lateral turbulence velocities acting on the vertical tail and to vertical velocities acting on the wing (see ref. 18). The lateral velocities can be approximated by the one-dimensional turbulence described by equation (22) or (24). For the vertical velocities, however, a two-dimensional turbulence expression of the type given by equation (21) must be used in order to take into account the influence of these velocities on the rolling moment. The frequency-response functions are approximated usually in terms of solutions of appropriate linear equations of airplane motion for flight at constant speed and at a given altitude through sinusoidal gust velocities acting on the vertical tail surface and on a number of sections along the span of the wing. The derivation follows generally along the same lines as those for the longitudinal equations and is described in reference 18.

Experimental Frequency-Response Functions

As indicated, the response spectra due to turbulence encounter may be calculated from equations (22), (24), or (25). It is frequently desired, however, to determine the airplane frequency-response functions from measured turbulence and response spectra for the purpose of comparison with calculated frequency-response functions. A major reason for determining the response functions experimentally is to assess the degree of complexity required to simulate analytically the dynamics of the airplane.

The solution for frequency response for longitudinal motion may be obtained from equation (22) as

$$\left|H_s(\omega)\right|^2 = \frac{\Phi_y(\omega)}{\Phi_w(\omega)} \tag{37}$$

or from equation (24) as

$$H_c(\omega) = \frac{\Phi_{wy}(\omega)}{\Phi_w(\omega)} \tag{38}$$

or from equation (25) as

$$H_c(\omega) = \frac{\Phi_y(\omega)}{\Phi_{yw}(\omega)} \tag{39}$$

Some information is given in appendix D on the practical aspects and interpretation of these methods.

The evaluation of frequency-response functions for lateral modes of motion requires more experimental information than that for the longitudinal short-period mode. As indicated in equation (21), not only must measurements be made which will provide the basic turbulence spectrum Φ_w, but additional measurements must also be made along the wing span to provide data from which the various cross spectra can be evaluated. As far as is known, no frequency-response functions for complete lateral motion involving coupling between yaw and roll have been obtained from experimental data.

The application of equations (37) and (38) to some longitudinal mode cases is given in the next section.

Comparison of Experimental and Calculated Frequency-Response Functions

The NASA has conducted flight tests and has made turbulence response calculations for two widely different airplane configurations: one a large flexible swept-wing subsonic airplane representative of turbojet bombers and transports; the other a delta-wing supersonic fighter airplane. Both experimental and calculated frequency-response functions are presented for these airplanes, together with a brief description of the degree of complexity of the mathematical model which formed the basis for the calculated functions.

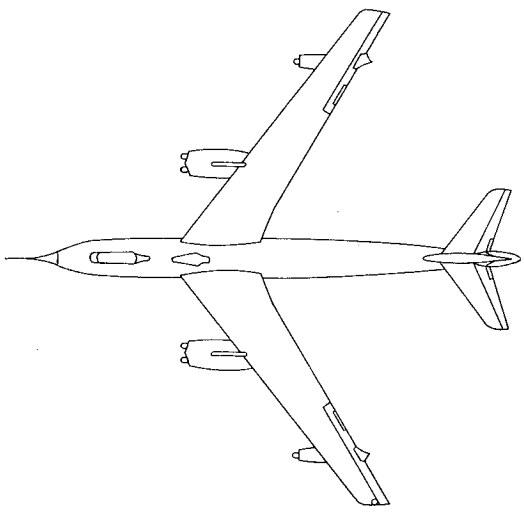

Figure 12.- Flexible swept-wing airplane.

Large flexible swept-wing airplane.- This airplane is illustrated in figure 12. The flight test was conducted at a Mach number of 0.581 at an altitude of 5,000 feet in clear-air turbulence. Calculated frequency-response functions were based on (1) rigid-body vertical translation, (2) rigid-body pitching motion, (3) first cantilever wing bending mode, (4) first cantilever wing torsion mode, and (5) the first vertical bending mode of the fuselage as a cantilever beam aft of the center of gravity. The method and complete results of the frequency-response-function calculations are given in reference 19.

Calculated results which emphasize the influence of various degrees of freedom are

shown in figure 13. Figure 13(a) applies to vertical acceleration of the center of gravity (the movement of the point on the structure which corresponds to the center-of-gravity location of the undeformed airplane, not the dynamical center-of-gravity location of the deformed airplane); figure 13(b) applies to wing bending strain at the 60-percent-semispan station. The quasi-static

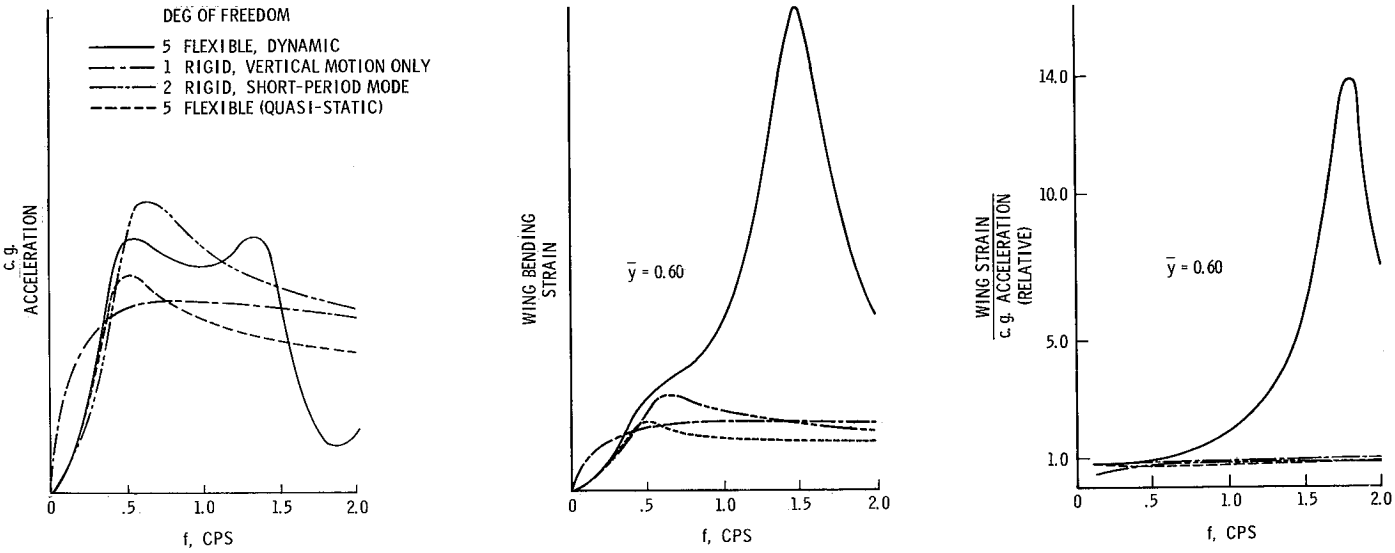

(a) Center-of-gravity acceleration.

(b) Wing bending strain at 60-percent semispan.

(c) Ratio of wing strain to center-of-gravity acceleration.

Figure 13.- Effects of various degrees of freedom on frequency-response functions for large swept-wing airplane.

condition referred to in the figure differs from the dynamic condition in that only the static-type aeroelastic deformations of the flexible structure are considered; the other conditions are as indicated. Although not shown specifically in the figure, calculations indicated that the contributions of wing torsion and fuselage bending were negligible for the frequency range considered.

It is apparent from figure 13 that, in addition to vertical motion, both pitching motion and dynamic wing deflections are important to the responses, particularly the bending strain. It is also apparent that there is no proportional relationship between center-of-gravity acceleration and wing bending-strain frequency responses for the flexible dynamic case, as has often been tacitly assumed in gust-loads studies of nearly rigid airplanes. To illustrate, division of the bending-strain response curves by the corresponding acceleration curve (fig. 13(c)) reveals that for rigid-body vertical motion only, for rigid-body short-period motion, and for the quasi-static condition, the ratio is indeed nearly independent of frequency; this ratio for the fully dynamic case, however, increases from about 1 at the short-period frequency ($f_{sp} \approx 0.5$ cps) to about 14 in the vicinity of the first natural frequency of the wing (indicating an amplification or overshoot on the order of 1,000 percent). Because of the drop of the input spectrum with frequency, this amplification effect becomes reduced in the output spectrum, but it is still important and yields a 50-percent amplification on the basis of a root-mean-square value

comparison between the quasi-static and the fully dynamic conditions.

Example comparisons between experimental and calculated results for the fully dynamic case are shown in figures 14 and 15. The experimental frequency-response functions were obtained by the cross-spectra relation of equation (38). The method and complete results are described in references 4 and 20. Figure 14 gives frequency-response functions for center-of-gravity acceleration and figure 15 gives functions for bending strain at several

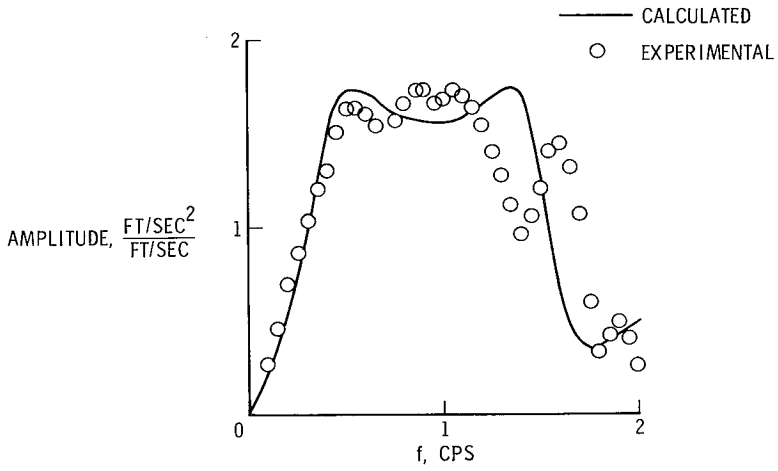

Figure 14.- Calculated and experimental center-of-gravity vertical-acceleration frequency responses for large swept-wing airplane.

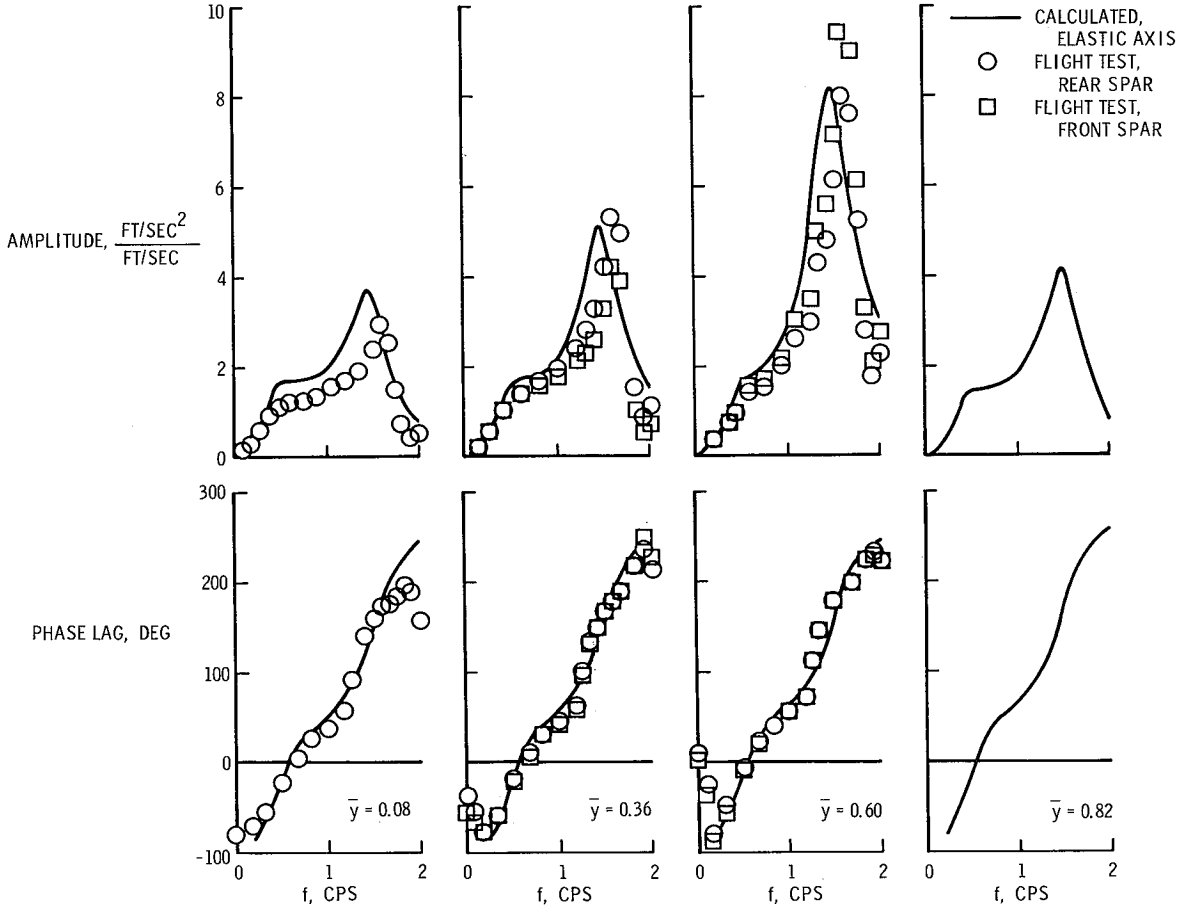

Figure 15.- Calculated and experimental bending-strain frequency responses for large swept-wing airplane.

stations on the wing semispan, where $\bar{y}$ is station location in fractions of a semispan. The dimensions of the ordinates in figure 15 are those for acceleration because the responses of the strain gages were calibrated in terms of the strain per unit normal acceleration experienced during a shallow pull-up maneuver. The agreement is good, considering the overall complexity of the problem. The experimental and calculated frequency-response functions for the wing displacements exhibited even better agreement than those presented here. It is to be noted that the number of modes used here appears quite adequate to determine the frequency-response function in this particular case, but is not necessarily sufficient for extended load studies where, for example, peak count is involved.

Delta-wing fighter airplane.- The delta-wing fighter airplane illustrated in figure 16 is equipped with an automatic pitch damper. Flights were made through thunderstorms under the following conditions:

Condition	Mach number	Altitude, ft
I	1.3	30,000
II	.92	35,000
III	.85	15,000

Experimental frequency-response functions were obtained by the spectra relation of equation (37); consequently, only the amplitude of the transfer functions could be evaluated. Because of the compact and rigid nature of the airplane, calculated frequency-response functions were based on rigid-body vertical translation and pitching motion only. The equations of motion differed in form from those previously described herein in that: (a) they were derived from the classical stability equations (described in ref. 21); (b) aerodynamic forces due to airplane motion were assumed quasi-steady and were calculated by using the manufacturer's design values of the stability derivatives; gust forces, however, were calculated by the numerical procedure which makes use of equation (30); and (c) the effect of the pitch damper was accounted for in terms of an effective pitch-damping stability derivative.

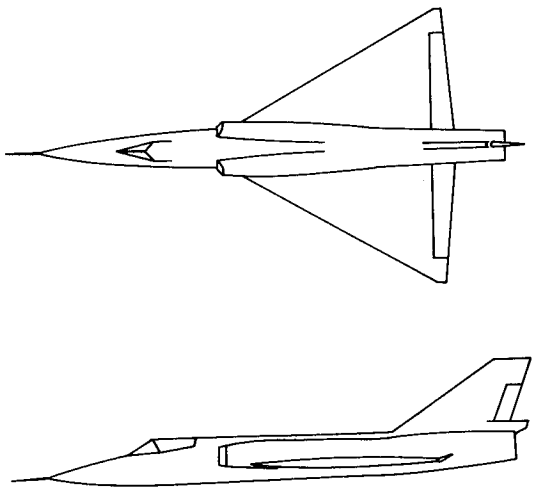

Figure 16.- Delta-wing fighter airplane.

Some examples of experimental and calculated frequency-response functions for acceleration at the center of gravity and for pitching velocity for both supersonic and subsonic speeds are presented in figure 17. Calculated results are given for pitch damper both on and off. The reason for considering both of these conditions is as follows: Examination of the flight records indicated that the damper saturated during the flights; that is, elevon deflections in excess of the mechanical limits were commanded by pitch rate but were not

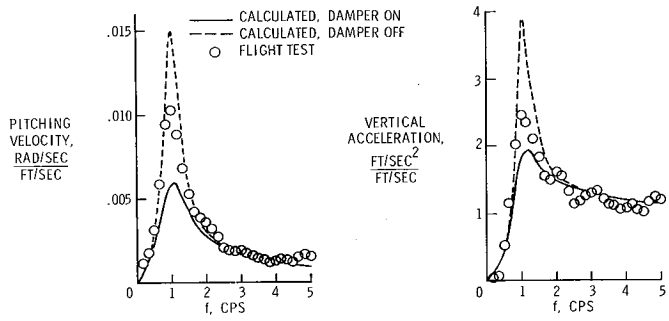

(a) M = 1.3; altitude = 30,000 feet; flight 1.

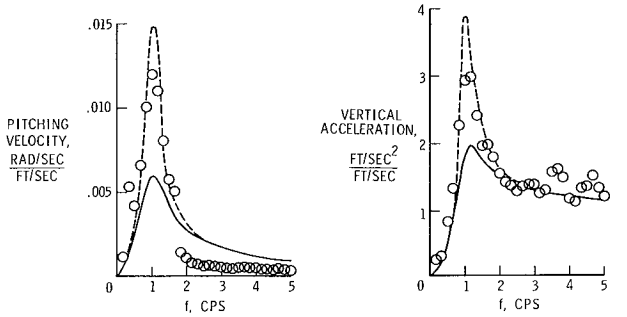

(b) M = 1.3; altitude = 30,000 feet; flight 2.

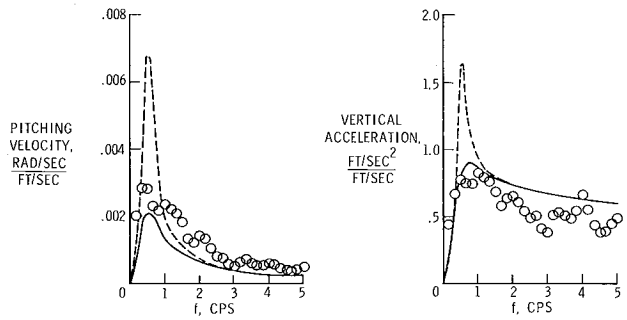

(c) M = 0.92; altitude = 35,000 feet.

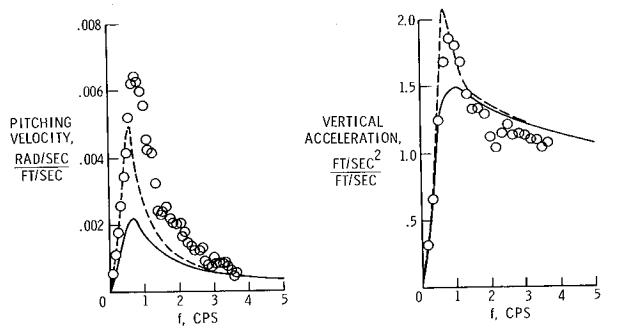

(d) M = 0.85; altitude = 15,000 feet.

Figure 17.- Frequency responses for delta-wing fighter airplane.

realized. The effective damping, therefore, lies somewhere between the values for an inoperative and a fully effective automatic damper. Inasmuch as linearized equations were used to calculate the frequency-response functions, the effective damping could not be calculated.

The experimental and calculated functions for the supersonic-flight conditions (figs. 17(a) and (b)) agree well; the agreement is good at the high and low frequencies, the frequency at which the curves peak agrees well, and at this frequency the experimental results fall between the two calculated damping conditions, thereby indicating as good an agreement as can be expected. The functions for the subsonic flights shown in figures 17(c) and (d) are not as well correlated. The precise reason for the poorer agreement is not known, but there are indications that the stability margins of the airplane were appreciably larger than the calculated values, and this would give a difference in the results of the type noted.

PREDICTION AND DESIGN FOR GUSTS BASED ON SPECTRAL TECHNIQUES

As mentioned in the section entitled "Evolution of Gust Design," the design of aircraft for gusts in past years has been based solely on the concept of a discrete gust and an associated gust-alleviation curve. In the earlier considerations, the airplane was considered to be a rigid body, but in later years the major flexibility of the aircraft, such as fundamental wing bending, was also included in an attempt to account for dynamic-response effects. In recent years design has usually incorporated both the single-gust concept and the concepts of power spectral analysis. The discrete-gust treatment normally constitutes the nucleus of the design approach, with the power spectral portion used as a means for bringing out dynamic-response effects more rationally, or possibly for uncovering unusual response effects that might otherwise be overlooked. Associated flight-test analysis by spectral procedures has also been used extensively.

The question may be raised as to whether the design for gust can be based completely on a power spectral concept, and it is believed that the answer is yes. In surveying the present situation, the following observations appear pertinent. Much work has been done in the application of spectral techniques to the gust-response analysis of aircraft; much has been accomplished and much is understood. The general method of describing atmospheric turbulence in power spectral terms and the general procedures for determining airplane response and for understanding the character of the random processes involved are now quite well established. It is not yet possible, unfortunately, to predict the statistical parameters of the gust-load history of an airplane in an absolute sense (i.e., independent of other airplanes and based on knowledge of the statistical description of the atmospheric turbulence and structural-response parameters of the airplane) because certain details of atmospheric-turbulence experience and of structural-response parameters as related to structural design have not been adequately defined. It appears to be only a

matter of time, however, before these parameters are defined adequately and spectral techniques can be used to predict the gust loads on an absolute basis.

In the following section three procedures are outlined which might form a basis for a power-spectral gust-design procedure. The procedures, in the order to be discussed, are: a spectral approach analogous to discrete gust design, a spectral approach on an absolute basis, and a spectral approach based on comparison with an existing aircraft. The first and third methods may be considered interim procedures in which considerable dependence is placed on past experience. The second method is cast completely in the spectral form but requires detailed information not completely available at the present time.

Spectral Approach Analogous to Discrete-Gust Design

The spectral approach analogous to discrete-gust design is shown in figure 18, where the analogous steps in a discrete-gust approach are shown for comparison. The example is expressed in terms of the center-of-gravity acceleration of the airplane, but it should be understood that the actual response quantities of concern, such as wing-bending stress or wing shear, would be used instead in actual design. From top to bottom the sketches on the left show: (1) the power spectrum of input gust velocity which depends on the atmospheric turbulence scale L (note that the mean-square gust velocity σ_w^2 has been extracted and that the spectrum has been normalized so that the area is unity); (2) the square of the nondimensional transfer function (the dimensions are contained in the factor $a\rho SV/2W$); and (3) the output response spectrum, which is the product of the preceding two items (K_Φ^2 represents the cross-hatched area). The sketches on the right indicate: (1) the gust velocity shape $\left(1 - \cos \frac{\pi V}{H} t\right)$, where H is the gust gradient distance, usually taken as 12.5 chords; (2) the response due to a unit-impulse gust velocity; and (3) the time-history response of the center-of-gravity acceleration to the gust input in item (1).

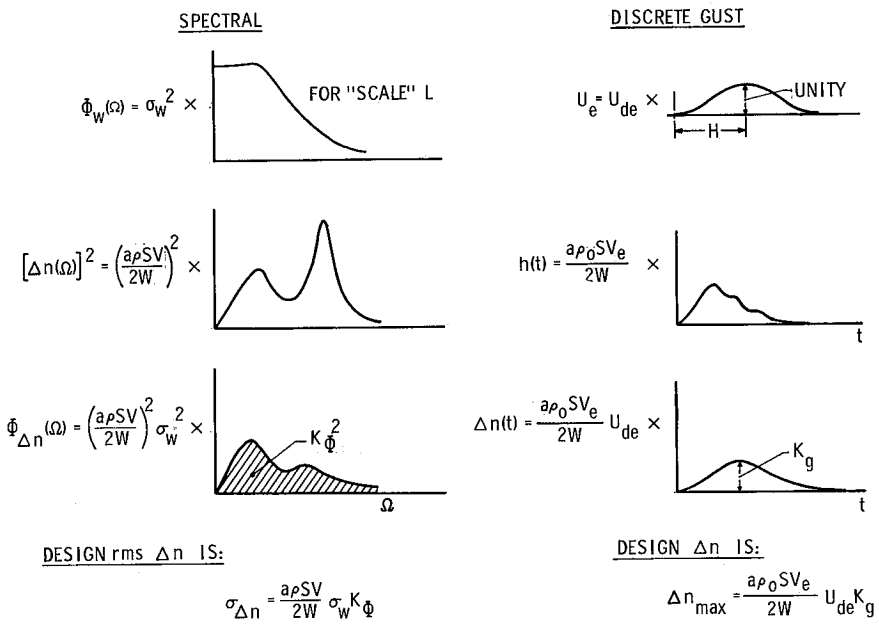

Figure 18.- Spectral analogy to discrete-gust design.

The equation for the root-mean-square acceleration $\sigma_{\Delta n}$ shown at the bottom of figure 18 is to be noted in particular,

since it provides the basis for this approach. For convenience, the equation is restated as follows:

The input-output relationship indicated in figure 18 in terms of the spectra and the transfer function is:

$$\Phi_{\Delta n}(\Omega) = \Phi_w(\Omega)\left[\Delta n(\Omega)\right]^2$$

and in terms of the root-mean-square values is:

$$\sigma_{\Delta n} = \frac{a\rho SV}{2W}\sigma_w K_\Phi \tag{40}$$

where

$$\sigma_w = \left[\int_0^\infty \Phi_w(\Omega)d\Omega\right]^{1/2}$$

and

$$\sigma_{\Delta n} = \left[\int_0^\infty \Phi_{\Delta n}(\Omega)d\Omega\right]^{1/2}$$

and, therefore,

$$K_\Phi = \frac{2W}{a\rho SV}\left\{\frac{\int_0^\infty \Phi_w(\Omega)\left[\Delta n(\Omega)\right]^2 d\Omega}{\sigma_w^2}\right\}^{1/2}$$

Note that equation (40) is analogous to the equation for Δn_{max} (shown at the lower right of fig. 18) which is the type of equation that has been used extensively through the years for discrete-gust design. The factor K_Φ in the spectral equation is of special significance; it is analogous to K_g, the commonly used gust-alleviation factor. Here, however, K_Φ can take account of the effects of vertical translation, pitch, and flexibility on the response of an airplane to a continuous random input. It may be recalled that on a mathematical approach basis K_g has been associated only with vertical translation effects (ref. 22).

The spectral equation for $\sigma_{\Delta n}$ may be transformed into the discrete-gust form as follows: Consider that the gust-load factor Δn for design is some factor η_d times $\sigma_{\Delta n}$, thus,

$$\Delta n_{design} = \eta_d \sigma_{\Delta n} \tag{41}$$

From a probability aspect, it is to be noted that a chosen value of η_d is associated with a given probability of exceeding the design load factor, that is, the probability that the load ratio $\frac{\Delta n_{design}}{\sigma_{\Delta n}} = \eta_d$ is exceeded. The substitution of $\sigma_{\Delta n}$ from equation (40) into equation (41) yields:

$$\Delta n_{design} = \frac{a\rho SV}{2W}\left(\eta_d \sigma_w\right) K_\Phi; \quad \Delta n_{design} = \frac{a\rho SV}{2W} w_d K_\Phi \tag{41a}$$

Remarkably, this equation is of the same form as the equation used in discrete-gust design; w_d assumes the role of U_{de}, and K_Φ replaces K_g. With respect to an appropriate value of the product $\eta_d \sigma_w$ for use in design, the following procedure is suggested. Suppose equation (41a) is equated to the discrete-gust equation indicated at the lower right of figure 18; there results

$$w_d = \eta_d \sigma_w = \frac{K_g}{K_\Phi} U_{de} \tag{42}$$

This equation can now be applied to several of the older gust-critical aircraft, thus permitting the establishment of a proper level of w_d; with this established, equation (41a) could then serve as the basis for design. It should be noted that if U_{de} is used as an equivalent velocity as is customary, then w_d will be expressed in the same manner. A point of interest with regard to this design method is that although the derivation originated from the spectral approach, the final form can be interpreted as a discrete-gust form which rationally includes some of the dynamic-behavior effects due to continuous turbulence.

(Equation (41a) may be established from another point of view as follows. Consider the ratio of a structural load value to the gust velocity producing this load. For a given airplane, it would appear reasonable that this ratio as established by power spectral considerations in terms of root-mean-square values should be equal roughly to the corresponding ratio as obtained in a discrete-gust approach, somewhat analogous to the concept of a spring constant. Thus, write

$$C_0 \frac{\sigma_{\Delta n}}{\sigma_w} = \frac{\Delta n_{design}}{U_{de}}$$

where C_0 is a factor of the order of unity. The substitution of $\sigma_{\Delta n}$ from this equation into the spectral equation for $\sigma_{\Delta n}$ in figure 18 then gives

$$\Delta n_{design} = \frac{a\rho SV}{2W}\left(C_0 U_{de}\right) K_\Phi$$

Thus, in this consideration $C_0 U_{de}$ takes on the role of w_d in equation (41a), and from equation (42), C_0 is noted to assume the character of K_g/K_Φ.)

If stress at a particular point had been considered instead of acceleration, equation (41a) would take the form

$$s_{design} = s_0 w_d K_{\Phi,s}$$

where s_0 is the stress quantity which takes the place of $a\rho SV/2W$, and $K_{\Phi,s}$ is the rms value of the nondimensional output spectrum for the particular stress being considered. Note that in this approach each response quantity has its own particular K_Φ, reflecting the fact that pitch and flexibility enter into each quantity to a different extent.

Equation (41a) or, more generally, the equation for s_{design} (just given) signifies only to a degree a rational design equation for a power spectral approach, one that is analogous to the commonly used discrete-gust approach. The design interest, however, is not only in the single large load but also in repeated loads at lower levels. In the application of these equations, the number of times a given load level, for example, the design level, is encountered in the life of the airplane is not taken into account explicitly; only the probability of exceeding a given load is known. The number of exceedances are expected to be closely related, however, to those of the gust-critical airplanes used in the establishment of a design level of w_d.

As an illustration that probability of exceeding a given load does not yield the number of exceedances, consider the following two sine waves.

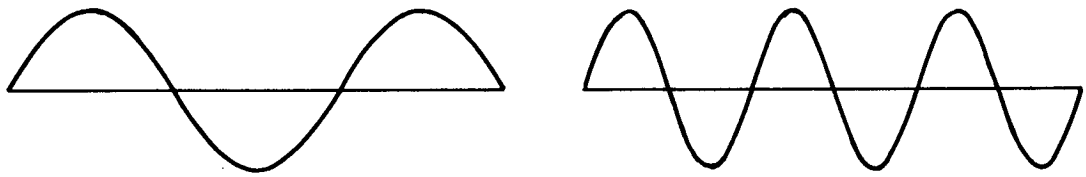

These two waves have the same probability distribution, but the number of times a given level is exceeded in a given length of time is much greater for the wave on the right. The treatment given in the subsequent section includes a consideration of this point.

Spectral Approach on an Absolute Basis

A more definitive but lengthier approach is one that extends the treatment of the preceding section so that number of exceedances of load levels, variation of severity of turbulence with altitude, and proportion of time spent in moderate and severe turbulence at each altitude, are explicitly taken into account. The approach leads to significant results in the form of average numbers of load level exceedances per unit flight distance or per unit flight time. It is based on the development given in references 10 to 12 and may be reviewed here with the use of figures 19 to 21.

Model considered.- Figure 19(a) illustrates the model or concept that is postulated as representing the atmospheric turbulence experienced by the airplane. The model is first considered to be made up of discrete patches of

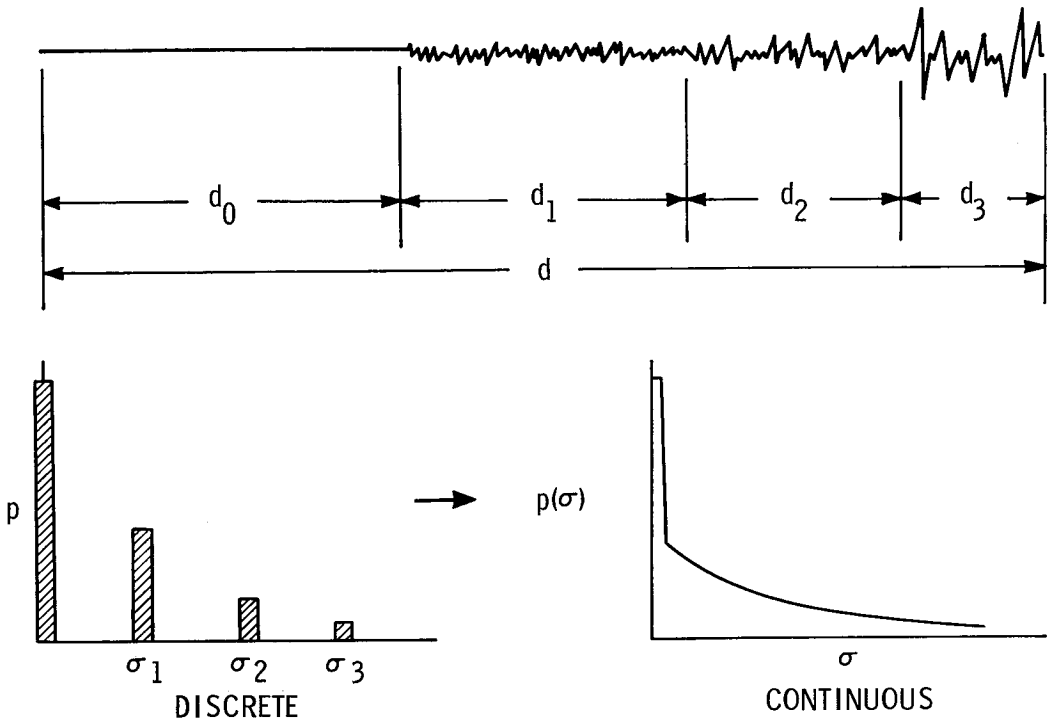

(a) Combined nonstorm and storm operation.

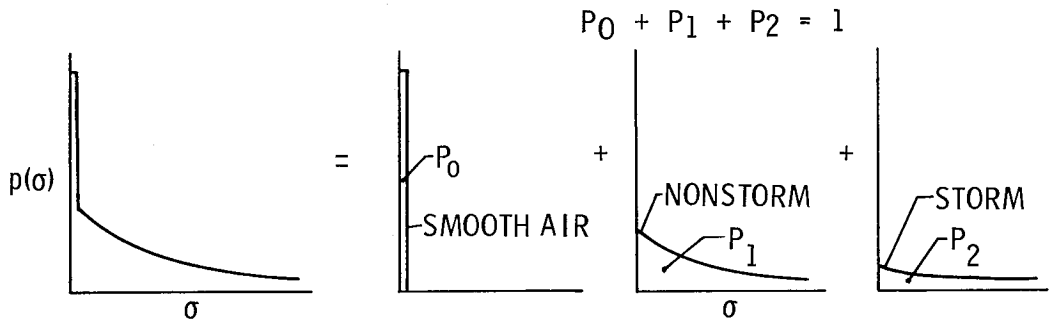

(b) Separated nonstorm and storm distributions.

Figure 19.- Composite gust encounter.

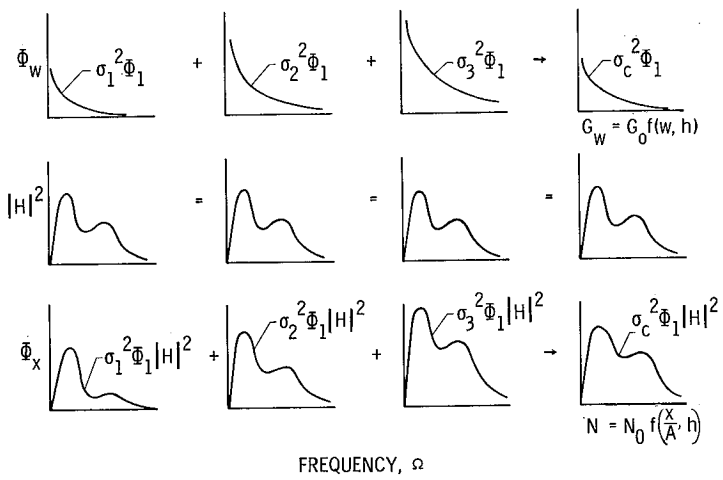

Figure 20.- Composite response to gusts.

disturbances of different mean-square intensity, each Gaussian and stationary in character, and then this model is replaced in a limiting-process sense by a model which has a continuously variable distribution of rms gust velocity. It is understood that the patches are encountered in random fashion, not necessarily in the succession shown. The σ's in figure 19 refer to the rms value of vertical gust velocity and correspond to the σ_w's used previously herein. In this section the subscript w will be dropped for convenience.

The use of radar, together with visual sightings and verbal reports, makes it possible to avoid flights through many storm areas during routine operations which could not have been avoided prior to the use of radar. Because of the changing flight experience in storm areas, it is desirable to have a means for specifically taking into account storm turbulence encounter to a varying extent. This may be done conveniently by splitting the continuous distribution curve shown in figure 19(a) into the components shown in figure 19(b); specifically, the first "Dirac delta" sketch to the right of the equality sign of area P_0 refers to the proportion of total flight distance that is spent in smooth flight (or below a threshold level), the second sketch is the distribution curve of σ for nonstorm turbulence encounter, the area P_1 being the proportion of total flight distance spent in this type of turbulence, while the third sketch is the corresponding curve for storm-turbulence encounter. (It may be noted that the sum of the fractional areas P_0, P_1, and P_2 is unity.)

Consistent with the model shown in figure 19(a), the resulting composite response of the airplane is shown schematically in figure 20. The situation pictured is for a given altitude, weight, and airspeed, but a similar picture is considered to apply at each altitude for other conditions. For simplicity, only the altitude h is shown as a parameter so that the response for various aircraft missions can be evaluated. The quantities and equations shown in the figure are derived as follows: The composite rms value σ_c of vertical velocity for the model would be

$$\sigma_c^2 = \frac{1}{d}\left[\int_{s_0}^{s_1} w_0^2(s)ds + \int_{s_1}^{s_2} w_1^2(s)ds + \int_{s_2}^{s_3} w_2^2(s)ds + \ldots\right]$$

$$= \frac{1}{d}\left[d_0\sigma_0^2 + d_1\sigma_1^2 + d_2\sigma_2^2 + d_3\sigma_3^2 + \ldots\right] = p_1\sigma_1^2 + p_2\sigma_2^2 + p_3\sigma_3^3 + \ldots \tag{43}$$

where p_n and σ_n represent, respectively, the proportion of time spent in an nth patch and the associated rms gust velocity, and σ_0 is zero. For the limiting case in which the turbulence model is represented by a continuous variation in rms gust velocity, equation (43) assumes the form

$$\sigma_c^2 = \int_0^\infty \sigma^2 p(\sigma) d\sigma \tag{44}$$

where $p(\sigma)$ is the probability density of σ. It should be noted carefully that the composite rms value σ_c as given by this equation is here mainly of conceptual interest and is that associated with the total flight time; its value is therefore quite small (less than 1 ft/sec) in comparison with the rms value of an individual turbulence patch.

Statistical description of gust velocities.- Composite information on the peak count of vertical gust velocity may be derived from reference 23 where equations applicable to the peak count of a Gaussian disturbance are developed. In application to the individually assumed Gaussian patches, the average number of peaks per unit distance in the nth patch which exceed a given level of vertical velocity is given approximately by

$$G_n(w) = G_0 e^{-\left(\frac{w^2}{2\sigma_n^2}\right)} \tag{45}$$

where G_0 is the average number of times per unit distance that $w(s)$ crosses the value zero with positive slope; its value depends only on the spectrum shape, and thus is the same for the various patches, and is given by

$$G_0 = \frac{1}{2\pi}\left[\frac{\int_0^\infty \Omega^2 \Phi_n(\Omega) d\Omega}{\int_0^\infty \Phi_n(\Omega) d\Omega}\right]^{1/2} \tag{46}$$

where it is recalled that

$$\sigma_n = \left[\int_0^\infty \Phi_n(\Omega) d\Omega\right]^{1/2}$$

Theoretically, equation (45) applies to the number of times per unit distance a given value of w is crossed with positive slope; it also happens to be a good approximation for determining the number of peaks above a given level for large values of w - for example, w greater than σ_n.

For the complete model, the equations for approximating the average number of peaks per unit distance which exceed a given level of vertical velocity are

$$G(w) = \frac{1}{d}\left[d_1 G_0 e^{-\left(\frac{w^2}{2\sigma_1^2}\right)} + d_2 G_0 e^{-\left(\frac{w^2}{2\sigma_2^2}\right)} + d_3 G_0 e^{-\left(\frac{w^2}{2\sigma_3^2}\right)} + \cdots\right]$$

$$= G_0\left[p_1 e^{-\left(\frac{w^2}{2\sigma_1^2}\right)} + p_2 e^{-\left(\frac{w^2}{2\sigma_2^2}\right)} + p_3 e^{-\left(\frac{w^2}{2\sigma_3^2}\right)} + \cdots\right] \tag{47}$$

For the limiting case of a continuous variation in the rms value σ_n, this equation becomes

$$G(w) = G_0 \int_0^\infty p(\sigma) e^{-\left(\frac{w^2}{2\sigma^2}\right)} d\sigma \tag{48}$$

As $p(\sigma)$ may vary with altitude, in effect

$$G = G_0 f(w,h)$$

Statistical description of airplane response.- Airplane response is described in the same manner as gust velocities except that allowance is made for variation of dynamic-response characteristics of the airplane with speed and weight as well as with altitude. Consider first the airplane response of a particular quantity x_n due to the nth discrete patch. The mean-square value of the output response $\sigma_{x,n}^2$ is equal to the area under the output spectrum, and the peak count for the response is given by an equation analogous to equation (45). The rms value and the approximate number of peaks per unit distance of the response that exceed a specified value are, therefore, given by the equations

$$\sigma_{x,n} = \left[\int_0^\infty \left|H(\Omega)\right|^2 \Phi_n(\Omega) d\Omega\right]^{1/2} \tag{49}$$

$$N_n(x) = N_0 e^{-\left(\frac{x^2}{2\sigma_{x,n}^2}\right)} \tag{50}$$

It is convenient to introduce a factor A such that

$$\sigma_{x,n} = A\sigma_n$$

or

$$A = \frac{\sigma_{x,n}}{\sigma_n}$$

where

$$\sigma_n = \left[\int_0^\infty \Phi_n(\Omega)d\Omega\right]^{1/2}$$

The quantity A is in the nature of a gust-response factor which depends on such airplane parameters as weight, wing area, speed, air density, and also directly reflects the number of degrees of freedom that are taking part in the response; in the example shown in figure 18, A has the value $\frac{a\rho SV}{2W} K_\Phi$. The parameter N_0, which is analogous to G_0, is the average number of times per unit distance that the response x crosses the value zero with positive slope and is given by

$$N_0 = \frac{1}{2\pi}\left[\frac{\int_0^\infty \Omega^2 \left|H(\Omega)\right|^2 \Phi_n(\Omega)d\Omega}{\int_0^\infty \left|H(\Omega)\right|^2 \Phi_n(\Omega)d\Omega}\right]^{1/2} \tag{51}$$

For the composite discrete-patch model the approximate number of peaks per unit distance of the response x becomes

$$N = \frac{1}{d}\left[d_1 N_0 e^{-\left(\frac{x^2}{2\sigma_1{}^2A^2}\right)} + d_2 N_0 e^{-\left(\frac{x^2}{2\sigma_2{}^2A^2}\right)} + d_3 N_0 e^{-\left(\frac{x^2}{2\sigma_3{}^2A^2}\right)} + \cdots\right]$$

$$= N_0\left[p_1 e^{-\left(\frac{x^2}{2\sigma_1{}^2A^2}\right)} + p_2 e^{-\left(\frac{x^2}{2\sigma_2{}^2A^2}\right)} + p_3 e^{-\left(\frac{x^2}{2\sigma_3{}^2A^2}\right)} + \cdots\right]$$

which in the limiting case of a continuous variation in σ_n becomes

$$N = N_0 \int_0^\infty p(\sigma) e^{-\left(\frac{x^2}{2\sigma^2A^2}\right)} d\sigma \tag{52}$$

These expressions apply to a given altitude (or altitude bracket) and strictly also to a given flight condition of weight and speed; that is, for the flight interval considered, the transfer function $H(\Omega)$ (hence N_0 and A) is assumed to be invariant.

It should be noted that the equations (48) and (52) for $G(w)$ and N refer to the number of exceedances per unit distance for positive w or x, or for negative values of w or x; for total peaks including positive and negative values of w or x, the equations should be multiplied by two.

Generalized prediction curves.- Consider now the implication of equation (52). In functional form the equation may be written

$$\frac{N}{N_0} = f\left(\frac{x}{A}, h\right) \tag{53}$$

where h is inserted as a reminder that the altitude is also a parameter. Equation (53) suggests the form and manner for analyzing gust-response data collected during routine airplane operations to obtain generalized curves for prediction purposes. A response quantity that has been collected in routine operations is the center-of-gravity acceleration. Such data can be processed to yield the number of exceedances N of given acceleration levels and should be separated according to altitude brackets and to flight conditions, if required. The values of A and N_0 for the monitored response quantity are calculated for the appropriate flight conditions (eqs. (49) to (51)). In accordance with equation (53), then, these data may be plotted as N/N_0 against x/A, thereby yielding generalized curves of the type shown in figure 21(a). Of significance is the fact that even though the curves are derived from a response

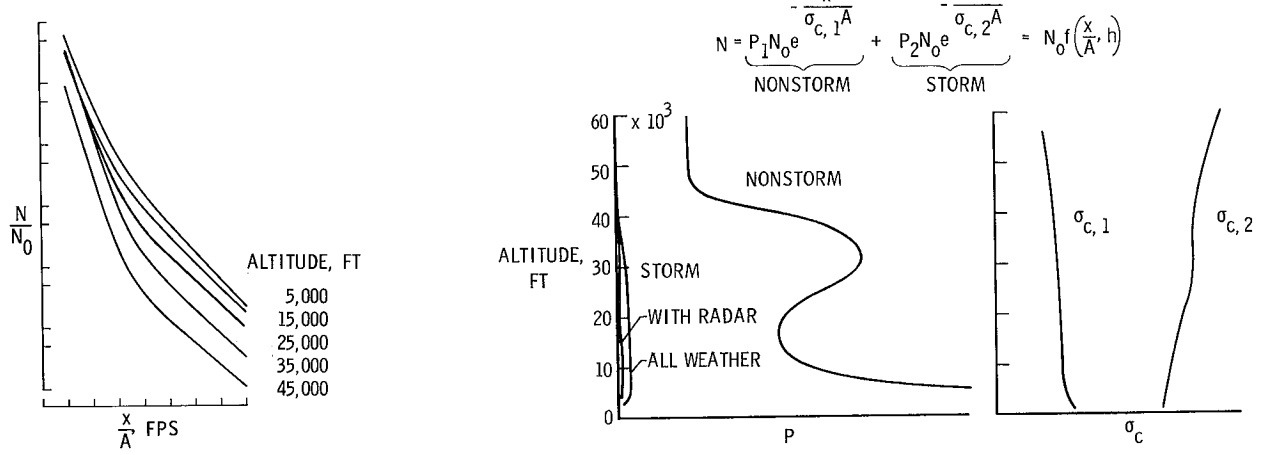

(a) Generalized curves for gust load experience.

(b) Variation of turbulence parameters with altitude.

Figure 21.- Turbulence and gust loads experiences in routine operations.

quantity which is convenient or easy to record, such as center-of-gravity acceleration, the generalized curves, because of their essentially nondimensional nature, apply to other response values as well. $\left(\text{Strictly, } \frac{x}{A\sigma_c} \text{ is the nondimensional quantity and } x/A \text{ has the dimension of a velocity.}\right)$ When necessary to distinguish the particular response quantity of interest N, N_0, and A will be identified by an appropriate subscript. For example, for the response quantity stress a parameter would be $N_{0,s}$.

To obtain peak count information on wing bending stress, it is only necessary to evaluate the factors A and N_0 appropriate to this stress (A_s and $N_{0,s}$) for a chosen location, and to use these factors in conjunction with the generalized curves of figure 21(a). Figure 21(a) thus represents the very heart of the approach being discussed - an approach which is a succinct method for determining the statistical data on peak count for flights of airplanes at any altitude. As will be shown subsequently, the expected results for any assumed mission can be derived from these curves.

A brief mention was made earlier of flight operations with and without storm avoidance. This operational factor may also be conveniently taken into account by the preceding approach. One way, for example, is to have a set of curves of the type shown in figure 21(a) for nonstorm operation, and another set for storm operation. A specific approach that is of interest, and is based on the work of references 10 to 12 follows. With reference to figure 19(b), analysis of the voluminous data collected during routine airline operations indicates that the empirically established probability density curves may be represented with fair accuracy by the equation

$$p(\sigma) = P_1 p_1(\sigma) + P_2 p_2(\sigma) \tag{54}$$

where

$$p_1(\sigma) = \sqrt{\frac{2}{\pi}} \frac{1}{\sigma_{c,1}} e^{-\left(\frac{\sigma^2}{\sigma_{c,1}^2}\right)}$$

$$p_2(\sigma) = \sqrt{\frac{2}{\pi}} \frac{1}{\sigma_{c,2}} e^{-\left(\frac{\sigma^2}{\sigma_{c,2}^2}\right)}$$

where P_1 and P_2 represent the proportion of total flight distance in nonstorm and storm turbulence, respectively, and $\sigma_{c,1}$ and $\sigma_{c,2}$ are the corresponding composite values of root-mean-square gust velocity in each type of turbulence. Note that P_0 associated with smooth air is dropped as before and the remaining flight experience has been regrouped into the two classes. The substitution of equation (54) into equation (52), keeping in view the form of equation (53), yields the following expression for peak count:

$$N = N_0 f\left(\frac{x}{A}, h\right)$$

$$N = P_1 N_0 e^{-\left(\frac{x}{\sigma_{c,1} A}\right)} + P_2 N_0 e^{-\left(\frac{x}{\sigma_{c,2} A}\right)} \tag{55}$$

The four parameters P_1, P_2, $\sigma_{c,1}$, and $\sigma_{c,2}$ depend on altitude and some representative curves evaluated from routine operations are shown in figure 21(b). Equation (55) is also included in figure 21(b); this figure, like the generalized curves of figure 21(a), represents an alternative condensed method for determining the statistical data on peak counts.

In the initial evaluation of the operational data to establish curves of the type given in figures 21(a) or 21(b), crude estimates for A and N_0 for the airplanes involved were used. Thus, to prevent the inappropriate use of the curves, the numbers on the scales have been purposely omitted. However, order of magnitude values may be indicated as follows. In figure 21(a) the logarithmic ordinate scale consists of six cycles with the largest value in the range of 10^{-2} to 10^{-3} and the linear abscissa scale covers a range of from 0 to 60 to 80 fps. In figure 21(b) the abscissa scale of the P curves ranges from zero to about 10^{-1} while the range of the σ_c curves extends from zero to roughly 10 ft/sec.

Extension to treat various missions.- The extension of the preceding analysis to treat complete missions where altitude, speed, and weight variations are involved follows easily. Thus, the equation which yields the composite total number of peaks per unit distance, on the average, that exceed a given value x during a complete mission of an airplane is as follows

$$N_c = \frac{1}{D}\left[D_1 N_{0,1} f\left(\frac{x}{A_1}, h_1\right) + D_2 N_{0,2} f\left(\frac{x}{A_2}, h_2\right) + \cdots\right] \tag{56}$$

where D_1, D_2, . . . are the distances traveled in each altitude bracket considered, and D the total flight distance. Subscripts referring to altitude bracket are also applied to N_0 and A to denote that these factors may change also with altitude. The effects of other flight conditions such as speed are contained implicitly in A and N_0. The repeated load history in a statistical sense for the entire mission is thus described by this equation. If necessary, each term in equation (56) may itself be separated into a suitable number of terms appropriate to the variable flight conditions considered. When applied to the determination of peak counts the equation is only suitable for the larger values of x as indicated by the statement following equation (46). Further, for total peaks including positive and negative x, the equation should be multiplied by two.

It should be noted that the appropriate characterization of peak counts for the gusts conflict somewhat with the characterization of peak counts for response. Since atmospheric turbulence is essentially space fixed, the number of zero crossings per unit distance is a logical parameter. A given airplane, on the other hand, tends to be frequency fixed; the logical parameter for airplane response therefore would be the number of zero crossings per unit time.

Equation (56) may be converted to the number of peaks per unit time N_c' above a given level as follows

$$N_c' = \frac{DN_c}{T} = \frac{1}{T}\left[\frac{D_1}{V_1} V_1 N_{0,1} f\left(\frac{x}{A_1}, h_1\right) + \frac{D_2}{V_2} V_2 N_{0,2} f\left(\frac{x}{A_2}, h_2\right) + \cdots\right]$$

or

$$N_c' = \frac{1}{T}\left[T_1 N_{0,1}' f\left(\frac{x}{A_1}, h_1\right) + T_2 N_{0,2}' f\left(\frac{x}{A_2}, h_2\right) + \cdots\right] \tag{57}$$

where T_1, T_2, . . . are the times traveled in each altitude bracket, and T the total flight time; $N_{0,1}' = V_1 N_{0,1}$, $N_{0,2}' = V_2 N_{0,2}$, . . . are the number of zero crossings per unit time at each altitude; for most cases these values should change very little with altitude, and for practical evaluation purposes, therefore, a single value might be taken for a given airplane to apply at all altitudes.

Since equation (56) gives the average number of peaks per unit distance that exceeds a given value x, the total distance D that must be flown (again on the average statistically) to encounter a total of $n_{p,x}$ peaks above this level is given by

$$DN_{c,x} = n_{p,x}$$

or

$$D = \frac{n_{p,x}}{N_{c,x}} \tag{58}$$

In an analogous manner, the equation for a unit of time, say in hours, that must be flown to encounter n_p peaks above a given level is found from equation (57) to be

$$T = \frac{n_{p,x}}{N_{c,x}'} \tag{59}$$

For design, the results obtained from either equation (58) or (59) would be assessed to judge whether the airplane is expected to be safe or satisfactory for routine and extended use. The number of miles, or alternatively the number

of hours, that can be flown in a statistical sense before exceeding a design load level, such as limit load, by a specified number of times is either stipulated, or more likely, is selected on the basis of past demonstrated performance of certain aircraft. The aim is to have the new design at least fulfill such a chosen requirement. How far the "life" of the airplane can go beyond this cannot be determined with certainty.

The question of to what extent the design should be based on miles of flight or hours of flight is of fundamental importance, and merits careful study and appraisal. As an illustration of the problem involved, consider a new fast airplane and an old slow airplane. The following sketches show schematically the differences in the expected statistical load behavior. On the left, the new airplane is designed to yield the same number of miles to exceed limit load

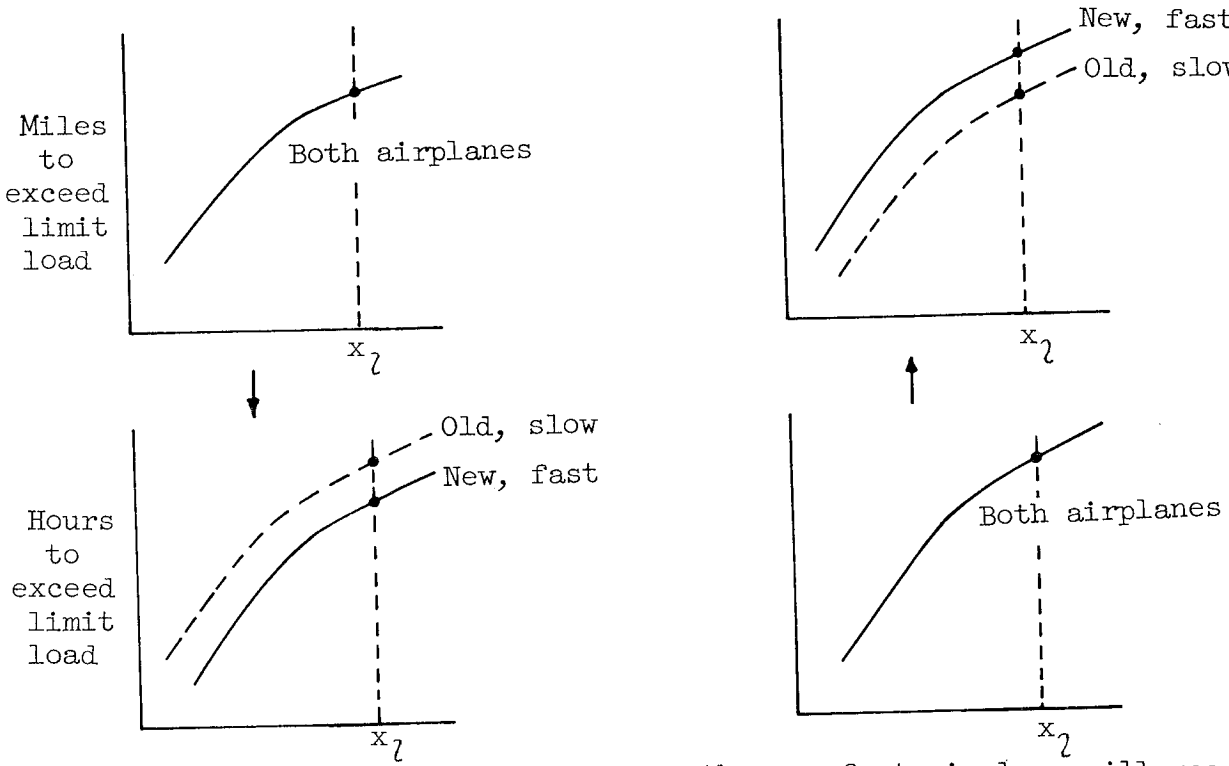

as for the old airplane. As a consequence, the new fast airplane will reach limit load in fewer hours of service than will the old. In contrast, on the right, the new and old airplanes have the same number of hours of service before reaching limit load. In this case, the new airplane may be expected to fly a greater number of miles before reaching limit load. The basic question briefly considered here is the relative significance of the experience in time or distance.

Comparison With Existing Aircraft

The third procedure is to compare the airplane being designed with an airplane that has been in use or service for a long time in order to obtain a new airplane that is at least as good as the "proven" design from the gust viewpoint. Generally, the details of the procedure have to be tailored to the

particular situation, depending on whether the design is still in the planning stage, whether a prototype exists, or whether there are flight data available on this prototype. A unique procedure therefore cannot be outlined for all cases. A procedure that may be applicable to many cases, however, is described herein.

Before presenting the details, the general sequence of steps in the method is indicated. In this method, an airplane that is known to be gust critical and for which extensive operational data exist, say in the form of peak counts of center-of-gravity accelerations Δn, is selected as the reference airplane, designated by subscript 1. The acceleration data for this airplane are converted by calculation to estimates of peak counts of other response quantities of interest such as wing bending stress. This process is also used for the airplane being designed (designated by subscript 2) to be "as good as" the reference airplane. The peak-count curves of the two airplanes are then compared, and, if necessary, changes in the new design are made so that its estimated stress experience is judged to be no more severe than that of the reference airplane.

The basic relation to be used is the composite peak count of acceleration Δn for the reference airplane given in a form which is essentially that of equation (53)

$$\left(\frac{N_c}{N_{0,\Delta n}}\right)_1 = \left[f\left(\frac{\Delta n}{A_{\Delta n}}\right)\right]_1$$

or, more explicitly, in the generalized nondimensional form for response x given by

$$\left[\frac{N_c\left(\frac{x}{A_x}\right)}{N_{0,x}}\right]_1$$

as a function of x/A_x where $N_{0,x}$ refers to the number of zero crossings for unit distance and x refers to a given response quantity; also, $N_{c,x}$ is the number of peaks exceeding a given value x of the response quantity in a unit distance.

This relation applies to all response quantities of interest on the basis of the representation of the airplane as a linear system. It is assumed that the new airplane will be subjected to the same turbulence model as the reference airplane. Therefore, identities such as the following hold

$$\left[\frac{N_c\left(\frac{s}{A_s}\right)}{N_{0,s}}\right]_2 \equiv \left[\frac{N_c\left(\frac{s}{A_s}\right)}{N_{0,s}}\right]_1 \equiv \left[\frac{N_c\left(\frac{\Delta n}{A_{\Delta n}}\right)}{N_{0,\Delta n}}\right]_1 \equiv Y(w) \qquad (60)$$

where
$$\left(\frac{s}{A_s}\right)_2 \equiv \left(\frac{s}{A_s}\right)_1 \equiv \left(\frac{\Delta n}{A_{\Delta n}}\right)_1 \equiv w \tag{61}$$

These relations provide a basis for expressing the peak counts of various response quantities in terms of those of, for example, accelerations.

It is also desirable to bring in explicitly the differences in flight distances traversed by the airplanes. The total number of stress response peaks $n_{p,s}$ that fall above the level s in a flight distance D is given by

$$n_{p,s} = DN_{c,s}$$

From this equation and equations (60) and (61), the following relations for peak count can be derived: The peak count of stress exceeded in the reference airplane is

$$(n_{p,s})_1 = D_1(N_{c,s})_1 = D_1(N_{0,s})_1 Y \tag{62a}$$

where the stress exceeded is

$$(s)_1 = w(A_s)_1$$

In terms of the acceleration exceeded in the reference airplane, the peak count of stress exceeded is (see eq. (60) for Y)

$$(n_{p,s})_1 = D_1(N_{c,s})_1 = D_1 \frac{(N_{0,s})_1}{(N_{0,\Delta n})_1}(N_{c,\Delta n})_1 \tag{62b}$$

where the stress exceeded is related to the acceleration exceeded by

$$(s)_1 = \frac{(A_s)_1}{(A_{\Delta n})_1}(\Delta n)_1$$

The application of equation (62b) to the conversion of $(N_{c,\Delta n})_1$ to $(N_{c,s})_1$ is illustrated by the following sketch (with D_1 canceled):

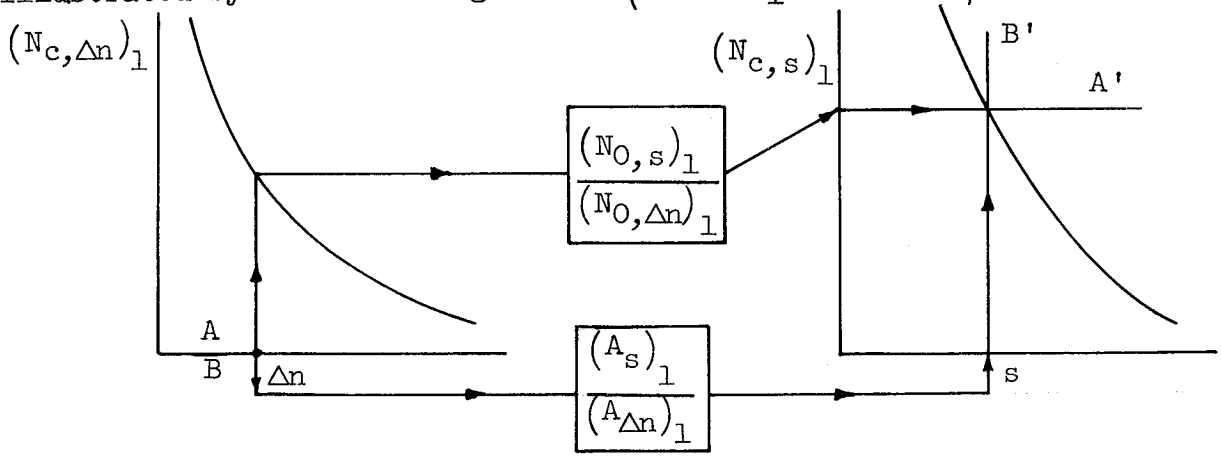

As indicated by path AA', the numerical value of the stress peak count $(N_{c,s})_1$ is determined by multiplying the value of $(N_{c,\Delta n})_1$ for a given value of $(\Delta n)_1$ by $\frac{(N_{0,s})_1}{(N_{0,\Delta n})_1}$. The value of the stress exceeded is obtained by multiplying the given value of $(\Delta n)_1$ by $\frac{(A_s)_1}{(A_{\Delta n})_1}$ as indicated by path BB'.

The relations between the peak count of stress in the new airplane to that of acceleration in the reference airplane are obtained in a similar manner. These relations are

$$(n_{p,s})_2 = D_2 \frac{(N_{0,s})_2}{(N_{0,\Delta n})_1}(N_{c,\Delta n})_1 \tag{63}$$

where

$$(s)_2 = \frac{(A_s)_2}{(A_{\Delta n})_1}(\Delta n)_1$$

The relations between peak counts of stresses in the two airplanes from equations (62) and (63) are:

$$(n_{p,s})_2 = \frac{D_2}{D_1} \frac{(N_{0,s})_2}{(N_{0,s})_1}(n_{p,s})_1 \tag{64}$$

where

$$(s)_2 = \frac{(A_s)_2}{(A_s)_1}(s)_1$$

The peak-count curves from equations (63) and (64) for the reference and new airplanes, respectively, are plotted on a common chart as illustrated in figure 22. For the example used in this figure; $(N_{c,\Delta n})_1$ is assumed to be known, $(n_{p,s})_1 = 3 \times 10^9 (N_{c,\Delta n})_1$, $(s)_1 = 2 \times 10^4 (\Delta n)_1$, $(n_{p,s})_2 = 2(n_{p,s})_1$, and $(s)_2 = 0.9(s)_1$. The adequacy of the new design is then judged by the relative position of the two curves. In general, it is desired to have the curve for the new airplane fall on or to the left of the reference curve. If this

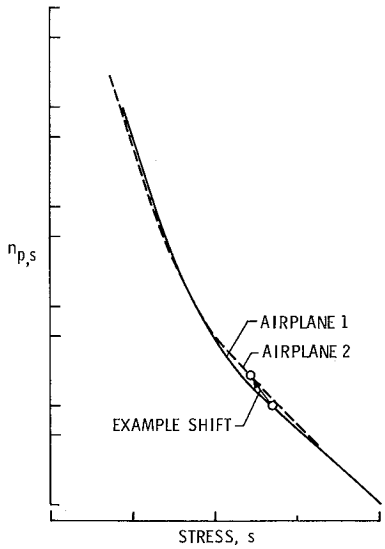

Figure 22.- Design comparison with "proven airplane."

is so, it is assumed that the load experiences of the new airplane will be no worse than that of the reference airplane.

As described, the method essentially assumes that the new airplane does not differ in major respects from the reference airplane and the method might be specially suited for application to a new design evolved from a predecessor design. If the new design should differ radically in its operating characteristics, it would be necessary to modify the method to account for such variations.

Since the peak-count history is strongly dependent on the two structural parameters A and N_0, it is of interest to see what must be considered relative to the behavior of A and N_0 when design changes are contemplated. A qualitative insight with respect to how changes in A or N_0 may alter the peak-count history can be obtained by reference to figure 23. Consider that curve 1 refers to the square of a frequency-response curve for the reference airplane, while curve 2 is the comparable curve for the new airplane. Because of the large peak in the curve for airplane 2, the value of N_0 will be larger than that for airplane 1 (because of the Ω^2 weighting in eq. (51)). To compensate for this larger value of N_0, from a peak-count point of view, the value of A for airplane 2 must be smaller than that for airplane 1. The value of A $\left(\text{that is, } A = \frac{\sigma_{\dot{x},n}}{\sigma_n}\right)$, however, is governed largely by the height of the frequency-response curve at the lower frequencies; thus, to reduce A for the new airplane, the frequency-response curve must have lower amplitudes at low frequencies than that of the comparison airplane. Specific or numerical trade-offs in N_0 and A depend, of course, on each particular situation.

This comparative or relative procedure has the feature of making the results somewhat insensitive with respect to whether or not the "correct" values of aerodynamic and structural parameters are used in the calculation of A and N_0. Often different individuals will select different values for the parameters involved, for example, in the choice of lift-curve slope, or whether the mid-span chord or the mean aerodynamic chord is used. By nonrelative procedures, estimated response results may differ significantly depending on these choices; here, however, there should not be a marked difference in results obtained by different individuals because only ratios of like quantities are involved; "errors" in chosen parameters will, therefore, tend to compensate, as long as each individual selects his parameters in a consistent manner. It is noted that while the procedure is believed to be potentially versatile, it has not as yet been pursued sufficiently.

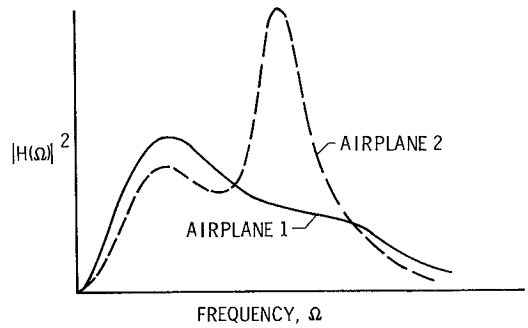

Figure 23.- Frequency-response functions for comparable peak count history.

CONSIDERATION OF COMBINED STRESSES

The question is sometimes raised as to whether spectral techniques can take into account the problems of stress due to combined loads and of interaction effects. Means for doing this are outlined below for two example situations.

Stresses Due to Superposition

Consider that the stress at a critical point in the structure is the result of several simultaneous loadings that occur during turbulence encounter, as indicated, for example, by the following equation:

$$s(t) = aM(t) + bV(t) + cT(t)$$

where M, V, and T refer to moment, shear, and torsion, respectively (see fig. 24). When considered individually, the stresses due to each of these three loads may be quite different in amplitude and phase, and it would be improper to determine separately the spectrum of the stress from each source, for there is no way to combine them to obtain the spectrum of the combined stress. The proper procedure is to determine the frequency-response function for the total or superimposed stress s(t)

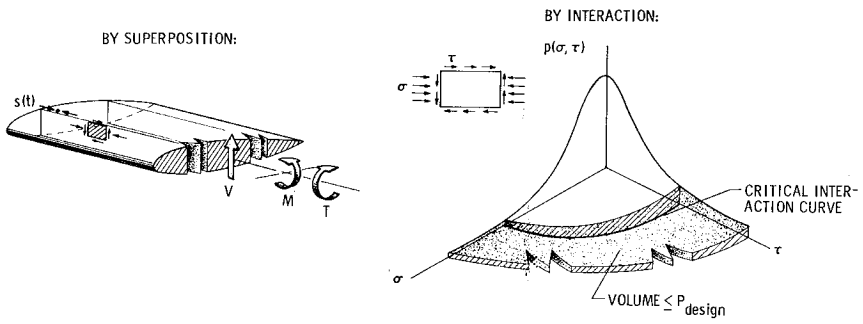

Figure 24.- Combined stress treatment.

$$H_S(\omega) = aH_M(\omega) + bH_V(\omega) + cH_T(\omega)$$

not for the individual stresses, and to use this frequency-response function to determine the power spectrum of s(t)

$$\Phi_S(\omega) = \Phi_W(\omega)\left|H_S(\omega)\right|^2$$

All phase relationships will then be taken into account automatically.

Critical Stresses by Interaction

The problem referred to here is the critical load in a structural element whose strength or stability is governed by an interaction curve (see ref. 24) of two or more stresses. This problem may be approached by joint probability

considerations as indicated by the following example: Suppose the critical loading of a panel is governed by an interaction curve involving shear stress τ and compressive stress σ. The joint probability-density distribution of the two stresses depicted on the right side of figure 24 is determined; the interaction curve is inserted in the σ-τ plane. The probability that a critical loading condition is exceeded is expressed by the volume lying outside the interaction region and contained between the σ-τ plane and the distribution surface; that is, the shaded region in figure 24. For design of the element, this probability should not exceed the design probability level established. (See also table I.)

CONCLUDING REMARKS

In this report which deals with determination of the dynamic response of aircraft to continuous atmospheric turbulence by power spectral techniques, a review is given and new information is presented on

(1) the description of atmospheric turbulence including cumulus cloud and thunderstorm turbulence,

(2) aircraft-response analyses and a comparison of results with several flight measurements, and

(3) prediction techniques based on power spectral methods for use in aircraft design for gust loads.

In the appendixes are given an outline of the origin and derivation of the correlation and spectral relations used in the report, the effect of possible extraneous signals on determination of the scale of turbulence, and a review of the basic procedures and mathematics that are involved in the practical applications of power techniques.

Some of the highlights of the report are summarized as follows:

1. Atmospheric turbulence measurements and spectral evaluations have been extended (beyond clear air) to include cumulus clouds and thunderstorms.

2. Analytical expressions for the autocorrelation and spectrum fitted to the measured atmospheric turbulence data were examined for two cases in which the spectrum varied at the higher frequencies as $\Omega^{-5/3}$ or Ω^{-2}. The $\Omega^{-5/3}$ case was found to give good internal consistency and a better fit than the previously used expression involving Ω^{-2}.

3. Distinction is made between two different root-mean-square values of gust velocity. One value, often quoted in the past, is associated only with the area under the portion of the spectrum that is evaluated and is, therefore, a truncated value. The other, which is associated with the area under the complete spectrum, is the overall or actual root-mean-square value. The actual root-mean-square value is two to two and one-half times as large as

the truncated root-mean-square value. Overall rms values of 32 ft/sec were found to be representative of thunderstorms; a value of 15 ft/sec is estimated for cumulus clouds.

4. Thunderstorms were found to have a scale of turbulence L of approximately 5,000 feet. A reexamination of results from clear-air-turbulence investigations made at a 5,000-foot altitude indicated that the value of L for clear air is also of this magnitude. (Where numerical values were available to permit use of the procedures outlined herein, the values of L ranged from 3,000 to 6,000 feet for the different traverses and methods of evaluation.)

5. Load and motion frequency responses from flight tests in rough air of a large flexible swept-wing airplane at subsonic speeds and of a delta-wing airplane at both subsonic and supersonic speeds are compared with calculated responses. In general, good agreement between the measured and calculated results was found.

6. Several approaches based on power spectral techniques for the design of airplanes for gust loads are outlined. In general, the basic spectral techniques for analyzing flight data, for determining aircraft response, and for predicting statistical load histories seem sound and well established. More work and understanding in a detailed sense are needed to be able to predict the gust loads of an aircraft on an absolute basis.

The present investigation indicates some problem areas which merit further study. The lateral-response problem including a development of an experimental technique needs further study to assess its importance more comprehensively. Procedures for calculating airplane response parameters in a consistent and accurate manner are needed. Following this, a reevaluation of the routine operational data is needed to establish more accurate generalized curves for gust-load experience. As regards prediction and design techniques, the approaches suggested herein warrant application to specific examples to work out details and to alter them as is found necessary. As a related item which is beyond the scope of this paper, but which is a logical extension, work should be done to determine how an analysis of the type given herein can be tailored or integrated into the fatigue problem. Specifically, the fatigue of structures under a random-force input and the manner or technique for appropriately simulating the fatigue testing of structures under combined loading need further study and development.

Langley Research Center,
National Aeronautics and Space Administration,
Langley Station, Hampton, Va., January 8, 1964.

APPENDIX A

SYMBOLS

The primary symbols used in this report are defined as follows:

A	airplane response parameter relating rms input and output values
$A(t)$	response of system to unit step
a	lift-curve slope; amplitude
a_i	generalized coefficient
a_n, b_n, a_o	Fourier series coefficients
a, b, c	stress coefficients
a_x, a_y, a_z	longitudinal, lateral, and vertical accelerations
c	wing chord; co-spectrum
$\hat{c}_h$	raw estimate of co-spectrum
c_r	root chord of wing
c_{xy}	co-component (in phase) of cross spectrum
D	flight distance
$d, d_0, d_1, d_2, \ldots$	flight distance in turbulence of given intensities
E_1, E_2	sampling error in amplitude and phase of frequency-response function
$E( )$	three-dimensional power spectrum
EI	elastic stiffness
$e( )$	spurious signal in measured quantity
$F( )$	nondimensional power spectrum of longitudinal component of random variable
f	frequency, cps
$f( )$	generalized function
$f(t)$	input force function

$f(r)$	nondimensional autocorrelation function of longitudinal component of random variable
G	average number of peaks per unit distance which exceed a given value of vertical gust velocity
G_0	average number of zero crossings per unit distance with positive slope for vertical gust velocity
$G(\ )$	nondimensional power spectrum of transverse component of random variable
g	acceleration due to gravity
$g(r)$	nondimensional autocorrelation function of transverse component of random variable
H	gust gradient distance
$H(\ )$	frequency-response functions; subscript s refers to function determined from spectral relations and subscript c refers to function determined by use of cross-spectra relations
h	altitude
$h(t)$	response due to unit impulse input
K	statistical degrees of freedom
K_g, K_Φ	gust alleviation factors
K_V	modified Bessel function of the second kind
k	reduced frequency, $\omega c/2V$
L_h	raw estimates of spectral power
L	scale of turbulence
L_r	scale of turbulence deduced from measurements containing spurious signal
l_x, l_z	longitudinal and vertical distances from accelerometer to flow vane
M	Mach number
M_i	generalized mass for ith mode
$\bar{M}_i$	bending-moment distribution associated with ith mode

$\overline{M}_g$ bending moment due to gust velocity

m structural mass density; maximum number of autocorrelation function lags

N, N_0 average number of peaks per unit distance which exceed a given level of response and average number of zero crossings per unit distance with positive slope

N_c composite average number of peaks per unit distance

n number of intervals used in time-history record $\left(T_L = n\epsilon = \frac{n\pi}{\omega_0}\right)$

n_p total number of peaks exceeding given level of response quantity

Δn vertical acceleration in g units

$P_0, P_1, P_2, \ldots$ proportion of total flight distance spent in given type of turbulence

p pressure; number of autocorrelation function lags

$p( ), p_c( )$ probability density function

p_g pressure distribution due to gust velocity

p_n proportion of time in nth patch of turbulence

$p_{t,0}$ total pressure on structure

Q_i generalized force

q dynamic pressure; number of time intervals; quadrature spectrum

$\hat{q}_h$ raw estimate of quadrature spectrum

$q_{xy}(\omega)$ quad-component (out of phase) of cross spectrum

$R( )$ correlation function

$R_e( )$ correlation function of spurious signal

$R_r( )$ correlation function of contaminated signal

$R(p)$ sum of lagged products used to estimate cross-correlation function

$R_{xy}( )$ cross-correlation function of x and y

r, r_1 correlation distances $r = V\tau$

r_c	value of r at which correlation function crosses zero
S	wing area
$s, s(\ )$	stress
T	general time limit
T_L	record length
t	time
U	maximum gust velocity
U_{de}	derived gust velocity
u	longitudinal component of true turbulence velocities
V	airplane speed
V_e	equivalent airspeed
v	lateral component of true turbulence velocities
W	airplane weight
$w_d = \eta_d \sigma_w = \frac{K_g}{K_\Phi} U_{de}$	
$w_{g,0}$	magnitude of sinusoidal gust velocity
w	vertical component of true turbulence velocities
w_0	local downwash; initial value of airplane vertical velocity
w_r	vertical component of true gust velocity containing spurious signal
x	general input function, or a general response quantity
x_c	location of downwash relative to a convenient reference point
X, Y, Z	longitudinal, lateral, and vertical axes
y	general response quantity
$\overline{y}$	semispan station
$y(t), y(T)$	general and truncated response time histories
z, z_i	mode shapes

$z(x,y,t)$ displacement of points x and y

α_v vertical vane angle

β damping coefficient

β_{cr} critical damping

β_v side vane angle

Γ gamma function

γ damping ratio

$\gamma^2(\omega)$ coherency function

Δ incremental value

δ Dirac delta function

ϵ time interval of sampling, T_L/n

$$\eta_d = \frac{\Delta n_{design}}{\sigma_{\Delta n}}$$

θ pitch angle

λ wavelength

μ mass ratio

ρ air density

ρ_o air density at sea level

σ root-mean-square value

σ_c composite rms value

σ_1, σ_w truncated and complete rms values, respectively

$\sigma_1, \sigma_2, \sigma_3, \ldots \sigma_n$ complete rms values for given patches of turbulence

τ time lag

Φ power spectrum

$\Phi_{a,i}$ power spectrum of displacement

$\Phi_{xy}(\ ),\Phi_{wy}(\ )$ cross spectrum of two quantities

φ roll angle

ψ yaw angle

ω angular or circular frequency

ω_i natural frequency of ith mode

$\Delta\omega$ effective filter bandwidth, $\frac{4\pi}{m\epsilon}$

Ω spatial frequency, $\frac{2\pi}{\lambda}$

Ω_0 highest spatial frequency to be evaluated

Ω_1 lowest spatial frequency to be evaluated

Subscripts:

av average

cr critical

e error

f filtered

g gust or turbulence

i ith mode of motion

m measured

M moment

n nth turbulence patch

Δn acceleration

r contaminated signal

s stress

sp short period

st static value

T	truncated in time; torsion
u,v,w	longitudinal, lateral, and vertical turbulence velocities
V	shear
x,y	general input or output response quantities

A dot over a symbol represents differentiation with respect to time.

The symbol $\hat{}$ over a figure indicates a prewhitened quantity.

APPENDIX B

CORRELATION AND SPECTRAL FUNCTIONS

A brief outline of the origin and derivations of the correlation and spectral relations used in the body of this paper is given in this appendix.

General Relations

Consider two points A and B in an isotropic turbulent field. The correlation of particle velocities at these two points is conveniently expressed in terms of five basic correlation functions; two are double correlation functions and three are triple correlation functions. Only the two double correlation functions need be considered here; they are as indicated by the following sketch and equations:

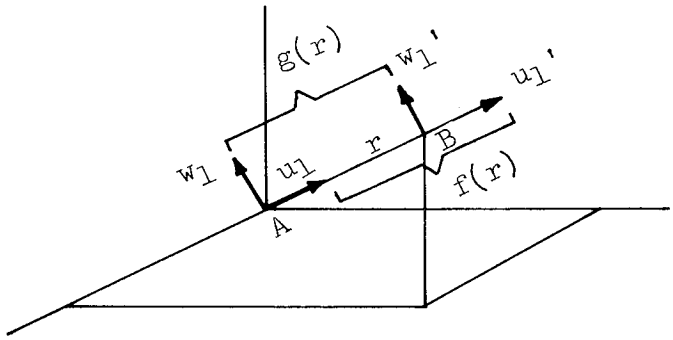

Longitudinal:

$$R_u(r) = \overline{u_1 u_1'} = \frac{1}{T}\int_0^T u_1(0,t)u_1(r,t)dt \qquad \text{(B1a)}$$

$$f(r) = \frac{R_u(r)}{R_u(0)} = \frac{R_u(r)}{\sigma_u^2} = \frac{\overline{u_1 u_1'}}{\overline{u_1^2}} \qquad \text{(B1b)}$$

Transverse:

$$R_w(r) = \overline{w_1 w_1'} = \frac{1}{T}\int_0^T w_1(0,t)w_1(r,t)dt \qquad \text{(B2a)}$$

$$g(r) = \frac{R_w(r)}{R_w(0)} = \frac{R_w(r)}{\sigma_w^2} = \frac{\overline{w_1 w_1'}}{\overline{w_1^2}} \qquad \text{(B2b)}$$

in which

$$\sigma_u^2 = R_u(0) = \overline{u_1^2} = \sigma_w^2 = R_w(0) = \overline{w_1^2} \tag{B3}$$

From the equation of continuity, it may be shown that these correlation functions are related by the equations

$$R_w = R_u + \frac{r}{2}\frac{\partial R_u}{\partial r} \tag{B4a}$$

or

$$g = f + \frac{r}{2}\frac{\partial f}{\partial r} \tag{B4b}$$

Thus, if one value is known, the other is automatically specified.

Associated with the two correlation functions in equations (B1a) and (B2a) are the one-dimensional power spectra defined by the following Fourier transform pairs:

$$\Phi_u(\Omega) = \frac{1}{\pi}\int_{-\infty}^{\infty} R_u(r)e^{-i\Omega r}\,dr = \frac{2}{\pi}\int_0^{\infty} R_u(r)\cos\,\Omega r\,dr \tag{B5a}$$

$$R_u(r) = \frac{1}{2}\int_{-\infty}^{\infty} \Phi_u(\Omega)e^{i\Omega r}\,d\Omega = \int_0^{\infty} \Phi_u(\Omega)\cos\,\Omega r\,d\Omega \tag{B5b}$$

and

$$\Phi_w(\Omega) = \frac{1}{\pi}\int_{-\infty}^{\infty} R_w(r)e^{-i\Omega r}\,dr = \frac{2}{\pi}\int_0^{\infty} R_w(r)\cos\,\Omega r\,dr \tag{B6a}$$

$$R_w(r) = \frac{1}{2}\int_{-\infty}^{\infty} \Phi_w(\Omega)e^{i\Omega r}\,d\Omega = \int_0^{\infty} \Phi_w(\Omega)\cos\,\Omega r\,d\Omega \tag{B6b}$$

For convenience, these equations are often expressed in terms of nondimensional spectral and correlation functions as:

$$F(\Omega) = \frac{\Phi_u(\Omega)}{\sigma_u^2} = \frac{2}{\pi}\int_0^{\infty} f(r)\cos\,\Omega r\,dr \tag{B7a}$$

$$f(r) = \frac{R_u(r)}{\sigma_u^2} = \int_0^{\infty} F(\Omega)\cos\,\Omega r\,d\Omega \tag{B7b}$$

and

$$G(\Omega) = \frac{\Phi_w(\Omega)}{\sigma_w^2} = \frac{2}{\pi} \int_0^\infty g(r)\cos \Omega r \, dr \tag{B8a}$$

$$g(r) = \frac{R_w(r)}{\sigma_w^2} = \int_0^\infty G(\Omega)\cos \Omega r \, d\Omega \tag{B8b}$$

From equations (B4) to (B8), it follows that the spectral functions are related by the equations

$$\Phi_w(\Omega) = \frac{1}{2} \Phi_u(\Omega) - \frac{\Omega}{2} \frac{d\Phi_u}{d\Omega} \tag{B9a}$$

or

$$G(\Omega) = \frac{1}{2} F(\Omega) - \frac{\Omega}{2} \frac{dF}{d\Omega} \tag{B9b}$$

As mentioned, the spectra defined by equations (B5) and (B6) are called one-dimensional spectra, and that of equations (B5) often being referred to as Taylor's spectral function. These spectra represent, in effect, one-dimensional cuts through a turbulence field which in reality is three dimensional in character. To represent the actual spatial character of the turbulence, a three-dimensional energy spectrum, or spatial spectrum, is used which involves the use of three-dimensional Fourier analysis (or the concept of a correlation tensor). This three-dimensional spectrum, designated here by $E(\Omega)$, is expressible in terms of the one-dimensional spectra; specific relations are:

$$E(\Omega) = \frac{1}{2} \Omega^2 \frac{\partial^2 \Phi_u}{\partial \Omega^2} - \frac{1}{2} \Omega \frac{\partial \Phi_u}{\partial \Omega} \tag{B10a}$$

or

$$\Phi_u(\Omega_1) = \int_{\Omega_1}^\infty \frac{E(\Omega)}{\Omega} \left(1 - \frac{\Omega_1^2}{\Omega^2}\right) d\Omega \tag{B10b}$$

and

$$\Phi_w(\Omega_1) = \frac{1}{2} \int_{\Omega_1}^\infty \frac{E(\Omega)}{\Omega} \left(1 + \frac{\Omega_1^2}{\Omega^2}\right) d\Omega \tag{B10c}$$

It is of interest to note how much energy is contained in the three-dimensional spectrum as compared with the one-dimensional spectrum; integration of equation (B10a) yields

$$\sigma_E^2 = \int_0^\infty E(\Omega)d\Omega = \frac{3}{2}\int_0^\infty \Phi_u(\Omega)d\Omega \tag{B11}$$

By equations (B5b) and (B3), however, the integral on the right equals σ_u^2; the mean-square value of the three-dimensional turbulence velocity σ_E^2 therefore bears the following relationship to the one-dimensional mean-square value:

$$\sigma_E^2 = \frac{3}{2}\sigma_u^2$$

Turbulence Scale and Limit Relations

It is common to introduce various lengths which are significant in characterizing the structure of turbulence. Two of these lengths are called the macro- or integral-scale, or simply scale, of the turbulence, and are defined by the equations

$$L_u = \int_0^\infty f(r)dr \tag{B12a}$$

$$L_w = \int_0^\infty g(r)dr \tag{B12b}$$

Interpreted physically, these lengths are a rough measure of the longest distance that two points in a turbulent field may be separated before the correlation between the velocities becomes zero. Another interpretation is that they are a measure of the average eddy size. By equations (B4), these lengths are found to be related by the equation

$$L_u = 2L_w \tag{B13}$$

With equations (B1), (B2), and (B12), the following useful limit relations follow from equations (B5) to (B8):

$$\left.\begin{aligned} f(0) &= \frac{R_u(0)}{\sigma_u^2} = \int_0^\infty F(\Omega)d\Omega = 1 \\ R_u(0) &= \int_0^\infty \Phi_u(\Omega)d\Omega = \sigma_u^2 \\ F(0) &= \frac{\Phi_u(0)}{\sigma_u^2} = \frac{2}{\pi}\int_0^\infty f(r)dr = \frac{2L_u}{\pi} \\ \Phi_u(0) &= \frac{2}{\pi}\int_0^\infty R_u(r)dr = \frac{2L_u\sigma_u^2}{\pi} \end{aligned}\right\} \tag{B14}$$

and

$$\left.\begin{aligned} g(0) &= \frac{R_w(0)}{\sigma_w^2} = \int_0^\infty G(\Omega)d\Omega = 1 \\ R_w(0) &= \int_0^\infty \Phi_w(\Omega)d\Omega = \sigma_w^2 \\ G(0) &= \frac{\Phi_w(0)}{\sigma_w^2} = \frac{2}{\pi}\int_0^\infty g(r)dr = \frac{2L_w}{\pi} \\ \Phi_w(0) &= \frac{2}{\pi}\int_0^\infty R_w(r)dr = \frac{2L_w\sigma_w^2}{\pi} \end{aligned}\right\} \qquad (B15)$$

Analytical Representation of Spectrum and Correlation Functions

Case I.- Equations (5) and (6) were derived by von Kármán (ref. 8) essentially as follows: Based on the work of Loitsianskii and others, it is reasoned that the three-dimensional spectrum for isotropic turbulence should be proportional to Ω^4 for small values of Ω. Further, by dimensional considerations, or by energy transfer considerations, it may be shown that the spectrum at high Ω should be proportional to $\Omega^{-5/3}$ (for large Reynolds numbers); this is a result of Kolmogoroff and others. On the basis of these two extremes of low and high values of Ω, von Kármán thus introduced the following interpolation formula for the three-dimensional spectrum:

$$E(\Omega) = C\frac{\left(\frac{\Omega}{\Omega_0}\right)^4}{\left(1 + \frac{\Omega^2}{\Omega_0^2}\right)^{17/6}} \qquad (B16)$$

where the two constants C and Ω_0 define the basic overall structure of the turbulence; their evaluation in terms of mean-square velocity and the turbulence scale is indicated subsequently.

The substitution of equation (B16) into equations (B10b) and (B10c) leads to the one-dimensional spectra; when these in turn are substituted in equations (B5b) and (B6b), the corresponding correlation functions are found. The equations so found and as used in the body of the paper for Case I are:

$$R_u(r) = \sigma_u^2 \frac{2^{2/3}}{\Gamma\left(\frac{1}{3}\right)}\left(\frac{r}{1.339L}\right)^{1/3} K_{1/3}\left(\frac{r}{1.339L}\right) \tag{B17a}$$

$$R_w(r) = \sigma_w^2 \frac{2^{2/3}}{\Gamma\left(\frac{1}{3}\right)}\left(\frac{r}{1.339L}\right)^{1/3}\left[K_{1/3}\left(\frac{r}{1.339L}\right) - \frac{1}{2}\left(\frac{r}{1.339L}\right)K_{2/3}\left(\frac{r}{1.339L}\right)\right] \tag{B17b}$$

$$\Phi_u(\Omega) = \sigma_u^2 \frac{2L}{\pi} \frac{1}{\left[1 + (1.339L\Omega)^2\right]^{5/6}} \tag{B17c}$$

$$\Phi_w(\Omega) = \sigma_w^2 \frac{L}{\pi} \frac{1 + \frac{8}{3}(1.339L\Omega)^2}{\left[1 + (1.339L\Omega)^2\right]^{11/6}} \tag{B17d}$$

where $L = L_u$. The constants

$$C = \frac{55}{9} \frac{L}{\pi} \sigma_u^2$$

and

$$\Omega_0 = \frac{1}{L} \frac{\Gamma\left(\frac{1}{2}\right)\Gamma\left(\frac{5}{6}\right)}{\Gamma\left(\frac{1}{3}\right)} = \frac{1}{1.339L}$$

necessary to establish equations (B17) are found by application of the limit values given by the second and fourth of equations (B14); involved in this evaluation is the use of the following gamma function relations:

$$x! = \Gamma(x + 1) = x\Gamma(x)$$

$$\Gamma(x)\Gamma(1 - x) = \frac{\pi}{\sin \pi x}$$

It is important to note that all equations (B17) are expressed arbitrarily in terms of the longitudinal scale $L = L_u$, even though equations (B17b) and (B17d) apply to the transverse velocity component. Thus the scale L deduced in the body of the report refers to the longitudinal "scale," not the transverse scale (see eq. (B13)).

Case II.- The correlation and spectrum functions, equations (7) and (8), for Case II are established in a manner somewhat inverse to that of the preceding section as follows. With reference to turbulence studies made in wind tunnels, exponential laws have often been used to fit the measured correlation

data. One function chosen in particular for longitudinal correlation is the following:

$$R_u(r) = \sigma_u^2 e^{-r/L} \tag{B18a}$$

Then from equations (B4a), (B5a), and (B6a), the transverse correlation and associated spectral functions may be deduced; specifically, the following equations are found:

$$R_w(r) = \sigma_w^2 \left(1 - \frac{r}{2L}\right) e^{-r/L} \tag{B18b}$$

$$\Phi_u(\Omega) = \sigma_u^2 \frac{2L}{\pi} \frac{1}{1 + L^2\Omega^2} \tag{B18c}$$

$$\Phi_w(\Omega) = \sigma_w^2 \frac{L}{\pi} \frac{1 + 3L^2\Omega^2}{\left(1 + L^2\Omega^2\right)^2} \tag{B18d}$$

Again, it is to be noted that all equations are expressed in terms of the longitudinal scale $L = L_u$.

It is of interest to see what three-dimensional spectrum is implied by equation (B18a). If equation (B18c) is substituted into equation (B10a), the following expression for $E(\Omega)$ is found:

$$E(\Omega) = \sigma_u^2 \frac{8L}{\pi} \frac{L^4\Omega^4}{\left(1 + L^2\Omega^2\right)^3} \tag{B19}$$

Interestingly, this equation is in accord with the requirement that for small values of Ω, E should behave as Ω^4; for large values of Ω, however, it exhibits a Ω^{-2} variation in contrast to the more appropriate $\Omega^{-5/3}$ variation for Case I.

APPENDIX C

EFFECT OF EXTRANEOUS SIGNALS ON SCALE DETERMINATION

The deduction of turbulence velocities from vane and airplane motion measurements by such means as equation (4) requires consideration of extraneous signals. In particular, one cannot be certain that all the airplane motion effects are eliminated, especially the very-low-frequency and d-c components which might result in spurious gust velocities. The problem is to determine what effect possible residual motion can have on the deduction of such parameters as turbulence scale. This problem is examined to some extent in this appendix.

Consider that the turbulence-velocity time history established by equation (4) is represented by the equation:

$$w_r(t) = w(t) + e(t) \tag{C1}$$

where $w(t)$ is the time history of the vertical gust velocities that would be obtained if they could be measured perfectly (the uncontaminated values) and $e(t)$ is the spurious gust velocity due to residual motion.

If w and e are uncorrelated, the autocorrelation function for w_r is

$$R_r(r) = R(r) + R_e(r) \tag{C2}$$

while the spectrum is

$$\Phi_r(\Omega) = \Phi(\Omega) + \Phi_e(\Omega) \tag{C3}$$

where the independent variable is distance instead of time. Obviously, the derivation of parameters, such as the scale of turbulence, depends on the nature of $R_e(r)$ or on the distribution of power in $\Phi_e(\Omega)$.

To establish possible effects, a specific type of error e will be considered in the remainder of the treatment. The waves that can be seen in the correlation function shown in figure 11 suggest that the turbulence-velocity deductions may contain a small periodic component, which might result, for example, if traces of short-period motion remain in the final time history. Thus, specifically assume

$$e(Vt) = a \sin \Omega_0 Vt \tag{C4}$$

For this case, equations (C2) and (C3) become

$$R_r(r) = R(r) + \frac{a^2}{2} \cos \Omega_0 r \tag{C5}$$

$$\Phi_r(\Omega) = \Phi(\Omega) + \frac{a^2}{4}\,\delta(\Omega + \Omega_0) + \frac{a^2}{4}\,\delta(\Omega - \Omega_0) \tag{C6}$$

where the symbol δ is a Dirac delta function.

If the scale is deduced from equation (C5) in accordance with equation (11), the following equations result:

$$L = 2\int_0^{r_1} \frac{R(r)}{R(0)}\,dr = \frac{R_r(0)}{R(0)}\left[2\int_0^{r_1} \frac{R_r(r)}{R_r(0)}\,dr - \frac{a^2}{\Omega_0 R_r(0)}\sin \Omega_0 r_1\right] = 0.746 r_1 \tag{C7}$$

Graphically, this equation appears as

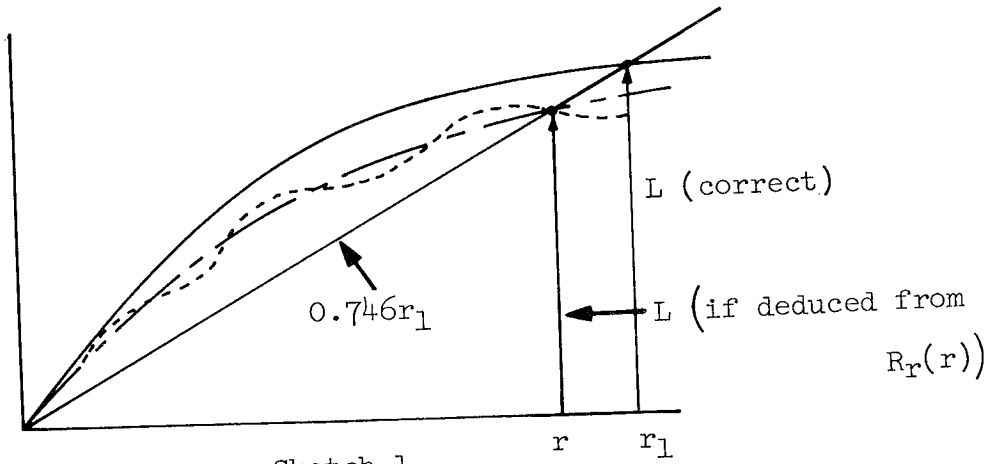

Sketch 1

where the solid curve refers to the integral on the left of equation (C7) and the dotted curve to the integral inside the brackets, the dash-dot curve represents the net quantity contained in the brackets. From this sketch and equation (C7), to a first approximation, the uncontaminated value of L is given by

$$L = \frac{R_r(0)}{R(0)}\,L_r \tag{C8}$$

where L_r is the scale value as deduced directly from the derived or impure vertical velocities; the ratio in this equation is found from equation (C5) to be

$$\frac{R_r(0)}{R(0)} = \frac{1}{1 - \dfrac{a^2}{2R_r(0)}} = \frac{L}{L_r} \tag{C9}$$

as will be used subsequently.

In contrast, if the scale is deduced from equation (C6) in accordance with equation (16), consider the following: Graphically the spectral functions of the assumed sinusoidal error signal e appear as follows in sketch 2(a):

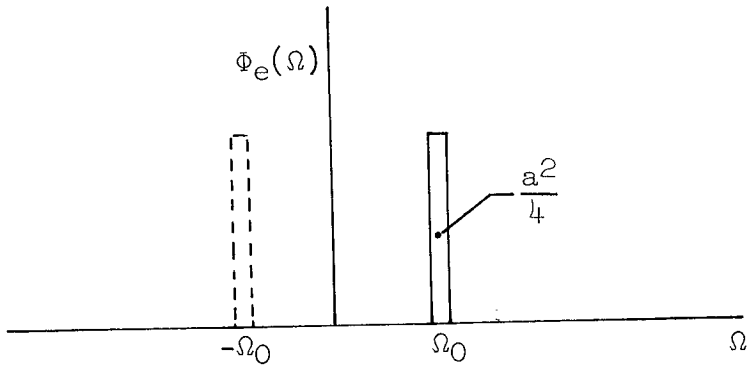

Sketch 2(a)

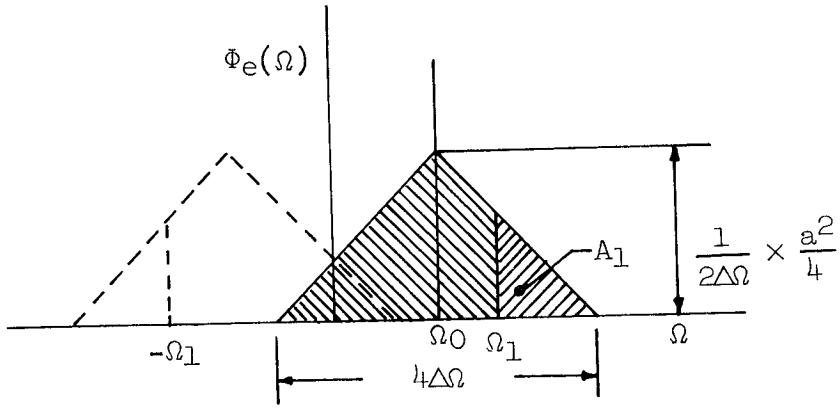

Sketch 2(b)

Sketch 2(a) depicts the Dirac delta functions that apply theoretically. In a numerical analysis, however, these Diracs would be "smeared" out since they, as well as the main spectrum $\Phi(\Omega)$, would effectively pass through the filter shown in figure 25; the result would be more like the pattern shown in sketch 2(b). The actual filter shape is nearly triangular and has minor lobes but is approximated here for convenience by the single triangles shown. The presence of this error spectrum, of course, influences the mean-square values of velocity that are deduced. Specifically, the overall mean-square value would appear

$$\sigma^2_{w,r} = \sigma_w{}^2 + \frac{a^2}{2} \qquad \text{(C10)}$$

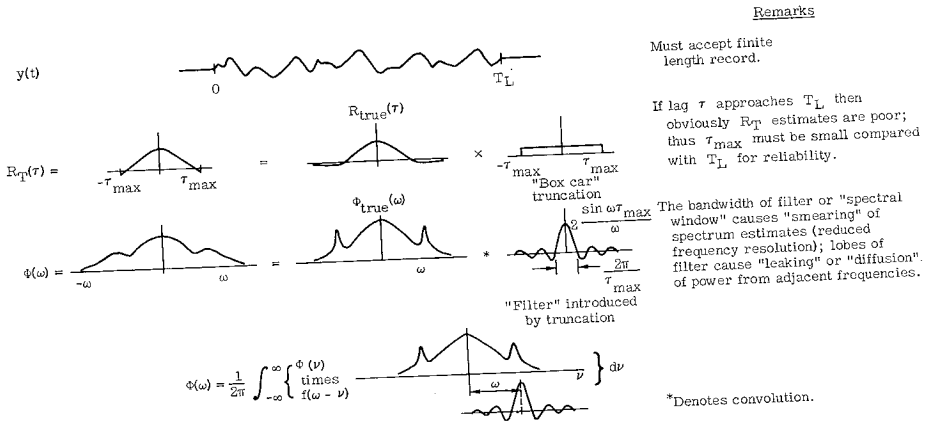

(a) Finite continuous samples.

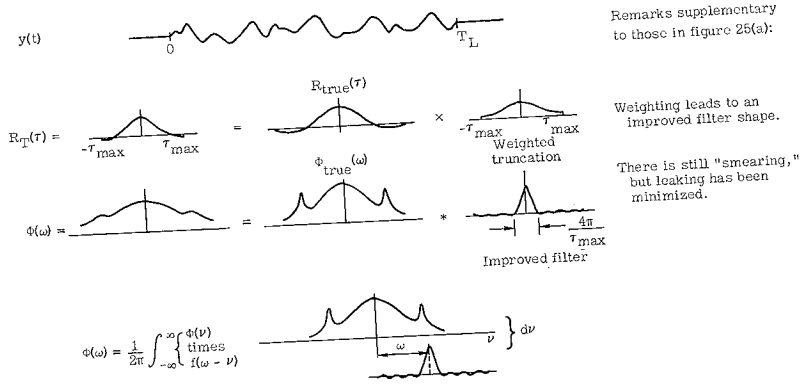

(b) Modifications to improve filter.

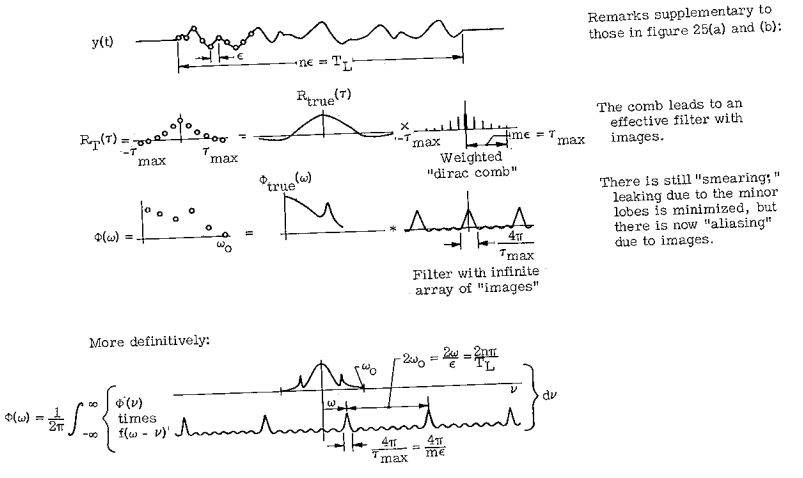

(c) Finite record with interval sampling.

Figure 25.- Practical evaluation of records.

If the lower truncation frequency Ω_1 is higher than the frequency Ω_0, then the mean-square value obtained from the record would be

$$\sigma_{1,r}^2 = \sigma_1^2 + 2A_1 \tag{C11}$$

where

$$A_1 = \frac{a^2}{8}\left[1 - \frac{(\Omega_1 - \Omega_0)}{2\Delta\Omega}\right]$$

and where σ_w and σ_1 are the overall and truncated rms values that would be obtained if the record contained no residual errors.

In accordance with equation (16), it follows that from the deduced L_r, the corrected L would be given by

$$L = \frac{\left(\frac{\sigma_w}{\sigma_1}\right)^3}{\left(\frac{\sigma_{w,r}}{\sigma_{1,r}}\right)^3} L_r$$

which from equations (C10) and (C11) may be written

$$L = \left(\frac{1 - \frac{a^2}{2\sigma_{w,r}^2}}{1 - \frac{2A_1}{\sigma_{w,r}^2}\frac{\sigma_{w,r}^2}{\sigma_{1,r}^2}}\right)^{3/2} L_r \tag{C12}$$

To illustrate the possible effects on scale deduction, consider the case of the spectrum function in figure 10, and the associated correlation function in figure 11 (note, in the terminology of this appendix, figure 11 represents a plot of $\frac{R_r(r)}{R_r(0)}$, not of $\frac{R(r)}{R(0)}$). Assume that the distortion shown in the correlation curve is due to an error of the type given by equation (C5); the frequency Ω_0 is about 0.0016, and the use of the equations in the range where $\frac{R_r(r)}{R_r(0)}$ and $\frac{R(r)}{R(0)}$ should be near zero indicates that $\frac{a^2}{2R_r(0)}$ is in the range of 0.02 to 0.04. With this value for Ω_0, which happens to coincide with Ω_1 used in the computations, the filtered error spectrum would appear

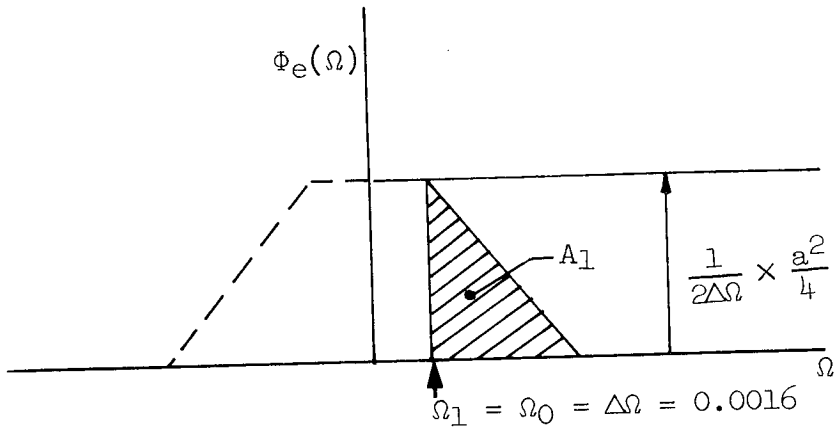

Sketch 3

From sketch 3, A_1 is seen to be $a^2/8$; equation (C12) thus becomes

$$L = \left(\frac{1 - \frac{a^2}{2\sigma^2_{w,r}}}{1 - \frac{a^2}{4\sigma^2_{w,r}} \frac{\sigma^2_{w,r}}{\sigma^2_{l,r}}} \right)^{3/2} L_r \qquad (C13)$$

For the case considered, $\frac{\sigma_{w,r}}{\sigma_{l,r}} = 2.41$, values of scale as deduced by equations (C8) and (C13) are given in the following table for various assumptions of $\frac{a^2}{2\sigma^2_{w,r}}$ $\left(\text{note, } \sigma^2_{w,r} = R_r(0)\right)$. The values of L_r are those given in the table included in the section entitled "The Evaluation of L."

$\frac{a^2}{2\sigma^2_{w,r}}$	Corrected scale, L, ft	
	From correlation (eq. (C8)) with $L_r = 5,720$	From spectrum (eq. (C13)) with $L = 5,550$
0.02	5,840	5,890
.03	5,900	6,080
.04	5,960	6,280

This analysis indicates that if a periodic error signal is present in the deduced vertical gust velocities, the correct scale of the turbulence may actually be larger than the scale value derived from the impure signal, contrary to what might be expected. Whether fortuitous or not, it is seen that the corrections derived herein lead to better agreement between the values of scale derived from the correlation and spectrum function.

The presence of a low-frequency periodic component in the evaluated gust velocities is not certain. If such a residual component does exist, a marked deterioration of the coherency function (see appendix D and table III) in the neighborhood of $\Omega = 0$ would result. This reduction has been observed in some analyses (see ref. 4). The analysis in this appendix shows, however, that even if a periodic error of the type assumed is present in the vertical-velocity values, there is negligible influence on the evaluated scale of turbulence.

APPENDIX D

ACQUISITION AND INTERPRETATION OF DATA BASED ON POWER SPECTRAL TECHNIQUES

Introduction

This appendix deals mainly with the analysis of linear systems which are in a random-process environment. The aim is to outline the major considerations that are involved, first, in the design and conduct of experiments with a system in this environment, and second, in the analysis and interpretation of the acquired data. The subject matter has an exceptionally wide scope and has entered into many fields; although it dates back many years, widespread application in the aeronautical and aerospace fields is relatively recent. The first six sections of the bibliography are representative of notable contributions in these fields; references 1 and 2, specifically, are summaries which show some of the main applications to airplane dynamics. Reference 25, in particular, gives an overall consideration of the application of statistics to the flight-vehicle problem. Although it does not delineate the turbulence characteristics of the atmosphere or the behavior of the airframe systems, it is a comprehensive compendious report on power spectrum concepts. This appendix presents a review of the main aspects of random-process phenomena and analysis which includes some details that might be helpful so that the individual mainly interested in application can grasp the general procedure and appreciate the significance of the various steps.

Objectives of Experiment

Random-process experiments may be divided basically into two broad areas

(1) Laboratory experiments

(2) Field experiments; for example, flight tests

and, with each of these, the data-collection procedure may be classified in two categories

(a) Establishment of a single time-history record which is to be analyzed by itself

(b) Establishment of a set or ensemble of records (as in the consideration of a number of segments of a long time history or as obtained in repeated tests analogous to the situation of a series of coin tosses).

In the following discussion, attention will be restricted mainly to the flight experiments and to the establishment and analysis of single time-history records.

Consider that the flight vehicle system that is undergoing a random forced-excitation test is represented by the following schematic:

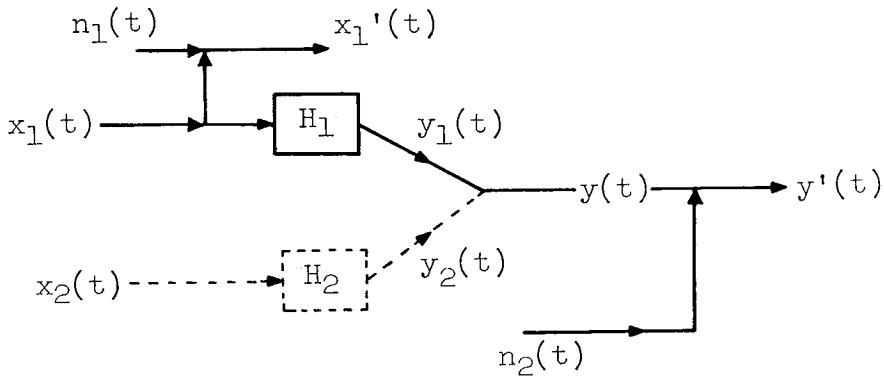

The main input and output of concern are $x_1(t)$ and $y_1(t)$, respectively. In measuring the input x_1, noise $n_1(t)$ enters and gives $x_1'(t)$. Another input $x_2(t)$, which is not really known, may enter and give an output $y_2(t)$ which adds to $y_1(t)$ and cannot be separated. Further, the measurement of $y(t)$ may be contaminated by another noise source $n_2(t)$ to yield $y'(t)$.

In making a test or repeated tests with the system, the final use of the data is an important consideration; the data may be used to:

(1) Establish dynamic environment for system

(2) Verify predictions

(3) Study fatigue

(4) Investigate human comfort

(5) Study any combination of items (1) to (4)

Specific objectives of items (1) and (2) are as follows:

(a) Given H_1 and $y'(t)$, deduce the nature of $x_1(t)$

(b) Given x_1' and H_1, deduce the nature of $y_1(t)$

(c) Given x_1' and $y'(t)$, deduce H_1

The material that follows deals with the interpretation of these specific problems from a statistical point of view considering that extraneous signal sources are present.

Elements of Problem

Environment.- Take as an example the responses of jet-powered airplanes. Consider, first, the environment and list what is known about it. Tables IV and V give dynamic-loads input and vibration-source information of the type that might be listed. This information provides a qualitative description of the excitation forces that are involved, and hence gives an indication of what the loads or structural-excitation problems might be. For jet noise and boundary-layer turbulence, the concern will be primarily structural panels, fastenings, and possibly instrument behavior. For gust loads, overall structural integrity is of concern and involves the climb, cruise, and descent portions of flight. For space-flight vehicles an analogous listing may be made to indicate the nature of the forcing functions that must be considered, measured, and analyzed. In any case the first step is to define the excitation as to the source, frequency content, severity, and duration so that the effects on the system can be considered in the light of this excitation.

System.- It is necessary to identify the areas or parts of the structure that are likely to be affected by the environment. One should be familiar with the response characteristics, particularly the natural frequencies, modes, and associated damping, and how the excitation is applied - whether by direct impingement or by structurally borne excitation. In general, the interest is in those modes which fall within the frequency spectrum of the input excitation and in whether the physical mechanism exists for exciting these modes; the latter point is often elusive. Modes often have frequencies which fall well within the frequency content of the excitation but are not excited because of large damping, or an averaging-out of the input forces, or their excitation may be secondary to other modes. A main objective of many experiments is to find out just what modes are excited.

Instrumentation.- One may distinguish two types of instrumentation - that used in the tests to measure and record, and that used in the subsequent analysis of the test records.

The measuring equipment used depends, of course, on the test objective and for flight vehicles includes such items as pressure gages, strain gages, accelerometers, position indicators, gyros, and flow-direction vanes. Data are collected by two basic schemes: (1) onboard recording using recording oscillographs or magnetic tapes, and (2) remote recording using telemetering techniques. In general, the telemetering of data imposes a greater restriction on the frequency range, dynamic range, and the number of sensors than the direct-recording method.

Data analysis may be digital or analog or a combination of the two. Digital analysis has been greatly facilitated by the modern high-speed computers. Analog analysis involves the use of a wide variety of common and special or unique instruments. This equipment includes voltmeters (including many rms instruments having various time constants and frequency responses), random-noise and sine-wave generators, band-pass filters, squaring circuits, spectrum analyzers, and probability density analyzers. Because the unique instruments such as spectrum analyzers and probability density analyzers are not generally

available, most of the discussion in this appendix will be slanted toward the digital-computing approach.

Whether for recording or analyzing, consideration should be given to the pertinent characteristics of the various instruments, such as range, frequency response, linearity, sensitivity, temperature sensitivity, and transverse sensitivity.

These characteristics are of concern, first, from the viewpoint of making certain that the transducers and recorders are selected with care so that they cover adequately the frequency range of the structure and of the forcing inputs as well as the expected amplitude ranges, and second, to appreciate fully the measuring and reading errors so that the effect of these errors on data interpretation can be assessed. As an example of one means for assessing the effect of instrument errors on results, see the study contained in reference 4.

Record evaluation considerations.- This section indicates briefly the steps that are involved in a record evaluation procedure.

Data analysis is divided logically into the two categories: (1) analysis of the statistical properties of a single time history and (2) analysis of the statistical properties of a collection of records.

Figures 26 and 27 are reproductions of the general procedure recommended in reference 25 for analyzing individual vibration records. Each step is

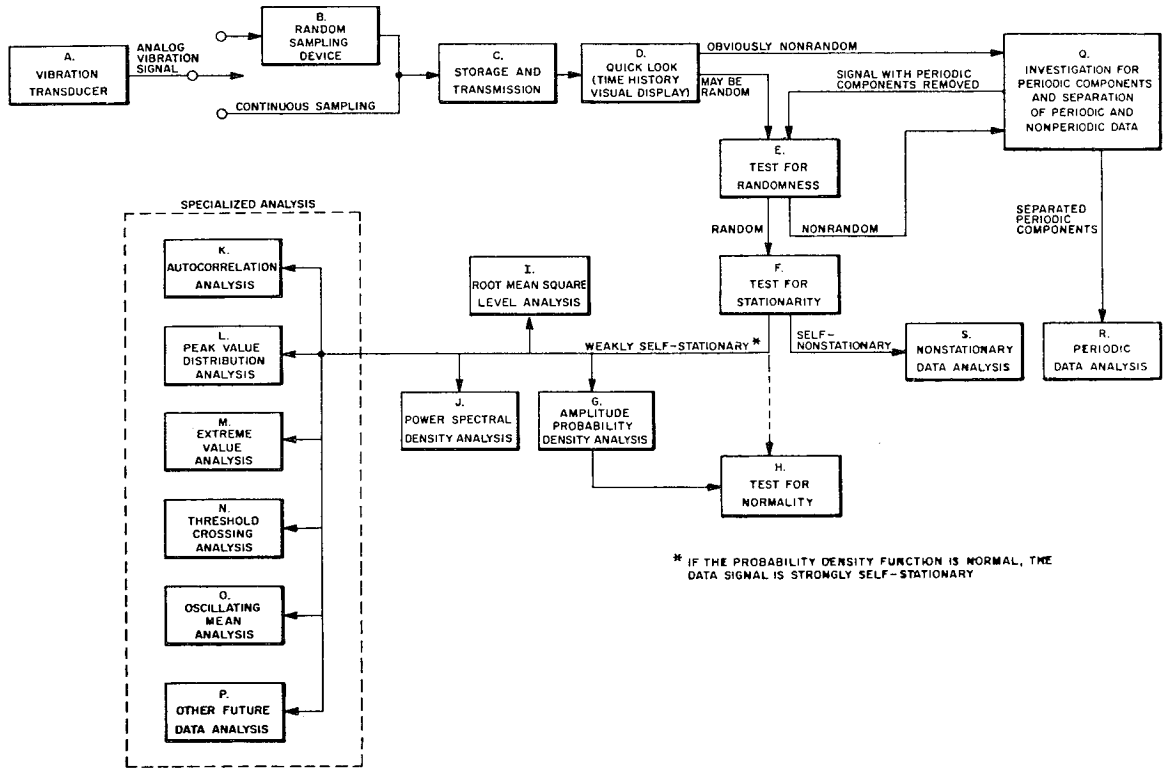

Figure 26.- Recommended procedure for analyzing individual vibration records (from ref. 25).

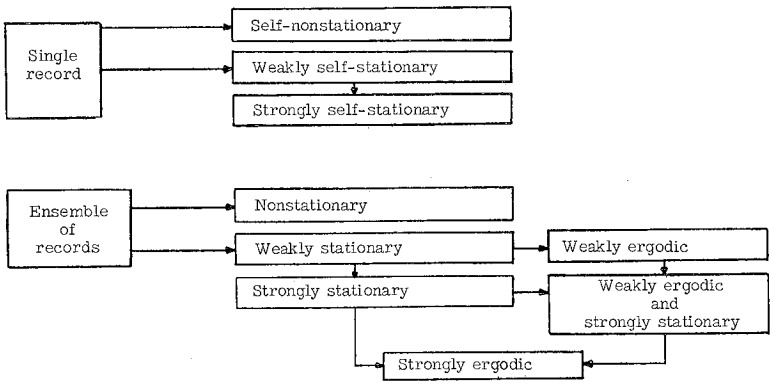

Figure 27.- Categories for single records and ensembles (from ref. 25).

discussed rather fully in this reference. Since the chief concern herein is random phenomena, main interest in the diagram is from block F (fig. 26) on, and subsequent discussion in this appendix will provide some insight as to what is involved in analytical procedures for executing these steps. It is remarked however, that an invaluable step in the overall procedure is the "quick-look analysis" indicated by Step D, whether by oscilloscope presentation or by visual inspection of the records.

Figures 27 to 29 indicate the general procedure recommended in reference 25 for handling a set or ensemble of records. A discussion of each step with the associate statistical mathematics is also given. Of fundamental importance in the consideration of repeated experiments and random sampling is the data-collection process. Of concern are the concepts of acceptance or rejection of records, the appearance of unexpected events, the number of samples required, and the consistency by which experiments are repeated involving, for example, the use of the same pilot, the conduction of flights in different weather, the use of different airplanes of the same type, the variability during any one flight, and the use of different missions.

Aside from determining the actual statistics of the process being investigated, much of the analysis may be concerned with ascertaining only the nature of the process, such as (1) randomness, (2) stationarity, (3) normality, (4) ergodicity, and whether the estimates are unbiased and consistent.

Fundamental in the analysis of any record or group of records is the consideration of the errors and noise in the entire system. These errors may be classed in two groups: (a) statistical estimation errors and (b) equipment errors. The basic aspects of statistical sampling such as the length of the record, the frequency content, and the intended use

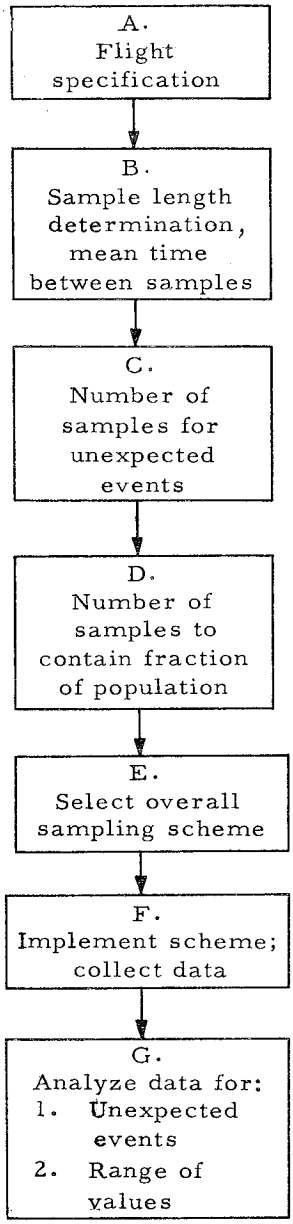

Figure 28.- Recommended procedure for selection of sampling scheme (from ref. 25).

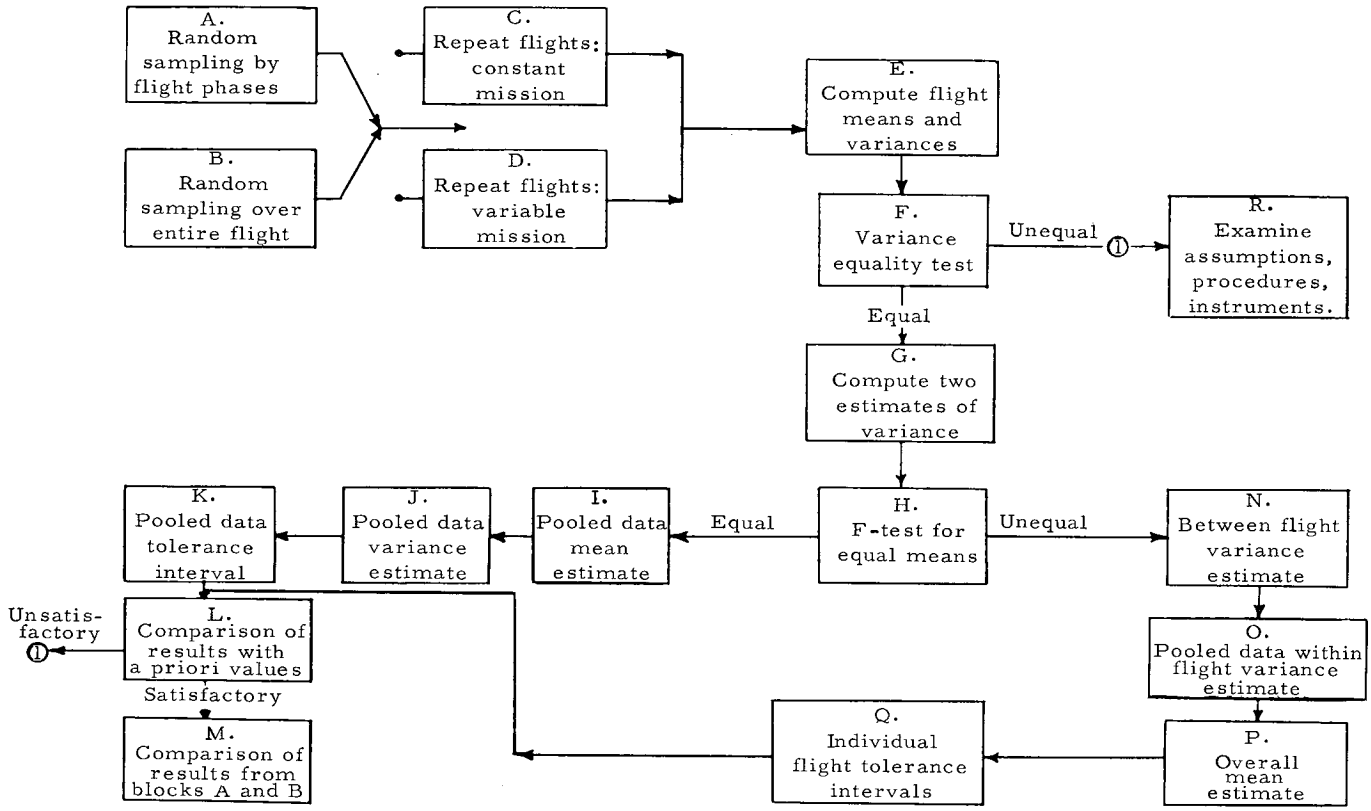

Figure 29.- Recommended procedure for analyzing collection of vibration records (from ref. 25).

of the data are discussed in some detail in the following section. In addition, some details of the equipment errors such as instrument errors, extraneous signal errors, and computational errors are also considered.

Procedures and Statistical Reliability

The following discussion proceeds on the basis that the process under consideration has been established as random Gaussian, and at least weakly stationary, and covers some of the mathematical techniques indicated in the blocks following block E in figure 26.

Mathematical representation.- Table I gives a summary of the equations that are involved in the analytic treatment of random time-history functions. Generalized harmonic analysis is the basic technique involved. For comparative purposes analogous equations that appear in the more commonly known analysis techniques are also shown.

Two basic principles underlie the generalized harmonic or power spectral approach

(1) That a concise picture of the nature of the random process being analyzed is obtained by representation in the frequency plane

(2) That quantities relating to the statistical characteristics of the time history are directly obtainable from this frequency-plane representation.

For principle (2) the columns pertaining to statistical information are also included in table I.

Input-output relations.- Tables II, VI, and VII indicate the basic input-output relations that are involved in power spectral treatment. Table VI gives the fundamental equations and, for comparison, shows the analogous equations that pertain to other basic techniques. Table II illustrates the input-output relations in application to gust loads on aircraft. One of the details brought out by the table is that the frequency scale may be expressed in various terms depending on the particular phenomenon under investigation. For the atmospheric gust problem, it is usually most convenient to make use of a spatial frequency defined in terms of sinusoidal wavelengths as shown, that is, $\Omega = 2\pi/\lambda$. This is in accord with Taylor's hypothesis. Three basic frequency arguments may be used: ω the circular frequency, f the frequency in cycles per second, and Ω the frequency in radians per foot. (Another parameter, the reduced frequency $k = \omega c/2V$ as used in flutter may also be used.) These frequencies and associated power spectra are related as follows:

$$\omega = 2\pi f = V\Omega = V\,\frac{2\pi}{\lambda}$$

$$\Phi(\omega) = \frac{1}{2\pi}\,\Phi(f) = \frac{1}{V}\,\Phi(\Omega)$$

Table VII shows a summary of the input-output situation with respect to a single-degree-of-freedom system for inputs having various characteristics.

Factors in practical evaluation and statistical interpretation of power spectra.- From a practical point of view it is not possible to analyze random time histories in strict accord with the governing equations. In general, the determined spectral values are altered statistical estimates of actual values; the extent of the alteration and the statistical reliability are dependent on the reduction process used - whether digital or analog. Fundamental in this consideration are the length of the record and the method by which the record is processed. The following discussion is intended to give some insight to the nature of the distortion and the quality of the estimates that are obtained. The discussion applies mainly to a digital approach, but similar considerations apply to the analog case.

The three parts of figure 25 (see p. 71) illustrate some of the main consequences of practical analysis. Most of the aspects should become evident by studying the sketches, by a comparison with the exact mathematical expression in table I and by referring to appendix E. The following explanatory comments are offered to pinpoint additional salient points:

Prewhitening:

With reference to lower sketch of figure 25(c), consider that the main lobe of the filter of the "spectral window" is placed at ω, as in the determination of the spectral estimate at this frequency. Also assume that the spectrum has very large power at low frequencies, as is often the case, even though the time history is expressed in terms of zero mean values. Then the side lobes of the filter, even though designed to be small by weighting of the correlation function, permit the power at the low frequency to leak or diffuse causing contamination or distortion of the power estimate being determined. This leaking is avoided in large part by first prewhitening the time-history data so that the power is distributed more evenly. Spectral estimates are then made of the prewhitened data, after which a postdarkening operation is performed to compensate for the initial prewhitening. The numerical procedure for prewhitening, making spectral estimates, and postdarkening is given in appendix E.

Aliasing:

Figure 25(c) shows that interval sampling of records leads to a spectral window with images. Spectrum estimates being made at a frequency ω therefore become distorted since these images permit a transfer of the spectrum power present at frequencies $\omega \pm 2\omega_0$, $\omega \pm 4\omega_0$ . . .. This phenomenon is known as "aliasing." It may be described in another way by reference to the following sketch:

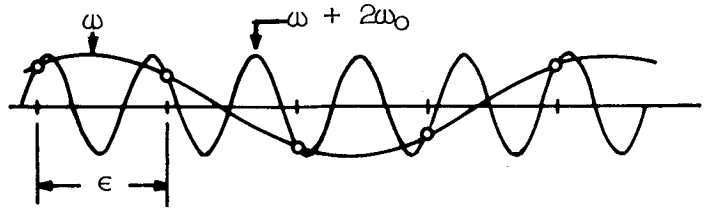

At the sampling interval of ϵ indicated in the sketch, it is not possible to distinguish whether the wave with frequency ω or the wave with frequency $\omega + 2\omega_0 = \omega + 2\pi/\epsilon$ is present. The frequency ω_0 is commonly called the Nyquist frequency.

The problem is avoided in practice by selecting a frequency ω_0 such that ostensibly there is negligible power above this value, and then by determining the sampling interval according to the relation

$$\epsilon = \frac{\pi}{\omega_0}$$

This equation evolves from a communication-sampling theorem which states that sampling with this interval will resolve frequencies up to ω_0. The choice may not always be practicable, however, and in such event, consideration must instead be given to the removal of the power at the higher frequencies either

by rejection in the measuring instruments or by filtering the recorded measurements.

Frequency resolution:

The filters indicated in figure 25 also cause a "smearing" of the spectrum estimates so that at best the estimates derived represent an average value over the effective bandwidth of the filter, which for the nearly triangular-shaped filter shown is approximately half the base width. The frequency resolution is this bandwidth $\left(2\pi/\tau_{max}\right)$ - that is, independent spectral estimates cannot be made for frequencies spaced closer than $2\pi/\tau_{max}$. The figure shows that the filter width may be decreased by increasing $\tau_{max} = m\epsilon$, which means increasing the number of correlation-function estimates. However, this increase will decrease statistical reliability, as discussed subsequently.

Coherency:

In block 7E of table I, the equation

$$\gamma^2(\omega) = \frac{\left|\Phi_{xy}(\omega)\right|^2}{\Phi_x(\omega)\Phi_y(\omega)}$$

defines the coherency function $\gamma^2(\omega)$, which is a measure of the degree to which the x and y processes are linearly related. If the two processes are in perfect linear relation, γ^2 is unity for all values of ω; if they are linearly independent or incoherent, $\gamma^2 = 0$. For a partially linearly related process, as is the case when extraneous noise is present, γ^2 will be between 1 and 0.

If the spectral input-output relations shown in table VI are substituted in this equation, the coherency function becomes

$$\gamma^2(\omega) = \frac{\left|H_c(\omega)\right|^2}{\left|H_s(\omega)\right|^2}$$

where H_c indicates the frequency-response function derived by use of the cross-spectrum equation, and H_s the frequency-response function derived from the equation involving power spectrum only. Consider this equation in light of the experimental objectives mentioned at the beginning of this appendix. If H_c and H_s are determined from the experiment and yield a γ^2 value of appreciably less than one, then a danger signal is provided which indicates that either one or both of the estimates are unreliable. In general, reductions in coherency reflect a loss of reliability in two distinct ways, namely (see fig. 30):

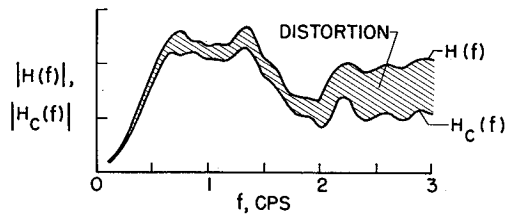

(a) Possible distortion of frequency-response function.

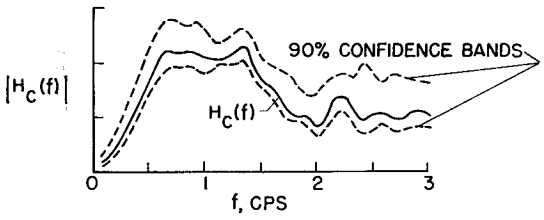

(b) Reduced statistical reliability.

Figure 30.- Effects of reduction in coherency on frequency-response functions.

(1) A possible distortion in the estimates of the frequency-response function from its true value

(2) A reduction in the statistical reliability as measured by the width of the associated confidence bands.

The basic mechanism leading to distortion is the presence of extraneous "noise" signals, such as pilot-control motions, instrumentation limitations, random errors in record reading, round-off errors, and the effects of other gust components such as side gusts (see system sketch in section entitled "Experimental Objectives" in this appendix). The nature of the distortion depends, of course, on the character of the noise and whether it affects the input or output signals. Several types of noise are examined in reference 4 to determine their effects on the coherency function and to establish how these noises distort spectral estimates or frequency-response evaluation; table III summarizes some of the results. It should be noted that for the special case of noises which are incoherent (unrelated) to the input or output signals (which fortunately appears to be the case in practice), the results are particularly simple.

A significant point to mention is that in some cases when the nature of the noise is known, corrections for the distortion are possible; the last column of table III lists the appropriate expressions for making these corrections. A recovery of uncontaminated estimates of the frequency-response function may then be feasible.

With respect to statistical reliability, losses in general cannot be recovered. The following section indicates the interrelation between coherency and statistical reliability.

Statistical reliability:

In consideration of the statistical reliability, assume that the experiment has been repeated many times. From the power spectrum estimates that are evaluated, a probability density distribution may be formed at any given frequency as shown in figure 31. The itemized information in this figure applies to an assumed normal or Gaussian distribution. Based on this assumption the results of reference 26 indicate that the spread of the distribution, as measured by σ_i (see item 1 in fig. 31), depends on the length of the record and the effective bandwidth of the filter (or $2\pi/\tau_{max}$ in fig. 25(a)), or alternatively on n and m, the number of time-history readings and the number of correlation-lag times. The confidence band within which the average value may be expected to

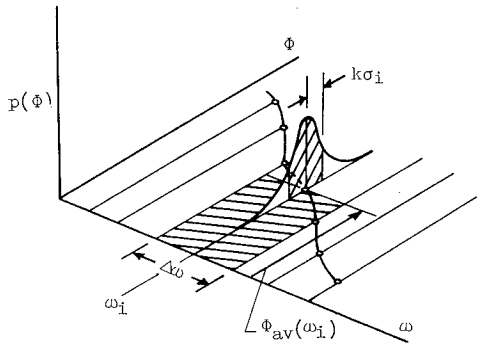

1. Values of Φ_i at $\omega = \omega_i$ have a standard deviation σ_i given by

$$\frac{\sigma_i}{\Phi_i} = \left[\frac{1}{2\pi}(\text{length of record})(\Delta\omega)\right]^{-1/2}$$

$$= \left(\frac{m}{n}\right)^{1/2} = \left(\frac{\tau_{max}}{T_L}\right)^{1/2}$$

2. Based on normal distribution, average value of Φ_i may be expected to fall within the confidence band defined by

$$\Phi_i \pm k\sigma_i$$

with probabilities as follows

k	Probability level
1.0	0.68
1.65	.90
1.96	.95
2.58	.99

3. For given values of $\frac{m}{n}$ and for probability set by k,

$$\left[1 - k\left(\frac{m}{n}\right)^{1/2}\right] < \frac{\Phi_m}{\Phi_{av}} < \left[1 + k\left(\frac{m}{n}\right)^{1/2}\right]$$

or, as indicated below with $K = \frac{2n}{m}$, the statistical degrees of freedom,

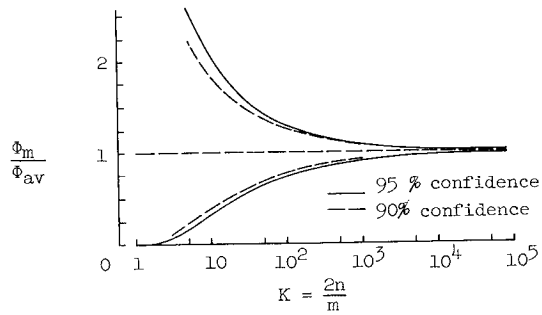

Figure 31.- Statistical reliability of spectrum estimates.

fall with a given level of probability is indicated in general terms in item 2 of figure 31. From items 1 and 2, item 3 gives the confidence limits of the quantity Φ_m/Φ_{av}, where Φ_m refers to a measured value of the power spectrum, and Φ_{av} represents the average of the power for this frequency. The abscissa $2n/m$ of the graph in item 3 denotes the number of statistical degrees of freedom. As an example of the use of this plot, assume $2n/m = 100$; then for 95-percent confidence

$$\left(1 + \frac{1.96}{\sqrt{50}}\right)\Phi_{av} = 1.277\Phi_{av} > \Phi_m$$

$$\left(1 - \frac{1.96}{\sqrt{50}}\right)\Phi_{av} = 0.723\Phi_{av} < \Phi_m$$

or

$$1.38\Phi_m > \Phi_{av} > 0.78\Phi_m$$

That is, the average power can be expected to be between $0.78\Phi_m$ and $1.38\Phi_m$ with a probability of 95 percent.

The statistical reliability of frequency response $\left(H_c(\omega) \text{ or } H_s(\omega)\right)$ derived from spectra of Gaussian processes depends on n and m as presented in the preceeding discussion and also on the coherency function $\gamma^2(\omega)$ between the measured input and output responses if noise is present (ref. 27). The effect of these quantities can be expressed in terms of a range of values within which the average or most probable value of the response $H(\omega)$ will fall with a given confidence level. Figure 32, taken from reference 4, gives the 90-percent confidence bands for the quantity

$$\pm E_1 = 100\,\frac{\left|H_c(\omega)\right| - \left|H(\omega)\right|}{\left|H(\omega)\right|}$$

which is the percent error in the amplitude of the frequency-response function, and for the quantity E_2, the error in the phase angle. As an example of their application, for $n = 1{,}000$, $m = 60$, and $\gamma^2 = 0.90$, the percent error E_1 in the amplitude is ± 15 percent. Thus,

$$-0.15 < \frac{\left|H_c(\omega)\right| - \left|H(\omega)\right|}{\left|H(\omega)\right|} < 0.15$$

with a probability of 90 percent. From this equation, it follows that the associated 90-percent confidence band for the true value of the amplitude of the frequency-response function $H(\omega)$ is given by

$$0.87\left|H_c(\omega)\right| < \left|H(\omega)\right| < 1.17\left|H_c(\omega)\right|$$

The error in phase E_2 for this example is $E_2 = \pm 0.15$. Thus the confidence band for phase angle is given by the interval defined by the measured phase angle plus and minus 0.15 radian.

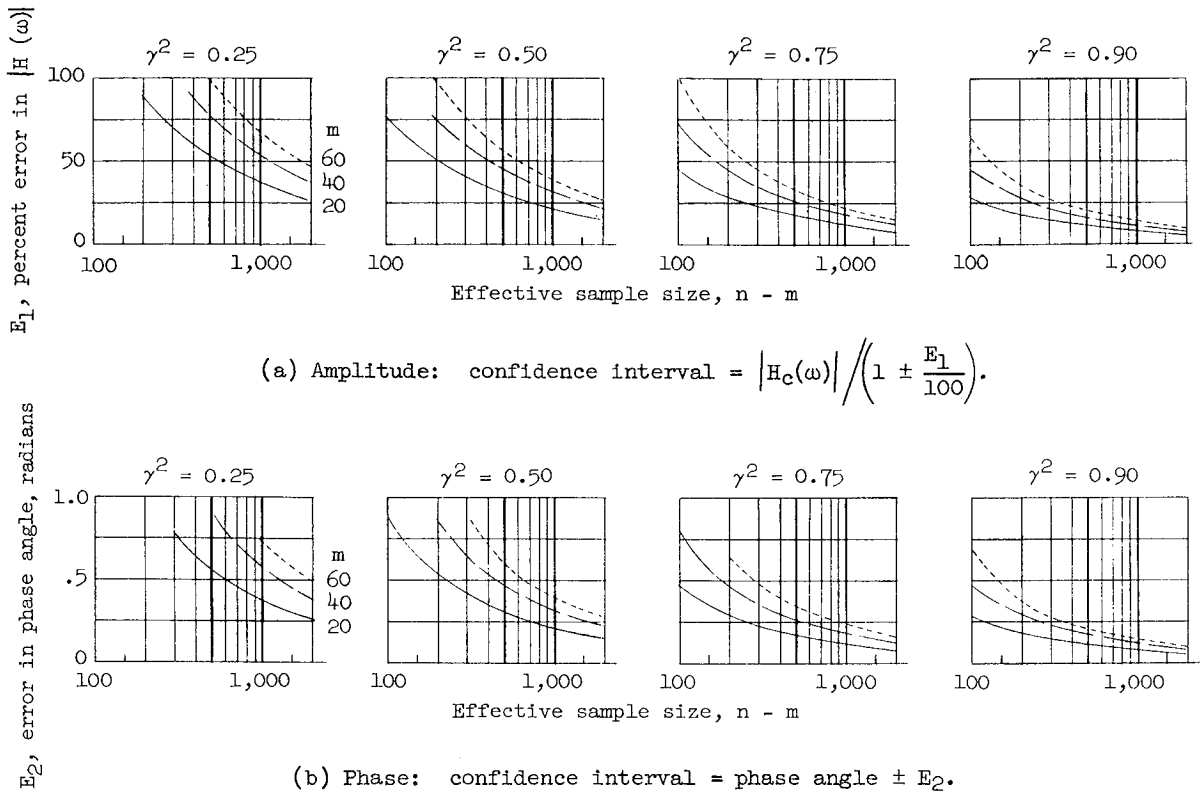

Figure 32.- Ninety-percent confidence intervals for amplitude and phase of estimates of frequency-response function for various values of coherency.

Procedure for selecting n and m.- Based on the information contained in the foregoing sections and for convenience in the planning of experiments, the following procedure is suggested, where digital analysis of the data is assumed (see also appendix E):

(1) Choose ω_0 so as to have negligible power outside of ω_0; this fixes the time-history sampling interval as

$$\epsilon = \frac{\pi}{\omega_0}$$

(2) Assume a practical and desirable record length T_L, then the total number of time-history values is

$$n = \frac{T_L}{\epsilon}$$

(3) Consider frequency resolution $\Delta\omega$; it is determined by computational filter-band width which is effectively one-half the base width, or

$$\Delta\omega = \frac{2\pi}{\tau_{max}} = \frac{2\pi}{m\epsilon}$$

where τ_{max} is maximum correlation-function shift. To have good frequency resolution, m ought to be large ($m = n$ being the best)

(4) However, for statistical reliability, the number of statistical degrees of freedom defined by

$$K \approx \frac{2n}{m} \quad \text{for interval sampling}$$

$$K = \frac{2T_L}{\tau_{max}} \quad \text{for continuous sampling}$$

should be large. (See figs. 31 and 32.) Therefore, for good statistical reliability, m ought to be small.

(5) Compromise between (3) and (4). As a guide, the numbers which have been commonly used with success for gust spectra and which do not involve excessive computation labor are: n from 1,500 to 4,000 and m from 40 to 60. (Note, with $n = 3{,}000$ and $m = 40$, the number of statistical degrees of freedom is 150.)

(6) If T_L is arbitrarily large, then the situation is more flexible; it is possible then to attain arbitrarily high resolution as well as good statistical reliability. After establishing ω_0 and ϵ, choose m to give a desired (but reasonable) frequency resolution. Thus choose a desired K, the number of statistical degrees of freedom. Now determine $n = mK/2$. Then establish the necessary record length $T_L = n\epsilon$ (the chief concern in this procedure is that n and T_L do not become so large that excessive analysis time is required and that stationarity of the process is not invalidated).

Postexperiment analysis.- The analysis procedure to be followed after the experiment has been conducted depends, of course, on the objective of the experiment. On the assumption that the experiment was conducted to determine the frequency-response function of the system, the following basic steps are involved:

1. Establish input and output time histories from measured quantities.

2. Evaluate power spectra of both the input and the output and the cross spectrum of the input and output, as outlined in appendix E.

3. Determine $\left|H_s(\omega)\right|^2$ and $H_c(\omega)$ from equations shown in table III or table VI.

4. Determine coherency function $\gamma^2(\omega)$, table I or table III.

5. If coherency γ^2 is near unity, estimates of $\left|H_s(\omega)\right|^2$ and $H_c(\omega)$ may be considered satisfactory and reliable.

6. If coherency γ^2 is appreciably less than unity, consult figure 32 to determine statistical reliability.

7. If reliability is judged not satisfactory, examine experimental procedure, recording instruments, adequacy of record length, and record reading in detail to try to ascertain whether distortions arise primarily from (a) noise in the input, (b) noise in the output, or (c) from a secondary input. If one of these three cases seems evident, then uncontaminated estimates of the frequency-response function may be obtained by use of the appropriate equation in the last column of table III:

8. If sources of error and distortion cannot be located, try to make a better experiment.

APPENDIX E

DETERMINATION OF POWER SPECTRA AND CROSS SPECTRA BY DIGITAL METHOD

The procedure for determining the power spectrum of vertical gust velocity, for example, from n equally spaced readings for increments of time $\Delta t = \epsilon$, is as follows. First, estimate the frequency ω_0 above which there should be negligible power and then determine the sampling interval as a convenient value near that given by the relation $\epsilon = \pi/\omega_0$. (For vertical gust velocity, experience has shown the $\Omega_0 = 0.1$ is near the upper value of concern; this would indicate an $\epsilon = \pi/V\Omega_0 = \pi/0.1V$ for this case.) Then perform the following steps:

For Spectrum Determination

Step 1.- Determine time history of w_g with zero mean for equally spaced intervals

$$w_g = V(\alpha_V - \bar{\alpha}_V) - V(\theta - \bar{\theta}) + \int_0^t (a_Z - \bar{a}_Z)dt + w_0 + l_x\left(\dot{\theta} - \dot{\bar{\theta}}\right)$$

where w_0 is the initial value of airplane vertical velocity.

Step 2.- Prewhiten values of w_g (response spectra usually do not benefit from prewhitening)

$$\hat{w}(t) = w_g(t) - w_g(t - \epsilon)$$

(see ref. 4).

Step 3.- Estimate values of autocorrelation function $\tilde{R}_{\hat{w}}(\tau)$ for $m + 1$ evenly spaced values of τ from 0 to $m\epsilon$ by numerically integrating

$$\tilde{R}_{\hat{w}}(\tau) = \frac{1}{T_L - \tau} \int_0^{T_L - \tau} \hat{w}(t)\hat{w}(t + \tau)dt$$

that is

$$\tilde{R}_{\hat{w},p} = \frac{1}{n - p} \sum_{q=1}^{n-p} \hat{w}_q \hat{w}_{q+p} \qquad (p = 0, 1, \ldots m)$$

where $n = \frac{T_L}{\epsilon}$, $p = \frac{\tau}{\epsilon}$, and $q = \frac{t}{\epsilon}$.

Step 4.- Obtain raw estimates of the spectral power by numerical evaluation of the Fourier transform of the autocorrelation function

$$L_h = \frac{2\epsilon}{\pi} \sum_{p=0}^{m} a_p \tilde{R}_{\hat{w},p} \cos \frac{hp\pi}{m} \qquad (h = 0, 1, \ldots m)$$

where

$$h = \frac{m\omega}{\omega_0}$$

$$a_p = \frac{1}{2} \qquad (p = 0, m)$$

$$a_p = 1 \qquad (p \neq 0, m)$$

Step 5.- Obtain smoothed estimates of power of $\hat{w}_g$ (from ref. 1)

$$\Phi_0 = \frac{1}{2} L_0 + \frac{1}{2} L_1 \qquad (h = 0)$$

$$\Phi_h = \frac{1}{4} L_{h-1} + \frac{1}{2} L_h + \frac{1}{4} L_{h+1} \qquad (1 \leqq h \leqq m - 1)$$

$$\Phi_m = \frac{1}{2} L_{m-1} + \frac{1}{2} L_m \qquad (h = m)$$

Step 6.- Postdarken smoothed estimates of power to obtain final estimate of power spectrum of w_g

$$\Phi_w(\omega) = \frac{\Phi_h}{2\left(1 - \cos \frac{\pi h}{m}\right)} \qquad \left(\omega = \frac{\pi h}{\epsilon m} = \frac{h}{m} \omega_0\right)$$

For Cross-Spectrum Determination

Step 1.- Determine time histories with zero mean for equally spaced readings for both input w_g and output y, as in the spectrum determination.

Step 2.- Prewhiten input time history (see step 2 above) to give $\hat{w}$.

Step 3.- Estimate values of cross-correlation function $\tilde{R}_{\hat{w}y}(\tau)$ for both positive and negative lags. (See step 3 above.)

$$\tilde{R}_{\hat{w}y,p} = \frac{1}{n - p} \sum_{q=1}^{n-p} \hat{w}_q y_{q+p} \qquad (p = -m, -(m - 1), \ldots m)$$

Step 4.- Obtain raw estimates of the co-spectrum and quadrature spectrum

$$\hat{c}_h = \frac{\epsilon}{\pi} \sum_{p=0}^{m} a_p \left[\tilde{R}_{\hat{w}y}(p) + \tilde{R}_{\hat{w}y}(-p) \right] \cos \frac{hp\pi}{m} \qquad (h = 0, 1, \ldots m)$$

$$\hat{q}_h = \frac{\epsilon}{\pi} \sum_{p=0}^{m} a_p \left[\tilde{R}_{\hat{w}y}(p) - \tilde{R}_{\hat{w}y}(-p) \right] \sin \frac{hp\pi}{m} \qquad (h = 0, 1, \ldots m)$$

where

$$a_p = \frac{1}{2} \qquad (p = 0, m)$$

$$a_p = 1 \qquad (p \neq 0, m)$$

Step 5.- Obtain smoothed values $\Phi_{\hat{w}y}(\omega)$ of prewhitened cross-spectrum estimates as in step 5 for single spectrum.

Step 6.- Postdarken $\Phi_{\hat{w}y}(\omega)$

$$\Phi_{wy}(\omega) = \frac{\Phi_{\hat{w}y}(\omega)}{1 - e^{i\frac{\pi h}{m}}} \qquad \left(\bar{\omega} = \frac{\pi h}{\epsilon m} = \frac{h}{m} \omega_0 \right)$$

APPENDIX F

ANALOG EQUIPMENT FOR ANALYZING RANDOM FUNCTIONS

Listed in this appendix are sketches of some of the analog equipment used in random-process analysis. Schematics for determining the following are shown:

(a) Power spectrum

(b) Cross spectrum

(c) Mean-square value (variance)

(d) Probability density

A brief analysis is made of the power spectrum analog to indicate the nature of its functions.

Determination of Power Spectrum

From an analog computer standpoint, the power-spectral-density function $\Phi_y(\omega)$ associated with a single random function $y(t)$ is defined as the limiting value of the mean-square value of the signal which comes from passing the signal through an ideal bandpass filter with center frequency ω, divided by the bandwidth $\Delta\omega$, as the bandwidth approaches zero. Accordingly, analog equipment for power-spectrum determination is usually built as illustrated in the following diagram:

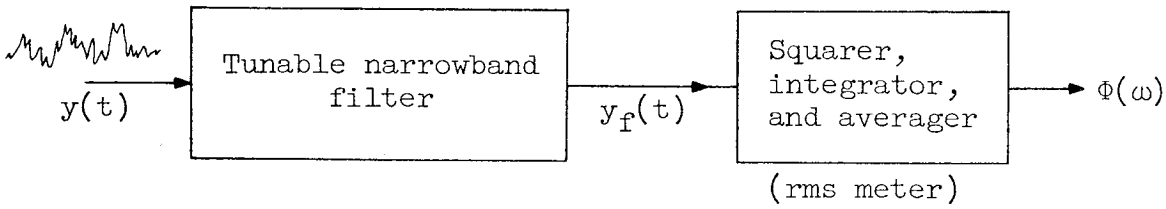

As a result of the filter

$$y_f(t) = \int_{-\infty}^{\infty} y(\tau)h(t - \tau)d\tau \tag{F1}$$

where $h(t)$ is the filter response to a unit impulse. From equation (F1), the power spectrum of y and y_f must be related as follows (see table VI):

$$\Phi_{y,f}(\omega) = \Phi_y(\omega)\left|H(\omega)\right|^2 \tag{F2}$$

where $H(\omega)$ is the frequency-response function of the filter for unit sinusoidal input and is given by

$$H(\omega) = \int_{-\infty}^{\infty} h(t)e^{-i\omega t}dt \tag{F3}$$

The filter is selected so as to reject frequencies except in a bandwidth defined by

$$\Delta\omega = \omega_h - \omega_l$$

where ω_h and ω_l define the frequency limits of the band which, for practical filters, usually correspond to the points on the frequency-response curve of the filter where the response is 3 decibels below the maximum.

For a true rms meter, the reading would be

$$\sqrt{\overline{y_f^2}} = \left[\frac{1}{T}\int_0^T y_f^2(t)dt\right]^{1/2} \tag{F4}$$

In terms of the spectral functions, however, the reading may be expressed as

$$\sqrt{\overline{y_f^2}} = \left[\int_0^{\infty} \Phi_{y,f}(\omega)d\omega\right]^{1/2} = \left[\int_0^{\infty} \Phi_y(\omega)\left|H(\omega)\right|^2 d\omega\right]^{1/2} \tag{F5}$$

For an idealized rectangular filter of bandwidth $\Delta\omega$ and a gradually varying spectrum, this operation indicates the following relation between the true power spectrum and the meter reading

$$\sqrt{\Phi_y(\omega)} = \frac{\sqrt{\overline{y_f^2}}}{\sqrt{\Delta\omega}} \tag{F6}$$

where $\Phi_y(\omega)$ denotes the power spectrum at the center frequency of the filter. Equation (F6) is reasonably true in practice. Thus, adjustment of the meter reading to take into account the bandwidth of the filter yields the estimate of the power spectrum.

It may be of interest to mention that equation (F6) is significant in noise studies, since noise-pressure data are presented in the literature for various filter bandwidths such as octave bands (ω_h twice ω_l), half-octave bands, third-octave bands, etc. It is frequently desirable, for purposes of comparison, to convert data obtained for a given bandwidth to a unit bandwidth, and thus establish an approximation to the square root of the power spectrum. When the square root of the power spectrum is plotted on a decibel scale, it is referred to as a spectrum-level plot.

Many meters are available for indicating the true root-mean-square value of any type of wave; however, they are not always suitable for field use. Many meters, used particularly in noise measurements, are basically rectified average types and are calibrated to give a true rms reading only for pure sine waves. It may be of interest to show the extent of the error in reading that results when an averaging meter is used instead of a true rms meter. In terms of the probability-density-distribution function $p(y)$ of the random signal, the following relations exist:

$$\overline{y^2} = \sigma^2 = \int_{-\infty}^{\infty} y^2 p(y)dy \tag{F7}$$

$$\left|\overline{y(t)}\right| = \int_{-\infty}^{\infty} |y| p(y)dy \tag{F8}$$

Then for a signal having Gaussian distribution,

$$p(y) = \frac{1}{\sigma\sqrt{2\pi}} e^{-\frac{y^2}{2\sigma^2}} \tag{F9}$$

the following values are found

$$\left.\begin{aligned} \left|\overline{y(t)}\right| &= 0.798\left(\overline{y^2}\right)^{1/2} \\ \text{or} \qquad \left(\overline{y^2}\right)^{1/2} &= 1.25\left|\overline{y(t)}\right| \end{aligned}\right\} \tag{F10}$$

Thus, if an averaging meter indicated the true rectified average value of the signal, the rms value would be 1.25 times as great. The averaging meter, however, is usually calibrated in terms of the rms value for a sinusoidal wave, that is,

$$\left(\overline{y^2}\right)^{1/2} = 1.11\left|\overline{y(t)}\right|$$

Therefore, the actual rms value of the random Gaussian signal is greater than the reading given by the usual averaging meter by a factor 1.25/1.11 which is approximately 1.125, thus indicating only a 12-percent error which is equivalent to about 1 decibel.

Cross-Spectrum Analyzer

A cross-spectrum analyzer has a schematic arrangement as follows:

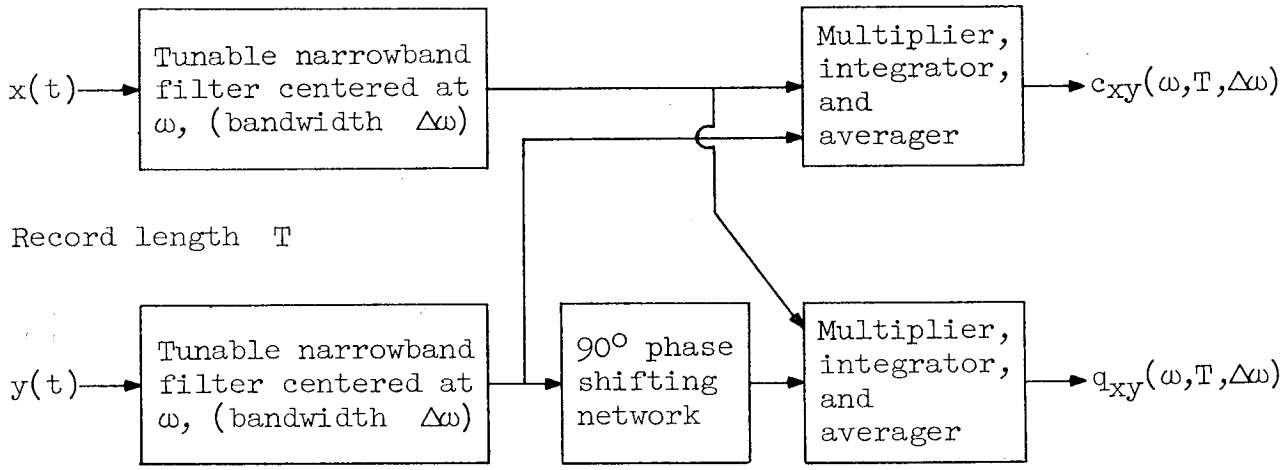

Mean-Square Measurement

Mean-square determination involves the use of the following type of circuit:

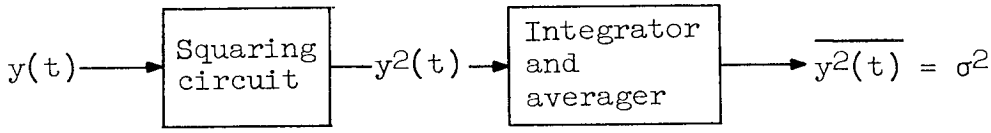

Probability-Density Analyzer

The probability-density function for a stationary random signal may be estimated as shown in the following sketch:

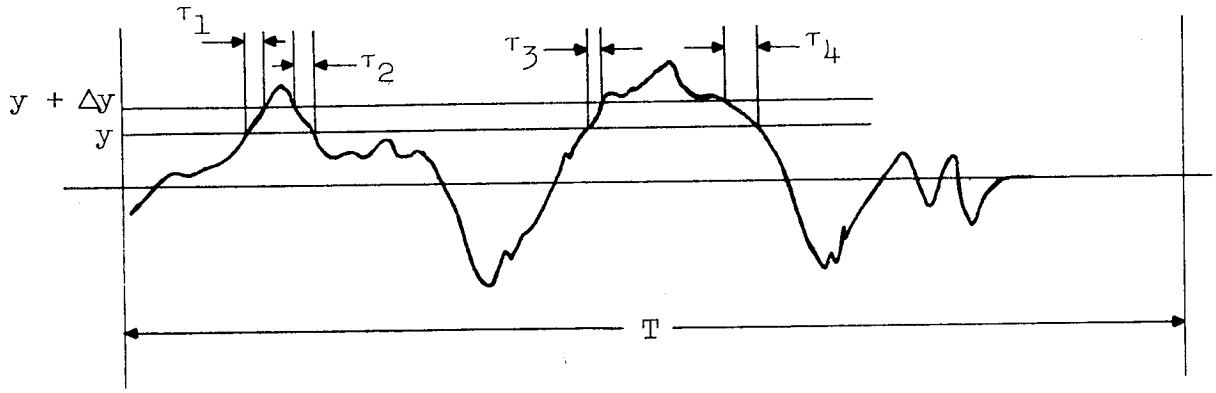

where

$$P(y,\ y + \Delta y) = \Delta y p(y) = \frac{1}{T} \sum_{n} \tau_n$$

or

$$p(y) = \frac{1}{T\ \Delta y} \sum_{n} \tau_n \qquad \text{(F11)}$$

Based on equation (F11), probability-density analyzers have a schematic arrangement as follows:

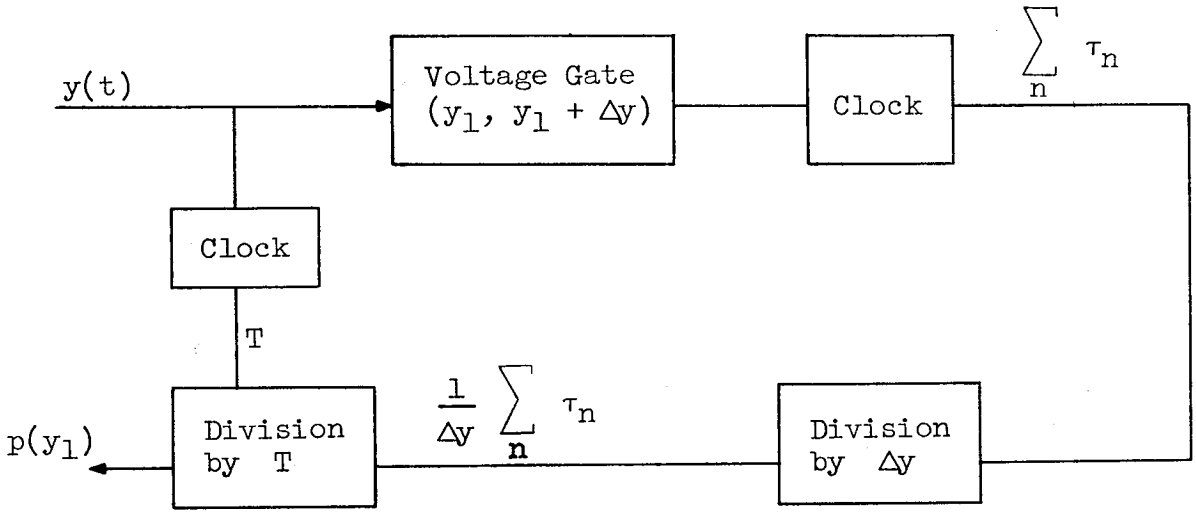

REFERENCES

1. Press, H., and Tukey, J. W.: Power Spectral Methods of Analysis and Their Application in Airplane Dynamics. Vol. IV of AGARD Flight Test Manual, Pt. IVC, Enoch J. Durbin, ed., North Atlantic Treaty Organization (Paris), pp. IVC:1-IVC:41.

2. Press, Harry, and Houbolt, John C.: Some Applications of Generalized Harmonic Analysis to Gust Loads on Airplanes. Jour. Aero. Sci., vol. 22, no. 1, Jan 1955, pp. 17-26, 60.

3. Houbolt, John C., and Kordes, Eldon E.: Structural Response to Discrete and Continuous Gusts of an Airplane Having Wing-Bending Flexibility and a Correlation of Calculated and Flight Results. NACA Rep. 1181, 1954. (Supersedes NACA TN 3006; also contains essential material from TN 2763 and TN 2897.)

4. Coleman, Thomas L., Press, Harry, and Meadows, May T.: An Evaluation of Effects of Flexibility on Wing Strains in Rough Air for a Large Swept-Wing Airplane by Means of Experimentally Determined Frequency-Response Functions With an Assessment of Random-Process Techniques Employed. NASA TR R-70, 1960. (Supersedes NACA TN 4291.)

5. Press, Harry, Atmospheric Turbulence Environment With Special Reference to Continuous Turbulence. Rep. 115, AGARD, North Atlantic Treaty Organization (Paris), Apr.-May 1957.

6. Dressel, T. L.: B-66B Low Level Gust Study. Vol. II. - Power Spectra. Pt. 1. - Plots of Vertical Gust Velocity. WADD Tech. Rep. 60-305, U.S. Air Force, Mar. 1961.

7. Dryden, Hugh L.: A Review of the Statistical Theory of Turbulence. Turbulence - Classic Papers on Statistical Theory, S. K. Friedlander and Leonard Topper, eds., Interscience Publ., Inc. (New York), c.1961, pp. 115-150.

8. Von Kármán, Theodore: Progress in the Statistical Theory of Turbulence. Turbulence - Classic Papers on Statistical Theory, S. K. Friedlander and Leonard Topper, eds., Interscience Publ., Inc. (New York), c.1961, pp. 162-174.

9. Chilton, Robert G.: Some Measurements of Atmospheric Turbulence Obtained From Flow-Direction Vanes Mounted on an Airplane. NACA TN 3313, 1954.

10. Houbolt, John C., and Steiner, Roy: Prediction of Gust Loads in Airplane and Missile Operations. WADC Tech. Rep. 59-507, U.S. Air Force, Aug. 11-13, 1959.

11. Press, Harry, and Steiner, Roy: An Approach to the Problem of Estimating Severe and Repeated Gust Loads for Missile Operations. NACA TN 4332, 1958.

12. Press, Harry, Meadows, May T., and Hadlock, Ivan: A Reevaluation of Data on Atmospheric Turbulence and Airplane Gust Loads for Application in Spectral Calculations. NACA Rep. 1272, 1956. (Supersedes NACA TN 3362 by Press, Meadows, and Hadlock and TN 3540 by Press and Meadows.)

13. Houbolt, John C.: On the Response of Structures Having Multiple Random Inputs. Jahr. 1957 der WGL, Friedr. Vieweg & Sohn (Braunschweig), pp. 296-305.

14. Diederich, Franklin W.: The Response of an Airplane to Random Atmospheric Disturbances. NACA Rep. 1345, 1958. (Supersedes NACA TN 3910.)

15. Watkins, Charles E., Runyan, Harry L., and Woolston, Donald S.: On the Kernel Function of the Integral Equation Relating the Lift and Downwash Distributions of Oscillating Finite Wings in Subsonic Flow. NACA Rep. 1234, 1955. (Supersedes NACA TN 3131.)

16. Watkins, Charles E., and Berman, Julian H.: On the Kernel Function of the Integral Equation Relating Lift and Downwash Distributions of Oscillating Wings in Supersonic Flow. NACA Rep. 1257, 1956. (Supersedes NACA TN 3438.)

17. Watkins, Charles E., Woolston, Donald S., and Cunningham, Herbert J.: A Systematic Kernel Function Procedure for Determining Aerodynamic Forces on Oscillating or Steady Finite Wings at Subsonic Speeds. NASA TR R-48, 1959.

18. Eggleston, John M., and Phillips, William H.: The Lateral Response of Airplanes to Random Atmospheric Turbulence. NASA TR R-74, 1960. (Supersedes NACA TN 3954 by Eggleston and TN 4196 by Eggleston and Phillips.)

19. Bennett, Floyd V., and Pratt, Kermit G.: Calculated Responses of a Large Sweptwing Airplane to Continuous Turbulence With Flight-Test Comparisons. NASA TR R-69, 1960.

20. Murrow, Harold N.: An Analysis of Flight-Test Measurements of the Wing Structural Deformations in Rough Air of a Large Flexible Swept-Wing Airplane. NASA MEMO 12-3-58L, 1959.

21. Pratt, Kermit G., and Bennett, Floyd V.: Charts for Estimating the Effects of Short-Period Stability Characteristics on Airplane Vertical-Acceleration and Pitch-Angle Response in Continuous Atmospheric Turbulence. NACA TN 3992, 1957.

22. Pratt, Kermit G., and Walker, Walter G.: A Revised Gust-Load Formula and a Re-Evaluation of V-G Data Taken on Civil Transport Airplanes From 1933 to 1950. NACA Rep. 1206, 1954. (Supersedes NACA TN's 2964 by Kermit G. Pratt and 3041 by Walter G. Walker.)

23. Rice, S. O.: Mathematical Analysis of Random Noise. Pts. I and II. Bell Syst. Tech. Jour., vol. XXIII, no. 3, July 1944, pp. 282-332; Pts. III and IV, vol. XXIV, no. 1, Jan. 1945, pp. 46-156.

24. Anon.: Metallic Materials and Elements for Flight Vehicle Structures. MIL-HDBK-5, U.S. Dept. Defense, Aug. 1962. (Supersedes MIL-HDBK-5, 1961.)

25. Bendat, Julius S., Enochson, Loren D., Klein, G. Harold, and Piersol, Allan G.: The Application of Statistics to the Flight Vehicle Vibration Problem. ASD Tech. Rep. 61-123, U.S. Air Force, Dec. 1961.

26. Tukey, John W.: The Sampling Theory of Power Spectrum Estimates. Symposium on Applications of Autocorrelation Analysis to Physical Problems. (Woods Hole, Mass.), June 13-14, 1949, pp. 47-67. (Sponsored by ONR, Dept. Navy.)

27. Goodman, N. R.: On the Joint Estimation of the Spectra, Cospectrum and Quadrature Spectrum of a Two-Dimensional Stationary Gaussian Process. Scientific Paper No. 10 (BuShips Contract Nobs-72018(1734-F) and David Taylor Model Basin Contract Nonr-285(17)), Eng. Statistics Lab., New York Univ., Mar. 1957.

BIBLIOGRAPHY

Survey Reports and General Theory

Press, H., and Tukey, J. W.: Power Spectral Methods of Analysis and Their Application in Airplane Dynamics. Vol. IV of AGARD Flight Test Manual, Pt. IVC, Enoch J. Durbin, ed., North Atlantic Treaty Organization (Paris), pp. IVC:1-IVC:41.

Press, Harry, and Houbolt, John C.: Some Applications of Generalized Harmonic Analysis to Gust Loads on Airplanes. Jour. Aero. Sci., vol. 22, no. 1, Jan. 1955, pp. 17-26, 60.

Bendat, Julius S., Enochson, Loren D., Klein, G. Harold, and Piersol, Allan G.: The Application of Statistics to the Flight Vehicle Vibration Problem. ASD Tech. Rep. 61-123, U.S. Air Force, Dec. 1961.

Houbolt, John C.: On the Response of Structures Having Multiple Random Inputs. Jahrb. 1957 der WGL, Friedr. Vieweg & Sohn (Braunschweig), pp. 296-305.

Coleman, Thomas L., Press, Harry, and Meadows, May T.: An Evaluation of Effects of Flexibility on Wing Strains in Rough Air for a Large Swept-Wing Airplane By Means of Experimentally Determined Frequency-Response Functions With an Assessment of Random-Process Techniques Employed. NASA TR R-70, 1960. (Supersedes NACA TN 4291.)

Houbolt, John C., and Steiner, Roy: Prediction of Gust Loads in Airplane and Missile Operations. WADC Tech. Rep. 59-507, U.S. Air Force, Aug. 11-13, 1959.

Press, Harry: Atmospheric Turbulence Environment With Special Reference to Continuous Turbulence. Rep. 115, AGARD, North Atlantic Treaty Organization (Paris), Apr.-May 1957.

Press, Harry, and Steiner, Roy: An Approach to the Problem of Estimating Severe and Repeated Gust Loads for Missile Operations. NACA TN 4332, 1958.

Diederich, Franklin W.: The Response of an Airplane to Random Atmospheric Disturbances. NACA Rep. 1345, 1958. (Supersedes NACA TN 3910.)

Fung, Y. C.: Statistical Aspects of Dynamic Loads. Jour. Aero. Sci., vol. 20, no. 5, May 1953, pp. 317-330.

Rice, S. O.: Mathematical Analysis of Random Noise. Pts. I and II. Bell Syst. Tech. Jour., vol. XXIII, no. 3, July 1944, pp. 282-332; Pts. III and IV, vol. XXIV, no. 1, Jan. 1945, pp. 46-156.

Atmosphere

Chilton, Robert G.: Some Measurements of Atmospheric Turbulence Obtained From Flow-Direction Vanes Mounted on an Airplane. NACA TN 3313, 1954.

Chippendale, George R., and Clement, Warren F.: A Statistical Study of Atmospheric Turbulence by Flight Measurements. Rep. No. T-2, M.S. Thesis, M.I.T., 1951.

Clementson, Gerhardt C.: An Investigation of the Power Spectral Density of Atmospheric Turbulence. Ph. D. Thesis, M.I.T., 1950.

Dressel, T. L.: B-66B Low Level Gust Study. Vol. II.- Power Spectra. Pt. 1.- Plots of Vertical Gust Velocity. WADD Tech. Rep. 60-305, U.S. Air Force, Mar. 1961.

Notess, Charles B., and Eakin, Grady J.: Flight Test Investigation of Turbulence Spectra at Low Altitude Using a Direct Method for Measuring Gust Velocities. Rep. VC-839-F-1 (Contract AF 33(616)174), Cornell Aero. Lab., Inc., July 1, 1954.

Press, Harry, Meadows, May T., and Hadlock, Ivan: A Reevaluation of Data on Atmospheric Turbulence and Airplane Gust Loads for Application in Spectral Calculations. NACA Rep. 1272, 1956. (Supersedes NACA TN 3362 by Press, Meadows, and Hadlock and TN 3540 by Press and Meadows.)

Summers, Robert A.: A Statistical Description of Large-Scale Atmospheric Turbulence. Sc. D. Thesis, M.I.T., 1954. (Also Rep. T-55, Instrumentation Lab., M.I.T., May 17, 1954.)

Airplane Response and Flight Studies

Bennett, Floyd V., and Pratt, Kermit G.: Calculated Responses of a Large Sweptwing Airplane to Continuous Turbulence With Flight-Test Comparisons. NASA TR R-69, 1960.

Connor, Roger J., Hawk, John, and Levy, Charles: Dynamic Analyses for the C-47 Airplane Gust Load Alleviation System. Rep. No. SM-14456, Douglas Aircraft Co., Inc., July 29, 1952.

Decaulne, Paul: Airplane Lateral Response to Statistical Gust Inputs. M.S. Thesis, M.I.T., 1952.

Diederich, Franklin W.: The Dynamic Response of a Large Airplane to Continuous Random Atmsopheric Disturbances. Jour. Aero. Sci., vol. 23, no. 10, Oct. 1956, pp. 917-930.

Eggleston, John M., and Phillips, William H.: The Lateral Response of Airplanes to Random Atmospheric Turbulence. NASA TR R-74, 1960. (Supersedes NACA TN 3954 by Eggleston and TN 4196 by Eggleston and Phillips.)

Houbolt, John C., and Kordes, Eldon E.: Structural Response to Discrete and Continuous Gusts of an Airplane Having Wing-Bending Flexibility and a Correlation of Calculated and Flight Results. NACA Rep. 1181, 1954. (Supersedes NACA TN 3006; also contains essential material from TN 2763 and TN 2897.)

Jackson, Charles E., and Wherry, John E.: A Comparison of Theoretical and Experimental Loads on the B-47 Resulting From Discrete Vertical Gusts. Jour. Aero/Space Sci., vol. 26, no. 1, Jan. 1959, pp. 33-45.

Liepmann, H. W.: Extension of the Statistical Approach to Buffeting and Gust Response of Wings of Finite Span. Rep. No. SM-15172, Douglas Aircraft Co., Inc., Feb. 1954.

Mayer, John P., and Hamer, Harold A.: Applications of Power Spectral Analysis Methods to Maneuver Loads Obtained on Jet Fighter Airplanes During Service Operations. NASA TN D-902, 1961. (Supersedes NACA RM L56J15.)

Murrow, Harold N.: An Analysis of Flight-Test Measurements of the Wing Structural Deformations in Rough Air of a Large Flexible Swept-Wing Airplane. NASA MEMO 12-3-58L, 1959.

Pratt, Kermit G., and Bennett, Floyd V.: Charts for Estimating the Effects of Short-Period Stability Characteristics on Airplane Vertical-Acceleration and Pitch-Angle Response in Continuous Atmospheric Turbulence. NACA TN 3992, 1957.

Pratt, Kermit G., and Walker, Walter G.: A Revised Gust-Load Formula and a Re-Evaluation of V-G Data Taken on Civil Transport Airplanes From 1933 to 1950. NACA Rep. 1206, 1954. (Supersedes NACA TN 2964 by Kermit G. Pratt and TN 3041 by Walter G. Walker.)

Press, Harry, and Mazelsky, Bernard: A Study of the Application of Power-Spectral Methods of Generalized Harmonic Analysis to Gust Loads on Airplanes. NACA Rep. 1172, 1954. (Supersedes NACA TN 2853.)

Shufflebarger, C. C., Payne, Chester B., and Cahen, George L.: A Correlation of Results of a Flight Investigation With Results of an Analytical Study of Effects of Wing Flexibility on Wing Strains Due to Gusts. NACA Rep. 1365, 1958. (Supersedes NACA TN 4071.)

Vitale, A. James, Press, H., and Shufflebarger, C. C.: An Investigation of the Use of Rocket-Powered Models for Gust-Load Studies With an Application to a Tailless Swept-Wing Model at Transonic Speeds. NACA TN 3161, 1954.

Buffeting

Graham, E. W., and Rodriguez, A. M.: Response of Some Linear Systems to Random Forces With Reference to Aircraft Buffeting. Rep. No. SM-14517, Douglas Aircraft Co., Inc., Sept. 1952.

Huston, Wilber B., and Skopinski, T. H.: Probability and Frequency Characteristics of Some Flight Buffet Loads. NACA TN 3733, 1956.

Huston, Wilber B.: A Study of the Correlation Between Flight and Wind-Tunnel Buffet Loads. Rep. 111, AGARD, North Atlantic Treaty Organization (Paris), Apr.-May 1957.

Huston, Wilber B., and Skopinski, T. H.: Measurement and Analysis of Wing and Tail Buffeting Loads on a Fighter Airplane. NACA Rep. 1219, 1955. (Supersedes NACA TN 3080.)

Liepmann, H. W.: On the Application of Statistical Concepts to the Buffeting Problem. Jour. Aero. Sci., vol. 19, no. 12, Dec. 1952, pp. 793-800, 822.

Luskin, Harold, and Lapin, Ellis: An Analytical Approach to the Fuel Sloshing and Buffeting Problems of Aircraft. Jour. Aero. Sci., vol. 19, no. 4, Apr. 1952, pp. 217-228.

Noise and Panel Response.

Eringen, A. C.: Response of Beams and Plates to Random Loads. Trans. ASME, Ser. E - Jour. Appl. Mech., vol. 24, no. 1, Mar. 1957, pp. 46-52.

Granick, Neal, and Thomas, C. E.: Aircraft Structural Vibration Induced by Jet Noise. Shock and Vibration Bulletin No. 24, Dept. of Defense, Feb. 1957, pp. 219-230.

Hess, Robert W., Lassiter, Leslie W., and Hubbard, Harvey H.: A Study of the Response of Panels to Random Acoustic Excitation. NACA RM L55E13c, 1955.

Lassiter, Leslie W., Hess, Robert W., and Hubbard, Harvey H.: An Experimental Study of the Response of Simple Panels to Intense Acoustic Loading. Jour. Aero. Sci., vol. 24, no. 1, Jan. 1957, pp. 19-24, 80.

Miles, John W.: On Structural Fatigue Under Random Loading. Jour. Aero. Sci., vol. 21, no. 11, Nov. 1954, pp. 753-762.

North, Warren J.: Summary Evaluation of Toothed-Nozzle Attachments as a Jet-Noise-Suppression Device. NACA TN 3516, 1955.

Schjelderup, H. C.: Prediction of Acoustical Fatigue Life. Symposium on Acoustical Fatigue. STM Special Tech. Pub. No. 284, c.1961, pp. 19-25.

Turner, M. J.: Environmental Vibration Problems on Large Jet-Propelled Aircraft. Shock and Vibration Bulletin No. 22, Dept. of Defense, July 1955, pp. 34-41.

Runway Roughness

Houbolt, John C.: Runway Roughness Studies in the Aeronautical Field. Jour. Air Transport Div., Proc. American Soc. Civil Eng., vol. 87, no. AT 1, Mar. 1961, pp. 11-31.

Houbolt, John C., Walls, James H., and Smiley, Robert F.: On Spectral Analysis of Runway Roughness and Loads Developed During Taxiing. NACA TN 3484, 1955.

Morris, Garland J., and Stickle, Joseph W.: Response of a Light Airplane to Roughness of Unpaved Runways. NASA TN D-510, 1960.

Thompson, Wilbur E.: Measurements and Power Spectra of Runway Roughness at Airports in Countries of the North Atlantic Treaty Organization. NACA TN 4303, 1958.

Walls, James H., Houbolt, John C., and Press, Harry: Some Measurements and Power Spectra of Runway Roughness. NACA TN 3305, 1954.

Spectral Evaluation

Chang, S. S. L.: On the Filter Problem of the Power-Spectrum Analyzer. Proc. IRE, vol. 42, no. 8, Aug. 1954, pp. 1278-1282.

Goff, Kenneth W.: An Analog Electronic Correlator for Acoustic Measurements. Jour. Acous. Soc. of America, vol. 27, no. 2, Mar. 1955, pp. 223-236.

Goff, Kenneth W.: The Application of Correlation Techniques to Some Acoustic Measurements. Jour. Acous. Soc. of America, vol. 27, no. 2, Mar. 1955, pp. 236-246.

Goodman, N. R.: On the Joint Estimation of the Spectra, Cospectrum and Quadrature Spectrum of a Two-Dimensional Stationary Gaussian Process. Scientific Paper No. 10 (BuShips Contract Nobs-72018(1734-F) and David Taylor Model Basin Contract Nonr-285(17)), Eng. Statistics Lab., New York Univ., Mar. 1957.

Kenimer, Robert L.: An Analog Cross-Spectrum Analyzer for Certain Telemetered Data. 1955 National Telemetering Conference (Chicago, Ill.), American Inst. Elec. Engineers, Inst. Aero. Sci., Inst. Radio Engineers, and Instr. Soc. America, May 1955, pp. 82-87.

Parzen, Emanuel: On Consistent Estimates of the Spectrum of a Stationary Time Series. Annals of Mathematical Statistics, vol. 28, no. 2, June 1957, pp. 329-348.

Parzen, Emanuel: On Choosing an Estimate of the Spectral Density Function of a Stationary Time Series. Annals of Mathematical Statistics, vol. 28, no. 4, Dec. 1957, pp. 921-932.

Smith, Francis B.: Analog Equipment for Processing Randomly Fluctuating Data. Aero. Eng. Rev., vol. 14, no. 5, May 1955, pp. 113-119.

Soffel, A. R.: How to Make Power Spectral Density Analyses of Measurement Signals. ISA Jour., vol. 6, no. 9, Sept. 1959, pp. 80-84.

Spetner, Lee M.: Errors in Power Spectra Due to Finite Sample. Jour. Appl. Phys., vol. 25, no. 5, May 1954, pp. 653-659.

Tukey, John W.: The Sampling Theory of Power Spectrum Estimates. Symposium on Applications of Autocorrelation Analysis to Physical Problems (Woods Hole, Mass.), June 13-14, 1949, pp. 47-67. (Sponsored by ONR, Dept. Navy.)

Zimmerman, J.: Correlation and Spectral Analysis of Time Varying Data. Shock and Vibration Bulletin No. 26, Pt. II, Dept. of Defense, Dec. 1958, pp. 237-254.

Miscellaneous

Blackman, R. B.: Applied Fourier Analysis. Bell Telephone Laboratories, Inc., Dec. 1, 1950.

Krendel, Ezra S., and Barnes, George H.: Interim Report on Human Frequency Response Studies. WADC Tech. Rep. 54-370, U.S. Air Force, June 1954.

Lin, C. C.: On the Motion of a Pendulum in a Turbulent Fluid. Quarterly Appl. Math., vol. I, no. 1, Apr. 1943, pp. 43-48.

Lyon, Richard H.: Response of a Nonlinear String to Random Excitation. Jour. Acous. Soc. of America, vol. 32, no. 8, Aug. 1960, pp. 953-960.

Mazelsky, Bernard: Extension of Power Spectral Methods of Generalized Harmonic Analysis to Determine Non-Gaussian Probability Functions of Random Input Disturbances and Output Responses of Linear Systems. Jour. Aero. Sci., vol. 21, no. 3, Mar. 1954, pp. 145-153.

McIntosh, Virgil C.: The Response of Mechanical Systems to Random Vibration as Determined by Analog Computer. WADC Technical Note 59-193, Wright Air Development Division, Feb. 1960.

Thomson, W. T., and Barton, M. V.: The Response of Mechanical Systems to Random Excitation. Jour. Appl. Mech., vol. 24, no. 2, June 1957, pp. 248-251.

Watkins, Charles E., Runyan, Harry L., and Woolston, Donald S.: On the Kernel Function of the Integral Equation Relating the Lift and Downwash Distributions of Oscillating Finite Wings in Subsonic Flow. NACA Rep. 1234, 1955. (Supersedes NACA TN 3131.)

Watkins, Charles E., and Berman, Julian H.: On the Kernel Function of the Integral Equation Relating the Lift and Downwash Distributions of Oscillating Wings in Supersonic Flow. NACA Rep. 1257, 1956. (Supersedes NACA TN 3438.)

Watkins, Charles E., Woolston, Donald S., and Cunningham, Herbert J.: A Systematic Kernel Function Procedure for Determining Aerodynamic Forces on Oscillating or Steady Finite Wings at Subsonic Speeds. NASA TR R-48, 1959.

Books

Bartlett, M. S.: Stochastic Processes. Cambridge Univ. Press, 1955.

Bendat, Julius S.: Principles and Applications of Random Noise Theory. John Wiley & Sons, Inc., c.1958.

Blackman, R. B., and Tukey, J. W.: The Measurement of Power Spectra. Dover Pub., Inc., 1959.

Campbell, George A., and Foster, Ronald M.: Fourier Integrals for Practical Applications. D. Van Nostrand Co., Inc., c.1948.

Crandall, Stephen H., ed.: Random Vibration. The Technology Press, M.I.T., and John Wiley & Sons, Inc., c.1958.

Dryden, Hugh L.: A Review of the Statistical Theory of Turbulence. Turbulence - Classic Papers on Statistical Theory, S. K. Friedlander and Leonard Topper, eds., Interscience Publ., Inc. (New York), c.1961, pp. 115-150.

James, Hubert M., Nichols, Nathaniel B., and Philips, Ralph S.: Theory of Servo-Mechanisms. McGraw-Hill Book Co., Inc., 1947.

Laning, J. Halcombe, Jr., and Battin, Richard H.: Random Processes in Automatic Control. McGraw-Hill Book Co., Inc., 1956.

Lawson, James L., and Uhlenbeck, George E., eds.: Threshold Signals. McGraw-Hill Book Co., Inc., 1950.

Von Kármán, Theodore: Progress in the Statistical Theory of Turbulence. Turbulence - Classic Papers on Statistical Theory, S. K. Friedlander and Leonard Topper, eds., Interscience Publ., Inc. (New York), c.1961, pp. 162-174.

Wax, Nelson, ed.: Selected Papers on Noise and Stochastic Processes. Dover Publications, Inc., c.1954.

Wiener, Norbert: Extrapolation, Interpolation, and Smoothing of Stationary Time Series With Engineering Applications. The Technology Press, M.I.T., and John Wiley & Sons, Inc., 1949.

Friedlander, S. K., and Topper, Leonard, (eds.): Turbulence, Classic Papers on Statistical Theory. Interscience Publishers, Inc., New York/London, 1961, pp. 115-150 and 162-174.

TABLE I.

	A Function	B Technique	C Time history	D Correlation function
1	Sinusoidal	Sine wave	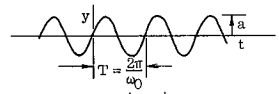 $y = a \sin \omega_0 t.$	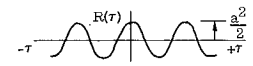 $R(\tau) = \frac{a^2}{2} \cos \omega_0 \tau$
2	Periodic	Fourier series	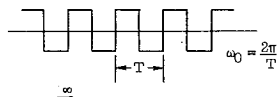 $y(t) = \sum_{n=0}^{\infty} (a_n \cos n\omega_0 t + b_n \sin n\omega_0 t)$ $= \sum_{n=-\infty}^{\infty} c_n e^{in\omega_0 t}$	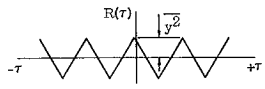
3	Nonrecurring but dissipating	Fourier integral	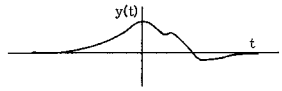 $y(t) = \frac{1}{2\pi} \int_{-\infty}^{\infty} F(\omega) e^{i\omega t} d\omega$ Provided $\int_{-\infty}^{\infty} \lvert y(t) \rvert dt$ exists	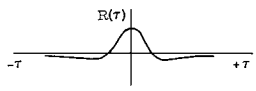 $R(\tau) = \lim_{T \to \infty} \frac{1}{2T} \int_{-T}^{T} y(t) y(t+\tau)\, dt$
4	Stationary random	Generalized harmonic analysis (power spectrum representation)	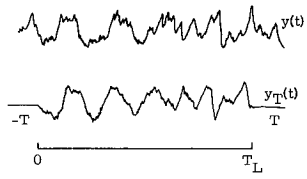	Autocorrelation function.- 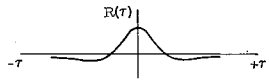 $R(\tau) = \lim_{T \to \infty} \frac{1}{2T} \int_{-T}^{T} y(t) y(t+\tau)\, dt$ $R(\tau) = R(-\tau);\ R(0) \geq \lvert R(\tau) \rvert;\ R(0) = \overline{y^2} > 0$ Note that $R(\tau) = \frac{1}{2} \int_{-\infty}^{\infty} \Phi(\omega) e^{i\omega\tau} d\omega = \int_{0}^{\infty} \Phi(\omega) \cos \omega\tau\, d\omega$
5	Stationary random Gaussian (with zero mean)	Same	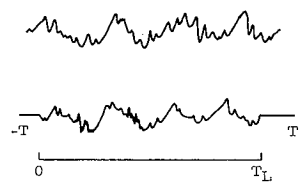	Same
6	Linked Gaussian (with zero mean values)	Same	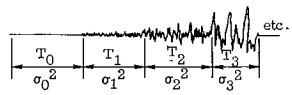 Mean-square values have distribution $p(\sigma)$	Each segment treated by block 4D
7	Two stationary random	Same	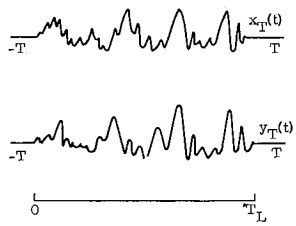	Cross-correlation function.- 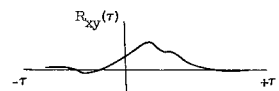 $R_{xy}(\tau) = \lim_{T \to \infty} \frac{1}{2T} \int_{-T}^{T} x(t) y(t+\tau)\, dt$ Note that $R_{xy}(\tau) = \frac{1}{2} \int_{-\infty}^{\infty} \Phi_{xy}(\omega) e^{i\omega\tau} d\omega$ If both x(t) and y(t) have zero mean values, with variances σ_x^2 and σ_y^2, respectively, then $\rho_{xy}(\tau) = \lim_{T \to \infty} \frac{1}{2T} \int_{-T}^{T} x(t) y(t+\tau)\, dt$ and correlation coefficient is $\Gamma_{xy} = \frac{\rho_{xy}(0)}{\sigma_x \sigma_y}$

E	F	G	H	I
Frequency plane representation	Statistical characteristics: Mean, average, or expected value $\bar{y}$	Mean square $\overline{y^2} = \sigma^2 + \bar{y}^2$ where σ^2 is variance	Probability density p(y)	Number of crossings and peaks per second
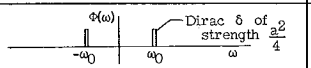 $\Phi(\omega) = \frac{a^2}{4}\delta(\omega - \omega_0) + \frac{a^2}{4}\delta(\omega + \omega_0)$	0	$\frac{a^2}{2}$	 $p(y) = \frac{1}{\pi\sqrt{a^2 - y^2}}$	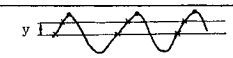 $N_o = N_y = N_{p,y} = \frac{\omega}{2\pi}$ $y < a$
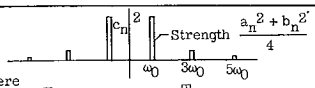 where $a_0 = \frac{1}{T}\int_0^T y(t)\,dt$; $a_n = \frac{2}{T}\int_0^T y(t)\cos n\omega_0 t\,dt$ $b_n = \frac{2}{T}\int_0^T y(t)\sin n\omega_0 t\,dt$ $c_n = \frac{1}{T}\int_0^T y(t)e^{-in\omega_0 t}dt$; $c_n = \frac{a_n - ib_n}{2}$ $c_{-n} = \frac{a_n + ib_n}{2}$	a_0	$\overline{y^2} = a_0^2 + \frac{a_1^2}{2} + \frac{a_2^2}{2} + \ldots + \frac{b_1^2}{2} + \frac{b_2^2}{2} + \ldots$	Depends on function	
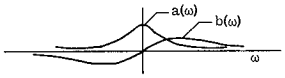 $F(\omega) = \int_{-\infty}^{\infty} y(t)e^{-i\omega t}dt = a(\omega) + ib(\omega)$ $a(\omega) = \int_{-\infty}^{\infty} y(t)\cos\omega t\,dt$ and $b(\omega) = \int_{-\infty}^{\infty} y(t)\sin\omega t\,dt$	$\bar{y} = \frac{1}{2T}\int_{-T}^{T} y(t)dt$	$\overline{y^2} = \lim_{T\to\infty}\frac{1}{2T}\int_{-T}^{T} y^2(t)dt$	Depends on function	
Power spectrum.- 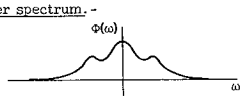 $\Phi(\omega) = \lim_{T\to\infty}\frac{1}{2\pi T}F(\omega)F(-\omega)$ where $F(\omega) = \int_{-\infty}^{\infty} y_T(t)e^{-i\omega t}dt$ or $\Phi(\omega) = \frac{1}{\pi}\int_{-\infty}^{\infty} R(\tau)e^{-i\omega\tau}d\tau = \frac{2}{\pi}\int_0^{\infty} R(\tau)\cos\omega\tau\,d\tau$ $\Phi(\omega) = \Phi(-\omega)$ and $\Phi(\omega) \geqq 0$ $\int_0^{\infty}\Phi(\omega)d\omega = R(0) = \overline{y^2}$	$\bar{y} = \frac{1}{2T}\int_{-T}^{T} y(t)dt$ or $\bar{y} = \int_{-\infty}^{\infty} yp(y)dy$	$\overline{y^2} = \frac{1}{2T}\int_{-T}^{T} y^2(t)dt$ or $\overline{y^2} = \int_{-\infty}^{\infty} y^2 p(y)dy$	Depends on function	
Same	0	$\sigma^2 = \frac{1}{2T}\int_{-T}^{T} y^2(t)dt = \int_0^{\infty}\Phi(\omega)d\omega$	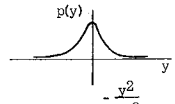 $p(y) = \frac{1}{\sigma\sqrt{2\pi}}e^{-\frac{y^2}{2\sigma^2}}$ i.e., the "normal" distribution	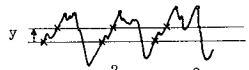 $N_y = \frac{1}{2\pi}\frac{\sigma_1}{\sigma}e^{-\frac{y^2}{2\sigma^2}} = N_0 e^{-\frac{y^2}{2\sigma^2}}$ $N_{p,y} \approx N_y$ $y > 2\sigma$ where $\sigma_1^2 = \int_0^{\infty}\omega^2\Phi(\omega)d\omega$
Each segment treated by block 4E'	0	$\sigma_c^2 = \int_0^{\infty}\sigma^2 p(\sigma)d\sigma$	$p_c(y) = \int_0^{\infty} p(\sigma)\frac{1}{\sigma\sqrt{2\pi}}e^{-\frac{y^2}{2\sigma^2}}d\sigma$	$N_{c,y} = N_0\int_0^{\infty} p(\sigma)e^{-\frac{y^2}{2\sigma^2}}d\sigma$ (See block 5I)
Cross spectrum.- $c_{xy}(\omega)$ = Co-spectrum $q_{xy}(\omega)$ = Quad-spectrum 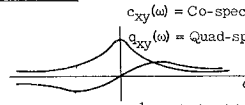 $\Phi_{xy}(\omega) = \lim_{T\to\infty}\frac{1}{2\pi T}F_x(-\omega)F_y(\omega)$ where $F_x(-\omega) = \int_{-\infty}^{\infty} x_T(t)e^{i\omega t}dt$ and $F(\omega) = \int_{-\infty}^{\infty} y_T(t)e^{-i\omega t}dt$ or $\Phi_{xy} = \frac{1}{\pi}\int_{-\infty}^{\infty} R_{xy}(\tau)e^{-i\omega\tau}d\tau = c_{xy}(\omega) - iq_{xy}(\omega)$ $\Phi_{xy}(\omega) = \overline{\Phi_{yx}(\omega)} = \Phi_{yx}(-\omega)$ $c_{xy}(\omega) = c_{xy}(-\omega) = c_{yx}(\omega)$ and $q_{xy}(\omega) = -q_{xy}(-\omega) = -q_{yx}(\omega)$. Coherency.- $\gamma_{xy}^2(\omega) = \frac{\lvert\Phi_{xy}(\omega)\rvert^2}{\Phi_x(\omega)\Phi_y(\omega)} \leqq 1$	----------	$\overline{x(t)y(t)} = \frac{1}{2T}\int_{-T}^{T} x(t)y(t)dt = \frac{1}{2}\int_{-\infty}^{\infty}\Phi_{xy}(\omega)d\omega = R_{xy}(0)$ For x(t) and y(t) with zero mean values, $R_{xy}(0)$ becomes the covariance $\rho_{xy}(0)$	A joint distribution which depends on the functions 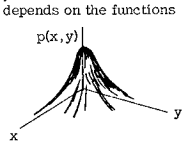 For a two-dimensional normal distribution (zero means); $p(x,y) = \frac{1}{2\pi\sigma^2}e^{-\frac{z^4}{2\sigma^4}}$ where $z^4 = \sigma_y^2 x^2 + \sigma_x^2 y^2 - 2\rho_{xy}xy$ $\sigma^4 = \sigma_x^2\sigma_y^2 - \rho_{xy}^2$ and $\rho_{xy} = \rho_{xy}(0)$	----------

TABLE II.- INPUT-OUTPUT RELATIONS FOR GUST RESPONSE

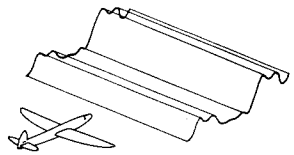

	Power-spectrum approach (Amplitude information only)	Cross-spectrum approach (Phase as well as amplitude information)
Input: Characterizes the atmosphere σ_w^2 = Mean-square value of gust velocity	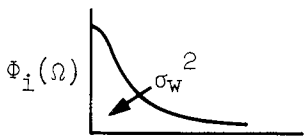	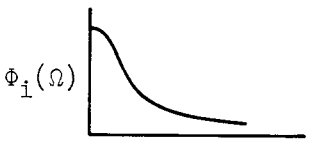
Frequency-response: Characterizes the airplane	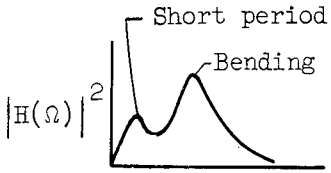	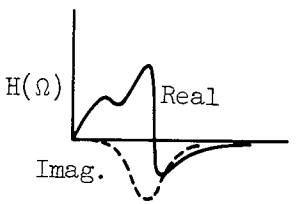
Output: Characterizes the response σ_x^2 = Mean-square value of response	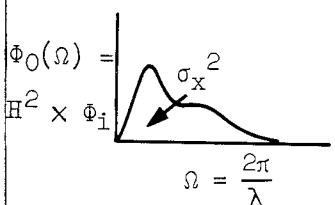 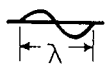	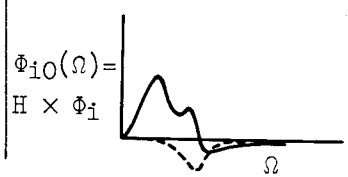

Spectral conversions

$$\omega = 2\pi f = V\Omega = V\frac{2\pi}{\lambda} \qquad \Phi(\omega) = \frac{1}{2\pi}\Phi(f) = \frac{1}{V}\Phi(\Omega)$$

TABLE III.- EFFECTS OF "NOISE" ON COHERENCY AND FREQUENCY-RESPONSE FUNCTIONS

Case	Basic spectra	Experimental transfer functions		Coherency functions		Uncontaminated transfer functions for incoherent noise
		Coherent noise	Incoherent noise	Coherent noise	Incoherent noise	
Pure linear system: 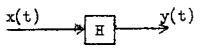	$\Phi_x(\omega)$ $\Phi_{xy}(\omega)$ $\Phi_y(\omega)$	—	$\lvert H_s(\omega)\rvert^2 = \frac{\Phi_y(\omega)}{\Phi_x(\omega)} \equiv \lvert H(\omega)\rvert^2$ $H_c(\omega) = \frac{\Phi_{xy}(\omega)}{\Phi_x(\omega)} \equiv H(\omega)$	—	$\gamma^2(\omega) = \frac{\lvert\Phi_{xy}(\omega)\rvert^2}{\Phi_x(\omega)\Phi_y(\omega)} = 1$ $\gamma^2(\omega) = \frac{\lvert H_c(\omega)\rvert^2}{\lvert H_s(\omega)\rvert^2} = 1$	$\lvert H(\omega)\rvert^2 = \lvert H_s(\omega)\rvert^2$ $H(\omega) = H_c(\omega)$
Noise in measured input: 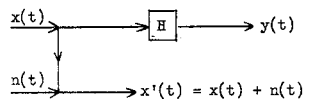	$\Phi_{x'}(\omega) = \Phi_x(\omega) + \Phi_n(\omega) + 2\mathrm{Re}\left[\Phi_{xn}(\omega)\right]$ $\Phi_{x'y}(\omega) = \Phi_{xy}(\omega) + \Phi_{ny}(\omega)$ $\Phi_y(\omega)$	See reference 4	$\lvert H_s(\omega)\rvert^2 = \frac{\Phi_y(\omega)}{\Phi_x(\omega) + \Phi_n(\omega)}$ $H_c(\omega) = \frac{\Phi_{xy}(\omega)}{\Phi_x(\omega) + \Phi_n(\omega)}$	See reference 4	$\gamma^2(\omega) = \frac{1}{1 + \frac{\Phi_n(\omega)}{\Phi_x(\omega)}}$	$\lvert H(\omega)\rvert = \frac{1}{\gamma}\lvert H_s(\omega)\rvert$ $H(\omega) = \frac{1}{\gamma^2} H_c(\omega)$
Noise in measured output: 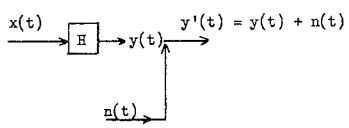	$\Phi_x(\omega)$ $\Phi_{xy'}(\omega) = \Phi_{xy}(\omega) + \Phi_{xn}(\omega)$ $\Phi_{y'}(\omega) = \Phi_y(\omega) + \Phi_n(\omega) + 2\mathrm{Re}\left[\Phi_{yn}(\omega)\right]$		$\lvert H_s(\omega)\rvert^2 = \frac{\Phi_y(\omega) + \Phi_n(\omega)}{\Phi_x(\omega)}$ $H_c(\omega) = \frac{\Phi_{xy}(\omega)}{\Phi_x(\omega)}$		$\gamma^2(\omega) = \frac{1}{1 + \frac{\Phi_n(\omega)}{\Phi_y(\omega)}}$	$\lvert H(\omega)\rvert = \gamma\lvert H_s(\omega)\rvert$ $H(\omega) = H_c(\omega)$
Noise in both input and output: 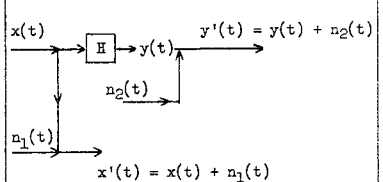	$\Phi_{x'}(\omega) = \Phi_x(\omega) + \Phi_{n_1}(\omega) + 2\mathrm{Re}\left[\Phi_{xn_1}(\omega)\right]$ $\Phi_{x'y'} = \Phi_{xy}(\omega) + \Phi_{xn_2}(\omega) + \Phi_{n_1y}(\omega) + \Phi_{n_1n_2}(\omega)$ $\Phi_{y'}(\omega) = \Phi_y(\omega) + \Phi_{n_2}(\omega) + 2\mathrm{Re}\left[\Phi_{yn_2}(\omega)\right]$		$\lvert H_s(\omega)\rvert^2 = \frac{\Phi_y(\omega) + \Phi_{n_2}(\omega)}{\Phi_x(\omega) + \Phi_{n_1}(\omega)}$ $H_c(\omega) = \frac{\Phi_{xy}(\omega)}{\Phi_x(\omega) + \Phi_{n_1}(\omega)}$		$\gamma^2(\omega) = \frac{1}{\left[1 + \frac{\Phi_{n_1}(\omega)}{\Phi_x(\omega)}\right]\left[1 + \frac{\Phi_{n_2}(\omega)}{\Phi_y(\omega)}\right]}$	Phase of $H_c(\omega)$ is uncontaminated
Additional input: 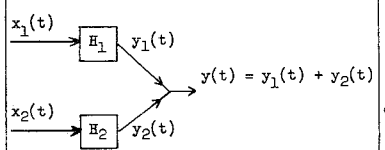	$\Phi_{x_1}(\omega)$ $\Phi_{x_1y}(\omega) = \Phi_{x_1y_1}(\omega) + \Phi_{x_1y_2}(\omega)$ $\Phi_y(\omega) = \Phi_{y_1}(\omega) + \Phi_{y_2}(\omega) + 2\mathrm{Re}\left[\Phi_{y_1y_2}(\omega)\right]$		$\lvert H_s(\omega)\rvert^2 = \lvert H_1(\omega)\rvert^2 + \frac{\Phi_{x_2}(\omega)}{\Phi_{x_1}(\omega)}\lvert H_2(\omega)\rvert^2$ $H_c(\omega) = H_1(\omega)$		$\gamma^2(\omega) = \frac{1}{1 + \frac{\Phi_{x_2}(\omega)}{\Phi_{x_1}(\omega)}\frac{\lvert H_2(\omega)\rvert^2}{\lvert H_1(\omega)\rvert^2}}$	$H_1(\omega) = H_c(\omega)$

TABLE IV.- DYNAMIC LOADS INPUTS FOR JET AIRPLANE

Flight phases	Approximate time duration	Vibration sources	Relative severity
Warmup	1 to 15 min	Jet exhaust	Medium
Taxi	5 to 15 min	Runway roughness; jet exhaust	Medium
Run-up	2 to 20 min	Jet exhaust	High
Take-off	1 to 5 min	Runway roughness; jet exhaust; atmospheric turbulence	High
Climb	3 to 30 min	Jet exhaust; atmospheric turbulence, boundary-layer turbulence	Medium to high
Cruise and mission, flight maneuvers, etc.	1 to 8 hr (might include a transonic region)	Jet exhaust; atmospheric turbulence, boundary-layer turbulence; buffet	Medium to high
Descent	5 to 15 min	Atmospheric turbulence; boundary-layer turbulence	Medium
Landing gear down, flaps down	1 to 15 min	Flap buffet; gusts (atmospheric turbulence)	Medium
Landing (runway or carrier)	5 sec to 2 min	Impact; runway roughness	Medium

TABLE V.- VIBRATION SOURCES

	Frequency range, cps	Most significant region, cps
Rocket exhaust noise*:		
Near field	20 to 5,000	100 to 1,000
Far field	10 to 1,000	20 to 200
Turbojet	50 to 10,000	100 to 1,000
Boundary-layer turbulence	100 to 10,000	500 to 5,000
Buffeting and oscillating shocks:		
Launch vehicles	1 to 500	2 to 200
Aircraft	5 to 500	5 to 50
Atmospheric turbulence	0 to 20	0 to 10
Wind shear	0 to 10	0 to 5
Runway roughness	0.5 to 30	0.5 to 5

*Depends strongly on rocket engine size; figures are for moderate size.

TABLE VI.- BASIC INPUT-OUTPUT RELATIONS

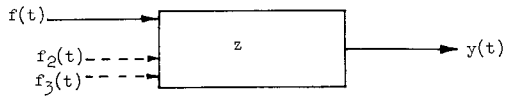

Function	Technique	Representation of input	Transfer function	Input-output relation	Nature of output information
Arbitrary	Superposition	$f(t)$	$h(t)$, response due to unit impulse $h(t) = \frac{d}{dt} A(t)1(t)$ $= \frac{dA}{dt} + A(0)\delta(t - 0)$ where $A(t)$ is response to unit step	$y(t) = \int_0^\infty f(\tau)h(t - \tau)d\tau$	Time history
Periodic	Fourier series	$f(t) = \sum_{n=-\infty}^{\infty} c_n e^{in\omega_0 t}$	$H(\omega) = \int_0^\infty h(t)e^{-i\omega t}dt$	$y(t) = \sum_{n=-\infty}^{\infty} H(n\omega_0)c_n e^{in\omega_0 t}$	Time history
Dissipating	Fourier integral	$f(t) = \frac{1}{2\pi} \int_{-\infty}^{\infty} F(\omega)e^{i\omega t}d\omega$	$H(\omega)$	$y(t) = \frac{1}{2\pi} \int_{-\infty}^{\infty} H(\omega)F(\omega)e^{i\omega t}d\omega$	Time history
Random	Generalized harmonic analysis	$\Phi_f(\omega) = \lim_{T \to \infty} \frac{1}{2\pi T} F(\omega)F(-\omega)$	$\lvert H(\omega) \rvert^2$ and $H(\omega)$	$\Phi_y(\omega) = \lvert H(\omega) \rvert^2 \Phi_f(\omega)$ $\Phi_{fy}(\omega) = H(\omega)\Phi_f(\omega)$ $\Phi_y(\omega) = H(\omega)\Phi_{yf}(\omega)$	Power spectrum and related statistical characteristics
Several random inputs	Generalized harmonic analysis	From inputs f_1, f_2, f_3, . . . f_n form $\Phi_1(\omega)$, $\Phi_2(\omega)$, $\Phi_3(\omega)$, . . . $\Phi_{12}(\omega)$, $\Phi_{23}(\omega)$, . . . $\Phi_{13}(\omega)$, ...	$H_1(\omega)$ $H_2(\omega)$ $H_3(\omega)$ . . . $H_n(\omega)$	$\Phi_y(\omega) = \Phi_1(\omega)H_1(\omega)H_1(-\omega) + \Phi_2(\omega)H_2(\omega)H_2(-\omega)$ $+ \Phi_3(\omega)H_3(\omega)H_3(-\omega) + . . .$ $+ 2\mathrm{Re}\left[\Phi_{12}(\omega)H_1(-\omega)H_2(\omega) + \Phi_{13}(\omega)H_1(-\omega)H_3(\omega)\right.$ $\left. + . . . + \Phi_{23}(\omega)H_2(-\omega)H_3(\omega) + . . .\right]$	Power spectrum and related statistical characteristics

TABLE VII.- INPUT-OUTPUT RELATIONS FOR SINGLE-DEGREE-OF-FREEDOM SYSTEM

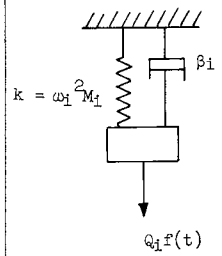

If response of continuous structure under loading $p(x,y,t)$ is expressed in terms of its natural modes $z_i(x,y)$ as follows

$$z(x,y,t) = a_1(t)z_1 + a_2(t)z_2 + a_3(t)z_3 + \ldots$$

then equation for individual mode response is

$$M_i\ddot{a}_i + \beta_i\dot{a}_i + \omega_i^2 M_i a_i = \int p(x,y,t)z_i \, dA$$

$$= f(t) \int g(x,y)z_i \, dA = Q_i f(t), \text{ for space-fixed loading}$$

where $M_i = \int z_i^2 dm$

Frequency-response function is:

$$H_i(\omega) = \frac{a_{i,st}}{1 - \frac{\omega^2}{\omega_i^2} + i2\gamma_i \frac{\omega}{\omega_i}}, \text{ in which } a_{i,st} = \frac{Q_i}{\omega_i^2 M_i}, \quad \gamma_i = \frac{\beta_i}{\beta_{i,cr}} = \frac{\beta_i}{2\omega_i M_i}$$

Function	Harmonic input	Several harmonic inputs	Random white noise input	Wide-band spectral input and highly tuned system
$f(t)$	$b_1 \sin \omega_1 t$ 	$b_1 \sin \omega_1 t + b_2 \sin \omega_2 t$ 		
$\Phi_f(\omega)$	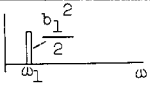	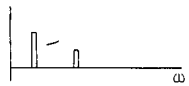		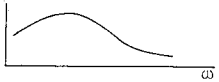
$\lvert H_i(\omega)\rvert^2$	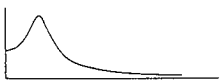	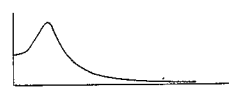	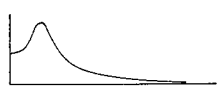	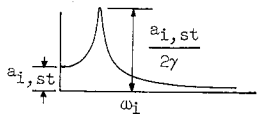
$\Phi_{a,i}(\omega) = \lvert H_i\rvert^2 \Phi_f$	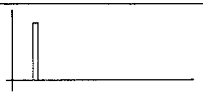	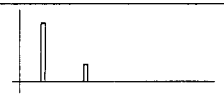	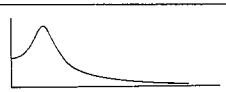	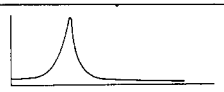
$a_i(t)$	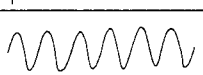	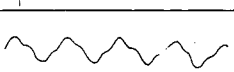	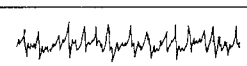	* 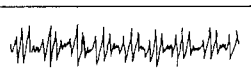
$\overline{a_i^2}$	$\frac{b_1^2}{2}\lvert H_i(\omega_1)\rvert^2$	$\frac{b_1^2}{2}\lvert H_i(\omega_1)\rvert^2 + \frac{b_2^2}{2}\lvert H_i(\omega_2)\rvert^2$	$\frac{\pi}{4}\frac{\omega_i a_{i,st}^2}{\gamma_i}\Phi_f$	$\frac{\pi}{4}\frac{\omega_i a_{i,st}^2}{\gamma_i}\Phi_f(\omega_i)$

*The envelope or amplitude variation of this response is approximated closely by the Rayleigh probability-density distribution $p(y) = \frac{y}{\sigma^2} e^{\left(-\frac{y^2}{2\sigma^2}\right)}$.